The Design of Wafer Swing-Disc Check Valves for Optimal Performance

Henry Hong

A Thesis

in the

Faculty of Engineering

Presented in Partial Fulfillment of the Requirements for

the Degree of Master of Engineering at

Concordia University

Montreal, Quebec

August 1983

ABSTRACT

THE DESIGN OF WAFER SWING-DISC CHECK VALVES

FOR

OPTIMAL PERFORMANCE

Henry Hong

The objective of this thesis is to optimize the design of wafer swing-disc check valves. Optimal valve design involves two major aspects of valve performance. The first performance criterion is minimum pressure loss when the valve is fully opened. The second performance requirement is minimum waterhammer pressure and non-slam seating action resulting from the valve closure. Also, the optimized valve design should retain the desirable features of simplicity, compactness and light-weight construction inherent to wafer type check valves.

Analysis of the pressure loss minimization study is verified experimentally. This concept is then applied to the redesign of wafer swing-disc check valves manufactured by Ritepro Inc. of Montreal. The redesigned valves result in a significant pressure loss improvement over existing Ritepro valves.

The criteria for minimum waterhammer pressure and non-slam seating action require the study of the valve mechanism dynamics, the interaction of the flow forces on the valve, and the analysis of fluid transients for pipe flow. The mathematics and model verification of a hydro-pneumatic mechanism acting as a combination spring and damper to control the wafer check valve dynamics, is reviewed. The flow characteristic of the check valve is determined experimentally. The transient flow through a pipeline is modelled by the method of lumped-parameters. The three studies are then combined and simulated on a digital computer. Conclusions and recommendations are drawn from the simulation study.

ACKNOWLEDGEMENTS

The author would like to express his gratitude and deep appreciation to his supervisors, Dr. J.V. Svoboda and the late Dr. S. Katz, for their suggestion of this research project and for providing guidance and inspiration throughout the author's graduate studies.

The author appreciates the cooperation and support given by Mr. D. Barclay, General Manager of Ritepro Inc. Also, The author would like to express his gratitude to Mr. P. Vogt, Designer for Ritepro Inc., for his technical assistance throughout the research.

The cooperation of Dr. A.S. Ramamurthy, Professor of Civil Engineering, for the use of his Water Resources Laboratory is appreciated. Also, the technical advice in flow measurement instrumentation given by Mr. G.M. Satish is highly appreciated.

The support of Mr. E. Heasman and his machine shop staff is highly appreciated. Special thanks to Mr. P. Scheiwiller for his fast and precise work. The technical assistance given by Mr. W. Fitch of the Fluid Power Control Research Laboratory during the experiments are appreciated.

The critical reading and tearing apart of the report's first draft, by the author's close friend, Dr. A. Fahim, is highly appreciated and honored. Also, the author would like to thank his close friends, Mr. R.S. Lee for beautifully drawing whatever figures were given to him (even during his vacation), and to Mr. N. Krouglicof who stayed up until the moon went down for the final printing of the report. Special thanks to Ms. P. Baktis, for the nuisance and overtime created by the rush jobs given to her for typing. The typing by Mrs. I. Crawford is also appreciated.

I am greatly indebted to my wife Suk Fung for her ever loving patience and understanding while I was intensely submerged in the preparation of the manuscript.

This work was supported by the Natural Sciences and Engineering Research Council of Canada under PRAI Grant No. P-7902.

TABLE OF CONTENTS

LIST OF FIGURES

LIST OF TABLES

NOMENCLATURE

A = disc cone and hinge arm projected area, m^2

A_1 = area of pipe, m^2

A_2 = area of orifice, m^2

A_3 = area of disc, m^2

A_4 = flow area provided by disc assembly, m^2

A_p = piston side piston area, m^2

A_r = rod side piston area, m^2

C = lumped capacitance of fluid-pipe section, m^2

C_{ND} = normal drag coefficient

C_{v1} = orifice flow coefficient, $m^3 s^{-1} Pa^{-\frac{1}{2}}$

C_{v2} = disc flow coefficient, $m^3 s^{-1} Pa^{-\frac{1}{2}}$

C_{v3} = valve flow coefficient, $m^3 s^{-1} Pa^{-\frac{1}{2}}$

C^*_{v1} = normalized orifice flow coefficient

C^*_{v2} = normalized disc flow coefficient

C^*_{v3} = normalized valve flow coefficient

E = Young's modulus of elasticity, N/m^2

F = flow force measured by load cell, N

F_a = actuator piston force, N

F_c = flow force normal to disc centre, N

H_R = resevoir pressure head, meters of water

H_T = tank pressure head, meters of water

H_i = pressure head at pipe location i (i = 1, 2, ...), meters of water

I = lumped fluid inertance within a pipe section, s^2/m^2

I_m = inertia of valve mechanism, kg-m^2

K_{L1} = orifice entrance contraction loss coefficient

K_{L2} = orifice exit expansion loss coefficient

K_{L3} = disc entrance contraction loss coefficient

K_{L4} = disc exit expansion loss coefficient

L = pipe length, m

$\overline{OA}$ = torque lever, mm

$\overline{OB}$ = reference pivot distance, mm

P_a = accumulator pressure, kPa, gage

P_{ao} = initial accumulator pressure, kPa, abs

P_{atm} = atmospheric pressure, kPa

P_i = static pressure at valve or pipe location i (i = 1, 2, ...), Pa

P_p = cylinder piston end pressure, kPa

P_r = cylinder rod end pressure, kPa

Q = flow rate through pipe or through valve, m^3/s

Q_a = accumulator flow rate, m^3/s

Q_i = flow rate through pipe section i (i = 1, 2, ...), m^3/s

Q_v = flow rate through valve, m^3/s

R = lumped pipe section resistance, s^2/m^5

R_c = check valve resistance, N-s^2/m^8

R_ℓ = lower cushion resistance, N-s^2/m^8

R_r = needle valve resistance, $N\text{-}s^2/m^8$

R_u = upper cushion resistance, $N\text{-}s^2/m^8$

R_v = wafer check valve resistance, $s/m^{2\frac{1}{2}}$

T_a = wafer check valve body length, mm

T_{cy} = torque generated by actuator, N-m

T_o = torque at the disc hinge arm, N-m

V = volume in a pipe section, m^3

V_a = accumulator volume, m^3

V_{ao} = initial accumulator volume, m^3

XY = Cartesian coordinate system

Y_p = actuator piston displacement, mm

$Y_{\ell c}$ = actuator lower cushion limit, mm

Y_{uc} = actuator upper cushion limit, mm

$\dot{Y}_p$ = actuator piston velocity, m/s

Z = normalized flow area provided by disc assembly

a = half the major diameter of an ellipse, mm

b = half the minor diameter of an ellipse, mm

c = circle or ellipse offset from ordinate axis, mm

c_o = velocity of pressure wave, m/s

d = disc pivot, mm

d_1 = pipe diameter, mm

d_2 = orifice diameter, mm

d_3 = disc diameter, mm

e	=	pipe wall thickness, mm
f	=	Darcy-Weisbach friction factor
g	=	gravitational acceleration, m/s^2
k_1, k_2	=	parameters to calculate disc to pipe edge clearance, mm
ℓ_A	=	hinge arm length, mm
m	=	fluid mass, kg
n	=	number of pipe sections
p_1, p_2	=	disc to pipe wall contact points
v_R	=	fluid velocity relative to disc, m/s
v_i	=	fluid velocity at valve location i (i = 1, 2, ...), m/s
v_1^*	=	fluid velocity calculated with respect to pipe area, m/s
v_2^*	=	fluid velocity calculated with respect to orifice area, m/s
w	=	orifice wall thickness, mm
x	=	abscissa
x'	=	limit of integration
y	=	ordinate
y'	=	integrand
α	=	width of seat ring face, mm
α_t	=	torque angle, rad
β	=	bulk modulus of elasticity, kPa
γ	=	valve overlap
δ	=	O-ring cross section diameter, mm
ε	=	dimension of disc seating surface, mm
η	=	disc to pipe bottom edge clearance, mm

θ	=	disc opening, rad or deg
θ_F	=	disc full opening, degrees
θ_N	=	disc limited opening, degrees
θ_{max}	=	maximum disc opening, rad
θ_{min}	=	minimum disc opening, rad
θ_o	=	initial disc opening, rad
λ	=	disc to pipe wall radial clearance, mm
μ	=	half the arm thickness, mm
ρ	=	fluid density, kg/m^3
σ	=	disc face thickness, mm
τ_o	=	shearing stress, kPa
ω	=	disc angular velocity, rad/s
ω_o	=	initial disc velocity, rad/s

CHAPTER 1

INTRODUCTION

1.1 General

Check valves are essentially used as safety devices in fluid pipeline networks. The check valve main function is to prevent fluid flow reversal. The undesired effects of flow reversal vary depending on the application. Some examples where check valves are used follow:

- In tank fill-up applications, a check valve is installed on a supply pipe which is below the water line to prevent draining the tank in the case of low supply pressure.

- A check valve installed on the output of a pump would prevent high downstream pressure from driving the pump in reverse in the event of a power failure.

- In an intermittent pumping application where the fluid supply level is below the pump, a check valve is installed at the foot of the inlet suction line to prevent draining of the pipe and hence unnecessary primming of the system.

Ideally, a check valve should offer no resistance to forward flow and instantaneous infinite resistance to reverse flow. Furthermore, the valve should close without slamming on its seat to prevent damage to the sealing surface. Practical valve design limitations, however, result in some resistance to forward flow and a slow valve response to reverse flow. A rapid valve response prohibiting reverse flow to develop reduces the waterhammer effects, as well as reverse flow forces which would cause the valve to slam on its seat.

The desired characteristics of a check valve are often traded off for such features like, simplicity of design, compactness, and low cost. Figure 1-1 shows a schematic drawing of a wafer type swing-disc check valve compared to a conventional swing-disc check valve. With reference to the figure, swing check valves are essentially composed of a valve body where the cavity within the body houses a valve seat and a swing-disc connected to a hinge arm. One end of the hinge arm is pivoted for the disc to swing open and close. When the disc is in its limiting position away from the valve seat, the valve is fully open and offers minimum resistance to the fluid flow. In the other extreme position the disc is in contact with the valve seat and the valve is fully closed. The main advantages of the wafer type check valve over conventional check valves are their compactness, their light-weight, and their

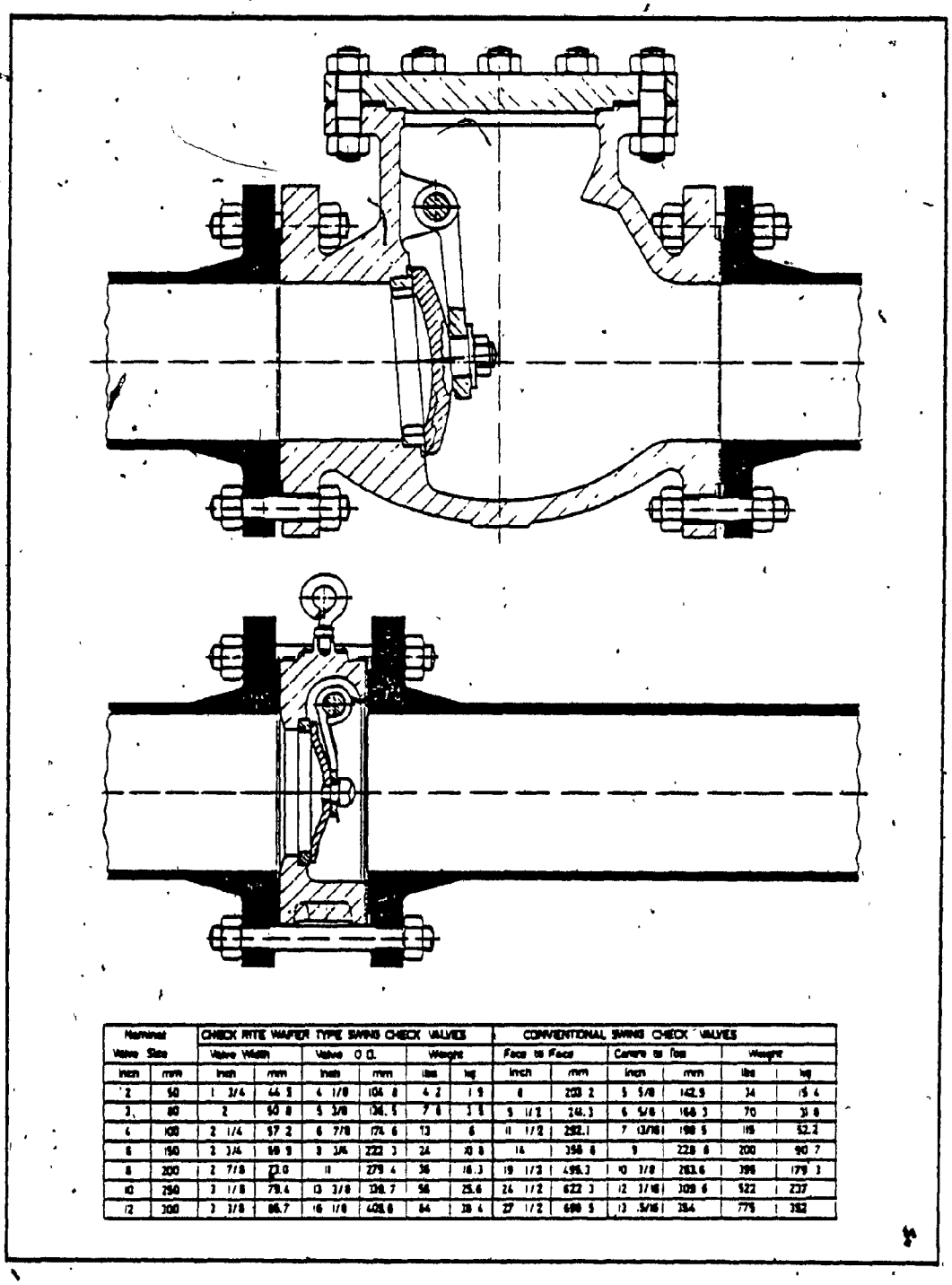

Nominal Valve Size		CHECK RITE WAFER TYPE SWING CHECK VALVES						CONVENTIONAL SWING CHECK VALVES					
		Valve Width		Valve O.D.		Weight		Face to Face		Centre to Top		Weight	
Inch	mm	Inch	mm	Inch	mm	lbs	kg	Inch	mm	Inch	mm	lbs	kg
2	50	1 3/4	44.5	4 1/8	104.8	4.2	1.9	8	203.2	5 5/8	142.9	34	15.4
3	80	2	50.8	5 3/8	136.5	7.8	3.5	9 1/2	241.3	6 5/8	168.3	70	31.8
4	100	2 1/4	57.2	6 7/8	174.6	13	6	11 1/2	292.1	7 13/16	198.5	115	52.2
6	150	3 3/4	69.9	8 3/4	222.3	24	10.8	14	355.6	9	228.6	200	90.7
8	200	2 7/8	73.0	11	279.4	36	16.3	19 1/2	495.3	10 7/8	283.6	395	179.3
10	250	3 1/8	79.4	13 3/8	339.7	56	25.6	24 1/2	622.3	12 7/16	309.6	522	237
12	300	3 3/8	86.7	16 1/8	409.8	84	38.4	27 1/2	698.5	13 5/16	334	775	352

Figure 1-1. Comparison of Wafer-Type Swing-Disc Check Valves and Conventional Swing-Disc Check Valves
(courtesy by Ritepro Inc. [25])

simplicity of design. Wafer type check valves, however, offer higher resistance to forward flow than conventional valves.

1.2 Review of Previous Work

To the knowledge of the author, no global and systematic investigation of all the essential aspects leading to an optimal design of the wafer type swing-disc check valve has been conducted. The literature survey indicates that only limited work has been done in the direction of energy minimization and controlling the dynamics of check valves in general. The work of several investigators are summarized as follows:

Esleeck and Rosser [1] showed that the problem of waterhammer due to pivoting check valves can be reduced to a single second order differential equation of disc motion. The valve is related to the piping system by knowing the "coastdown" characteristic (flow versus time) of the pipeline in the absence of the check valve. This assumes that the check valve exerts negligible effect on the pipe "coastdown" flow until the valve is nearly closed. The motion of the valve disc results from the fluid momentum. At the instant when the disc seats, the corresponding reverse flow velocity is calculated and converted into waterhammer pressure.

Pool, Porwit and Carlton [2] have extended the work from Esleeck and Rosser [1] to get agreement with experimental results. Their work focused on modelling the check valve dynamics more accurately to obtain better surge pressure predictions. Swing-disc and tilting-disc check valves were considered. The tilting-disc check valve pivots about a point within its disc diameter. Extrapolation of the valve mathematical model to pivoting check valves of any size in any system was established. This requires a knowledge of the check valve design parameters and the valve fluid flow characteristics.

Pool [3] then optimized pivoting check valves so that the disc reached the seat as fast as possible after the pipe flow decelerated to zero. If no reverse flow occurs, waterhammer pressure is minimum. Internal valve body, disc shape and pivot location were considered. Pool suggested that the best pivot location is at half of the disc radius. This calculation was based on an assumption considering the swinging disc as an oscillating pendulum. Addition of a torsional spring decreases the period and valve closure is faster. Methods to determine the least pressure drop across the valve was not considered.

Csemniczky [4] studied the hydraulic performance characteristics of pressure drop and momentum for tilting-disc check valves. The emphasis of his work was to derive a

semi-empirical formula describing the moment acting on the disc shaft. Csemniczky showed that the moment characteristic does not depend only upon the disc angle, but also on the eccentric location of the pivot. Experimental pressure drop results showed little difference for various pivot locations. No method of obtaining the least pressure drop for the tilting-disc check valve at full opening was presented.

Krane and Cho [5] experimentally determined the pressure drop and moment coefficients for a tilting-disc check valve. Both forward and reverse flow through the valve were considered. The similarity in variation with disc angle between these two coefficients indicated that the fluid flow generated moment on the disc is related to the pressure drop across the valve. Knowledge of these two hydraulic variables were used to predict pressure drops during normal operation and to estimate pressure surges during valve closure. The check valve studied incorporated a dash-pot mechanism for non-slamming closure action. The authors indicated that from test results, there was no appreciable throttling of the flow (agreeing with Esleeck and Rosser [1]) until the disc made contact with the dash-pot. At the dash-pot contact, water hammer resulted from the sudden change in valve resistance. Although a generalized equation describing the fluid torque on a moving disc was derived, no method was established to predict the

least pressure drop across the check valve. The research concluded that the pressure drop occurred almost entirely across the valve-disc.

Both Gwinn [6] and Uram [7] investigated the dynamics of a swing-disc check valve in order to estimate the disc impact velocity due to "steam-hammer". Gwinn calculated the valve life by requiring the closing impact stresses to be below the disc and seat yield strenghts. Both investigators considered the closing moment on the disc to be due to the valve pressure drop caused primarily by the disc. Hence, the motion of the valve disc can be estimated if the pressure loss across the valve is known.

1.3 Thesis Outline

The object of this thesis is to optimize the design of wafer type swing-disc check valves for improved performance, yet maintaining its simple design. The research focuses on two major areas of study:

1. Energy losses and their minimization.

2. Valve dynamics in order to limit pressure surges and mechanical shock.

For the sake of brevity, a "check valve" will refer

throughout the thesis to mean the wafer swing-disc check valve type, unless otherwise specified.

The different topics investigated in this thesis and the interactions between them, are shown in block diagram form in Figure 1-2. To minimize the check valve energy loss, the valve discharge coefficient and valve flow passage areas are considered in the valve design. The check valve dynamic performance investigation is divided into three separately related areas of study. These include the valve mechanism dynamics, the flow forces acting on the valve, and the waterhammer resulting from the valve dynamics. A brief outline of these subject areas is described in the following paragraphs.

Chapter 2 presents the energy loss investigation across a wafer type check valve. The pressure loss is minimized by altering two parameters associated with the valve geometry. One parameter is the discharge coefficient and other minor losses. The second parameter is the flow passage area ratio. The investigation results in an analytical prediction of the pressure drop across the check valve in terms of a normalized flow coefficient. This analytical flow coefficient is verified experimentally.

In Chapter 3, the design of the wafer swing-disc check valves manufactured by Ritepro Inc. in Montreal is

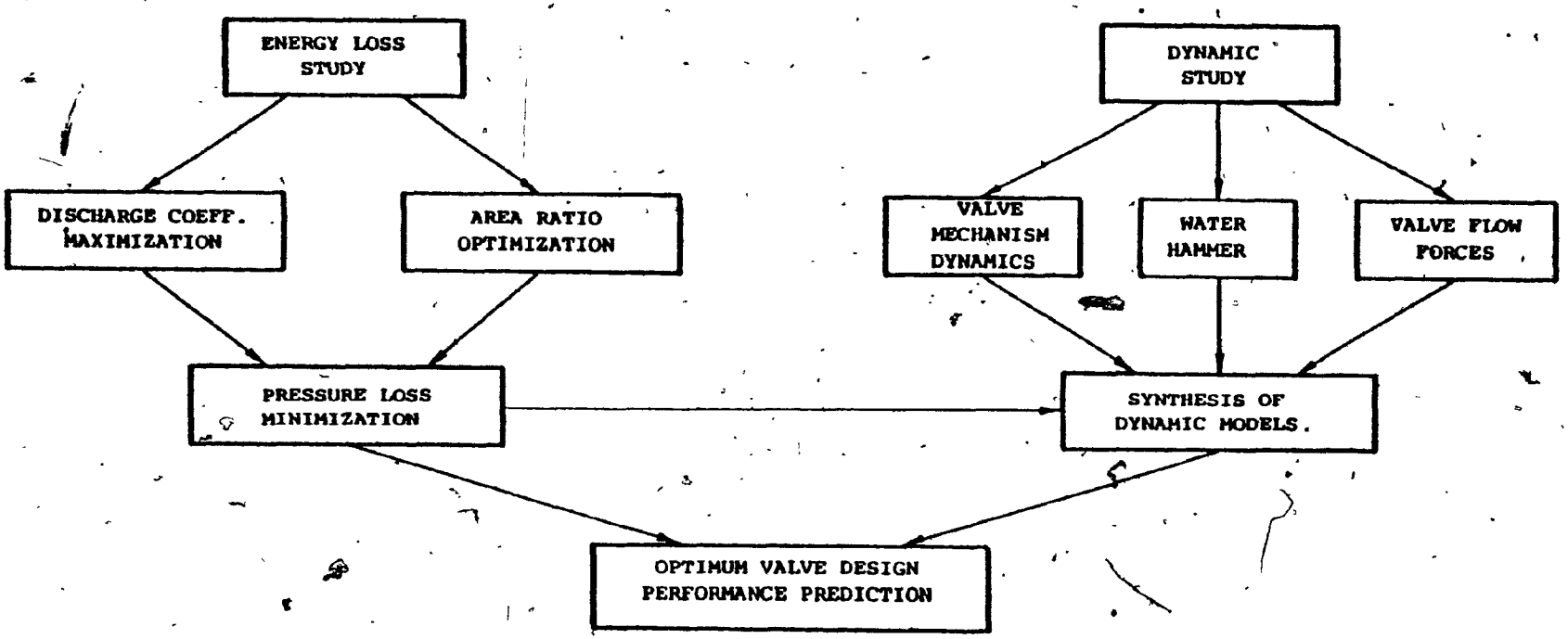

Figure 1-2. Check Valve Design Topic Areas and their Interactions

studied. The study is aimed at improving the pressure drop characteristic of the valve. Two types of wafer valves are manufactured by Ritepro. The first type is used in fire prevention systems and requires a pressure drop less than 20.7 kPa when the water flow velocity is 4.57 m/s. The second type of wafer valve is used in general industrial applications and has no upper limit on the pressure drop, however, the design is improved to give the valve a better pressure loss characteristic. The results from the energy loss study in Chapter 2 are applied to redesign the Ritepro wafer valves. Further pressure drop improvements are achieved by changing the valve disc pivot location. On the basis of this investigation a totally new generation of Ritepro wafer check valves was designed. The redesigned fire prevention valve prototypes meet the required pressure drop values.

Chapter 4 reviews the work by Svoboda and Lee [8], Lee [9], and Lee, Svoboda and Kwok [10] in conjunction with this project. The work considers the modelling of a hydro-pneumatic mechanism that has been incorporated together with a wafer check valve. The hydro-pneumatic system acts as a combination spring and damper for quick valve closure and non-slam action. System dynamics relate the angular position of the disc opening to an input torque.

Chapter 5 presents the study of flow forces acting on the valve disc. The flow forces are determined by experiment and describe the valve flow characteristics in terms of a flow coefficient and drag coefficient. The flow coefficient relates the fluid flow to the pressure drop across the valve. The drag coefficient relates the force normal to the disc surface to the flow rate through the valve. Both coefficients are determined for various openings of disc angle and pipe flow Reynolds numbers. Forward and reverse flow conditions are considered.

In Chapter 6, a generalized model for a pipeline using the method of lumped-parameters is presented. The model is used to study waterhammer effects in a fluid system incorporating the check valve. The fluid system is modelled as a circuit composed of lumped capacitances, inductances, and resistances. Volumes, fluid compressibility, and pipe material elasticity form the capacitance. The fluid inductance is due to the change of fluid flow velocity in the pipeline. Pressure drop across the valve, as well as the pressure drop due to the pipe roughness are represented by the resistance.

A case study, using computer simulation, evaluates the dynamic performance of a check valve. The check valve includes the hydro-pneumatic spring-damper mechanism [8] [9][10]. Similar to the method of calculating pipe flow

waterhammer transients by lumping the fluid and pipe parameters, the check valve is considered as a lumped variable resistor. The valve resistance and the disc shaft torque required to open the valve is a function of the disc swing angle. The flow forces characterized by the flow coefficient and the drag coefficient relate the pipeline waterhammer calculations to the valve dynamics.

To summarize, the energy loss and dynamic behaviour of the current wafer type swing-disc check valve design is studied so that its advantages can be retained. At the same time, the limitations of the present valve are established and guidelines to improve the performance are developed. In conclusion, the study results will help valve manufacturers and users to design and select the required swing-disc check valve performance based upon their application requirements.

The results of this thesis have been summarized and reported to the Natural Sciences and Engineering Research Council of Canada (NSERC) and to Ritepro Inc. by Svoboda, Hong and Katz [11].

CHAPTER 2

THE CONCEPT OF PRESSURE LOSS MINIMIZATION

2.1 Introduction

Ideally, there should be no pressure drop across a check valve. In practice, however, a pressure drop occurs across the valve. This pressure drop depends on the valve design parameters. In tilting-disc and conventional swing-disc check valves, the valve seat forms an orifice approximately equal to the pipe diameter. Also, the conventional valve provides a cavity to partially remove the disc from the flow stream. The pressure drop for these types of valves is primarily due to the disc alone [5][6][7]. Wafer swing-disc check valves do not have a cavity to partially remove the disc from the flow. When the valve is fully opened the disc still restricts the pipe flow area. Also, the valve seat forms an orifice which is always smaller than the internal pipe diameter. The pressure drop across the wafer swing-disc check valve is due to the combined effect of the disc obstruction in the flow as well as to the orifice restriction of the flow.

In this chapter, the wafer valve is modelled as two flow restrictions in series. One restriction is due to the orifice followed by the second restriction due to the disc. Analytical equations are derived to relate the total

pressure drop across the valve to the parameters of each of the restrictions. These equations are used as the basis for developing the concept of the pressure loss minimization. Experiments performed on each of the restrictions separately and on conbinations of both the restrictions together verifies the analysis.

This work has been published by Svoboda, Katz and Fitch [12] in conjunction with this project.

2.2 Wafer Swing-Disc Check Valve Analysis

2.2.1 Valve Description

A schematic drawing of the wafer swing-disc check valve is shown in Figure 2-1 sandwiched between two flanges. In the closed position, a disc seats over an orifice smaller than the internal pipe diameter. Diameters d_1, d_2 and d_3 are the pipe, orifice and disc diameters, respectively. With reference to the figure, as the force due to the pressure upstream of the valve exceeds the combined forces due to the pressure downstream of the valve and spring required to keep the valve closed, the disc will start to swing open about its pivot pin. As flow forces increase the disc opens further until the nut securing the disc to its hinge arm, or until the web on the backside of the hinge arm comes to rest against the upstream pipe wall. The nut or

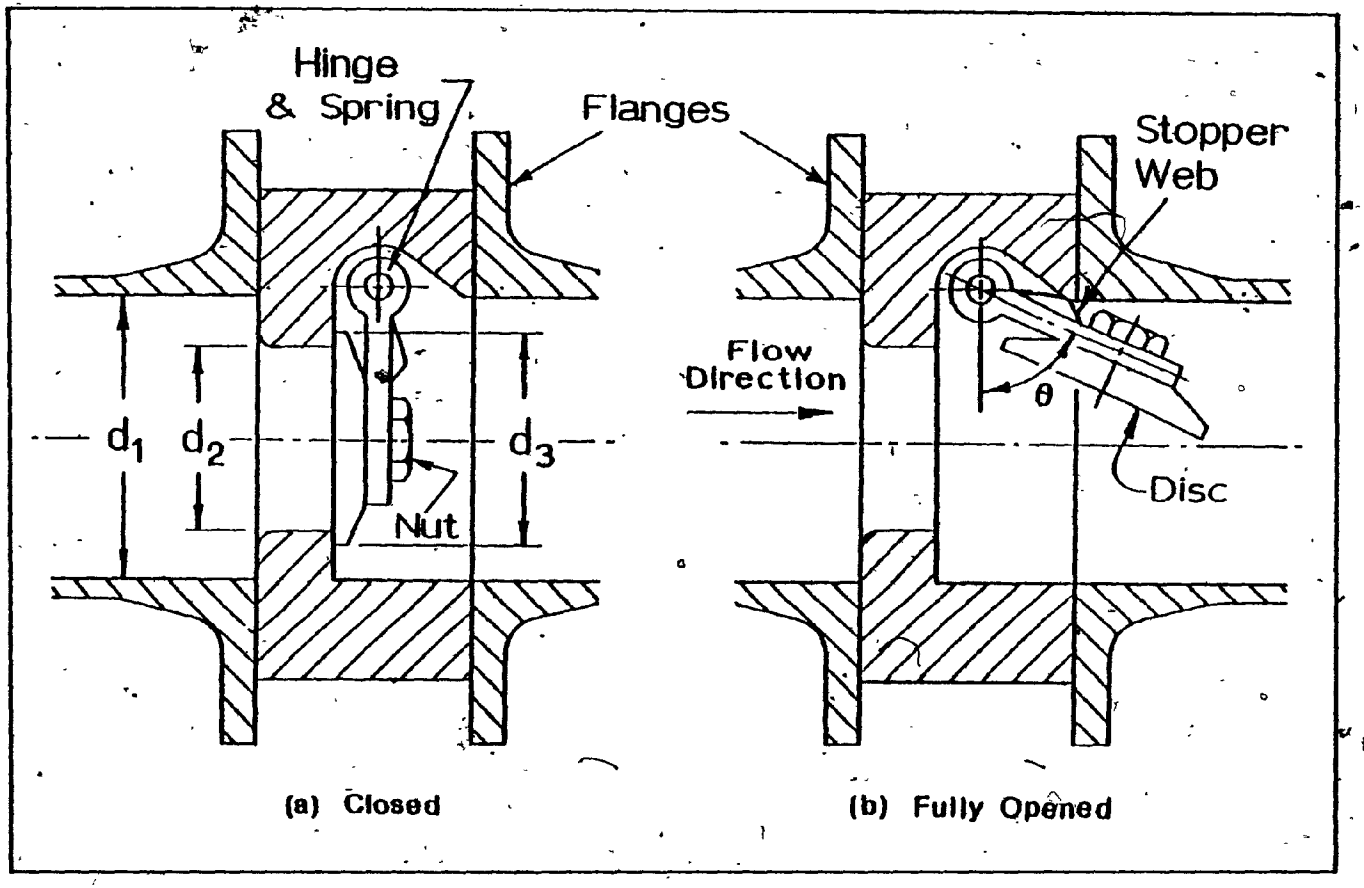

Figure 2-1. Schematic Drawing of Wafer-Type Swing-Disc Check Valve

the web is used to prevent the disc from wedging into the connecting pipe.

Check valves are usually spring loaded to keep the valve closed. When the disc is partially open, an additional pressure loss is created due to the spring force. Once the disc is completely opened, the spring force has no further effect on the pressure drop. The analysis deals with the valve always at its fully opened position, and the pressure drop due to the spring force will not be considered. Furthermore, the projection of the nut or the web on the back of the disc will be ignored in the analysis, and the disc will be assumed to touch the downstream pipe walls. When the disc is fully opened at angle θ, the disc extends beyond the valve in the adjacent connecting pipe. In this position, the disc is restrained by the pipe and remains in the pipe flow area.

2.2.2 Normalized Flow Coefficients

As shown in Figure 2-2, the wafer swing-disc check valve is modelled as two restrictions in series. The upstream restriction is due to the orifice and the downstream restriction is due to the wide open disc. Each restriction is composed of an entrance contraction followed by an exit expansion. The velocities along each indicated section, 1 to 5, are assumed uniform. Sections 1, 3 and 5

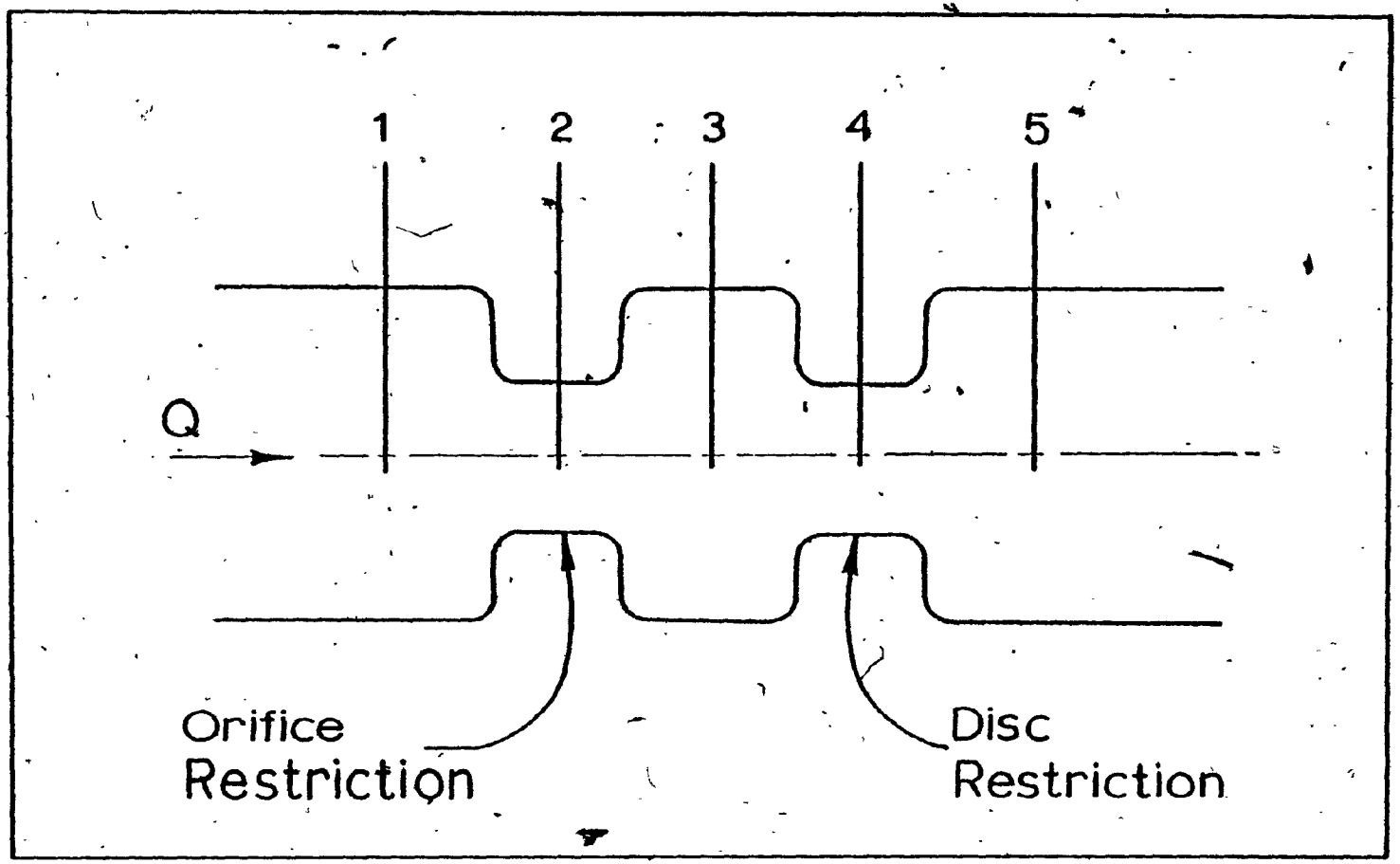

Figure 2-2. Flow Model for Wafer-Type Swing-Disc Check Valve

are of equal area and hence their velocities are the same. By applying the energy equation between each adjacent section, we get:

$$P_1 + \frac{\rho v_1^2}{2} = P_2 + \frac{\rho v_2^2}{2} + K_{L1} \cdot \frac{\rho v_2^2}{2} \tag{2.1a}$$

$$P_2 + \frac{\rho v_2^2}{2} = P_3 + \frac{\rho v_3^2}{2} + K_{L2} \cdot \frac{\rho v_2^2}{2} \tag{2.1b}$$

$$P_3 + \frac{\rho v_3^2}{2} = P_4 + \frac{\rho v_4^2}{2} + K_{L3} \cdot \frac{\rho v_4^2}{2} \tag{2.1c}$$

$$P_4 + \frac{\rho v_4^2}{2} = P_5 + \frac{\rho v_5^2}{2} + K_{L4} \cdot \frac{\rho v_4^2}{2} \tag{2.1d}$$

where P is the static pressure, v is the velocity, ρ is the fluid density, and the subscript numbers refer to the respective sections. K_{L1} and K_{L2} are the respective contraction and expansion loss coefficients of the orifice. Similarly, K_{L3} and K_{L4} are respectively the contraction and expanssion loss coefficients of the wide open disc.

The static pressure drop across the orifice alone is obtained by combining Equations 2.1a and 2.1b with $v_1 = v_3$ to give:

$$P_1 - P_3 = (K_{L1} + K_{L2}) \frac{\rho v_2^2}{2} \qquad (2.2)$$

This equation is expressed in terms of the flow coefficient C_{v1} as:

$$Q = C_{v1} \sqrt{P_1 - P_3} \qquad (2.3a)$$

$$C_{v1} = \frac{A_2 \sqrt{2/\rho}}{\sqrt{K_{L1} + K_{L2}}} \qquad (2.3b)$$

where Q is the flow rate and A_2 is the orifice area.

Normalizing the flow coefficient with respects to pipe area A_1 and fluid density $\sqrt{2/\rho}$ gives the normalized flow coefficient for the orifice as:

$$C^*_{v1} = \frac{C_{v1}}{A_1 \sqrt{2/\rho}} = \frac{A_2/A_1}{\sqrt{K_{L1} + K_{L2}}} \qquad (2.4)$$

In a similar manner, substituting $v_3 = v_5$, and rearranging Equations 2.1c and 2.1d gives the normalized flow coefficient for the disc as:

$$C^*_{v2} = \frac{C_{v2}}{A_1 \sqrt{2/\rho}} = \frac{A_4/A_1}{\sqrt{K_{L3} + K_{L4}}} \qquad (2.5)$$

where C_{v2} is the non-normalized flow coefficient for the disc and A_4 is the flow area provided by the disc at the fully open position.

The flow coefficients for the orifice and the disc are assumed as independent. The overall normalized flow coefficient for the check valve is the series combination of C^*_{v1} and C^*_{v2} and is given by:

$$C^*_{v3} = \frac{C_{v3}}{A_1\sqrt{2/\rho}} = \frac{C^*_{v1} \cdot C^*_{v2}}{\sqrt{C^{*2}_{v1} + C^{*2}_{v2}}} \qquad (2.6)$$

where C_{v3} is the non-normalized overall flow coefficient.

To evaluate the valve flow coefficients, entrance contraction and exit expansion loss coefficients must first be determined for the orifice and for the fully opened disc position.

2.2.3 Evaluation of the Loss Coefficients

As mentioned earlier, the valve pressure loss can be reduced by altering the valve geometry, such that:

1. the discharge coefficients of valve passages will be maximized,

2. the valve passage areas will be maximized.

By referring to Equations 2.4 and 2.5, the discharge coefficients are increased by decreasing both entrance and exit loss coefficients, for the orifice and for the disc. To increase these coefficients there should be no sudden changes in passage areas through the valve. Ideally, using a venturi shape entrance region and a diffuser shape exit region for the restrictors, would reduce the discharge coefficient of the valve. In practice, there is no control over the shape of the exit region of the orifice and the disc, and over the entrance region to the disc. However, rounding the entrance to the orifice would increase the flow coefficient slightly and would be easily implemented. Major improvements are attained by increasing the flow passage area ratios. This will be shown in Section 2.2.4 and its practicality will be implemented in actual valve designs in Chapter 3. The advantage of increasing the flow passage area ratio does not impair the desired valve compactness and light-weight features.

References [13][14][15] give the loss coefficients, for a well rounded entrance and for a sudden enlargement, respectively, as:

$$K_{L1} = 0.05 \qquad (2.7a)$$

$$K_{L2} = [A_2/A_1 - 1]^2 \qquad (2.7b)$$

Substituting Equation 2.7b in Equation 2.4 gives the normalized flow coefficient for the orifice as:

$$C^*_{v1} = \frac{(d_2/d_1)^2}{\sqrt{K_{L1} + ([d_2/d_1]^2 - 1)^2}} \qquad (2.8)$$

The loss coefficients K_{L3} and K_{L4} for the disc, and the flow area A_4 provided by the disc, are not known. The disc flow area is assumed to be related to the projected area of the tilted disc normal to the pipe flow. The extent of disc tilt is approximated by the opening of the disc until its diameter d_3 becomes a chord of the pipe diameter circle d_1. Minor variations in the area due to the hinge arm is neglected. Following the above assumptions, the flow area A_4 provided by the opened disc is given in Appendix [A] by:

$$\frac{A_4}{A_1} = 1 - \frac{A_3}{A_1}\left(1 - \sqrt{1 - A_3/A_1}\right) \qquad (2.9)$$

where A_3 is the area of the disc.

The disc restriction is assumed equivalent to an

orifice with entrance and exit loss coefficients given by:

$$K_{L3} = 0.1 \tag{2.10a}$$

$$K_{L4} = [A_4/A_1 - 1]^2 \tag{2.10b}$$

These values are chosen with the assumption that the equivalent orifice has a slightly rounded entrance and a sudden enlargement at the exit.

Substituting K_{L4} and Equation 2.9 in Equation 2.5 gives the disc normalized flow coefficient as:

$$C_{v2}^* = \frac{Z}{\sqrt{K_{L3} + (Z - 1)^2}} \tag{2.11a}$$

where

$$Z = \frac{A_4}{A_1} = 1 - \left(\frac{d_3}{d_1}\right)^2 \cdot \left[1 - \sqrt{1 - \left(\frac{d_3}{d_1}\right)^2}\right] \tag{2.11b}$$

The effect of varying the diameter of the pipe, orifice, and the disc on the flow coefficients will be discussed in the following sections.

2.2.4 Valve Overlap and Passage Area Ratio

In order to achieve a proper valve seal, a certain amount of overlap has to be provided between the disc and its seat orifice. With reference to Figure 2-1, the overlap is defined as:

$$\gamma = \frac{d_3 - d_2}{d_1} \qquad (2.12)$$

The pressure drop across the valve is affected by the overlap. Smaller valve overlap ratios result in smaller pressure losses.

Figure 2-3 shows a plot of the flow coefficients C^*_{v1}, C^*_{v2} and C^*_{v3} versus the orifice to pipe diameter ratio for an overlap of 10.6%. With reference to the figure, the orifice flow coefficient C^*_{v1} increases with the increase in diameter ratio. This increase in flow coefficient is due to the increase of the orifice flow area and the decrease of the exit expansion losses. The disc flow coefficient C^*_{v2} is shown to decrease with the increase of the diameter ratio. This decrease in flow coefficient is due to the decrease in the flow area around the disc and to the increase of the exit expansion losses. The overall flow coefficient C^*_{v3} is shown, in the figure, to increase with the increase in diameter ratio up to approximately 0.75 with the coefficient approximately equal to 0.871. This maximum value of the

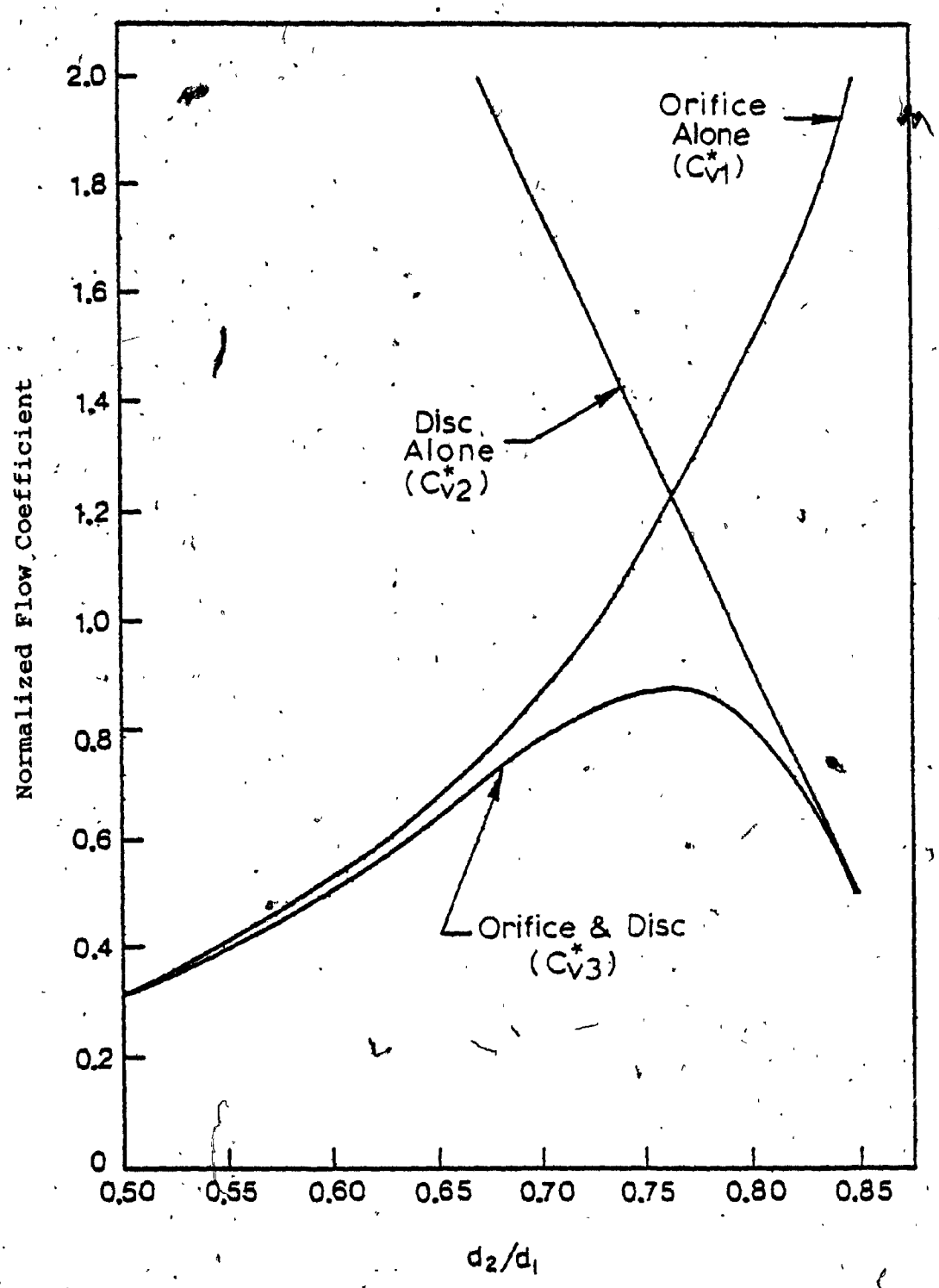

Figure 2-3. Theoretical Flow Coefficients vs Diameter Ratio
($\gamma = [d_3 - d_2]/d_1 = 0.106$)

overall flow coefficient occurs in the region where the individual flow coefficients C_{v1}^* and C_{v2}^* are approximately equal. For small values of diameter ratio, the contribution of C_{v2}^* to the overall coefficient is minimal, and the orifice losses become dominant. The disc restriction losses become dominant for larger values of diameter ratio.

Figure 2-4 show plots of the overall flow coefficient versus diameter ratio for different valve overlaps. The plot shows that as the overlap decreases the maximum value of the flow coefficient increases and occurs at larger values of orifice to pipe diameter ratio. For the limiting case when there is no overlap, the maximum flow coefficient is 1.19 and occurs at a diameter ratio of 0.82.

2.3 Test Results to Verify Valve Analysis

The test arrangement and procedure to verify the valve analysis are presented in Appendix B. The experimental results for the orifice alone are plotted in Figure 2-5 with the corresponding theory derived from Equation 2.8. The data is also given in Table 2-1. Maximum discrepancy occurs at the large diameter ratio d_2/d_1, of 0.85. The maximum difference in flow coefficient C_{v1}^* is about 10 percent. Errors may be attributed to the measurement procedure since pressure differences at larger diameter ratios are small. The overall close agreement

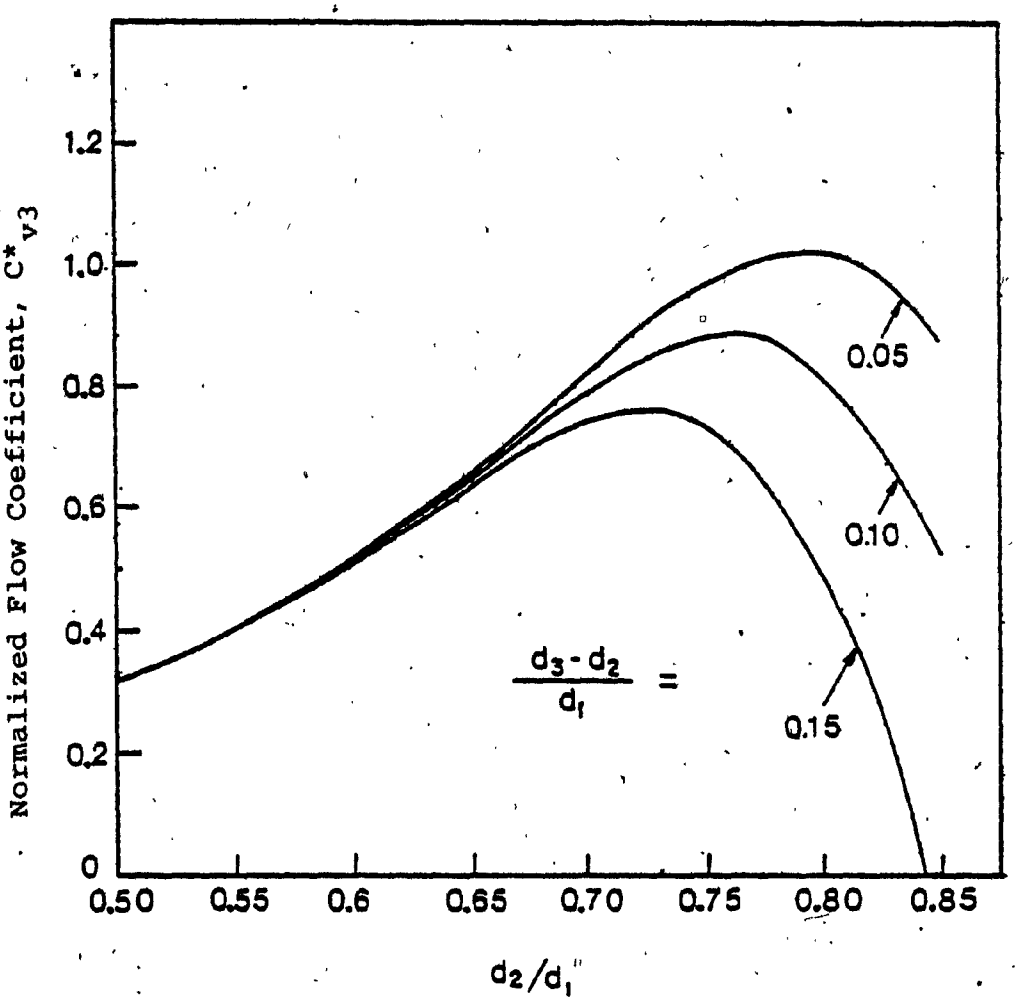

Figure 2-4. Effect of Overlap on Theoretical Flow Coefficient

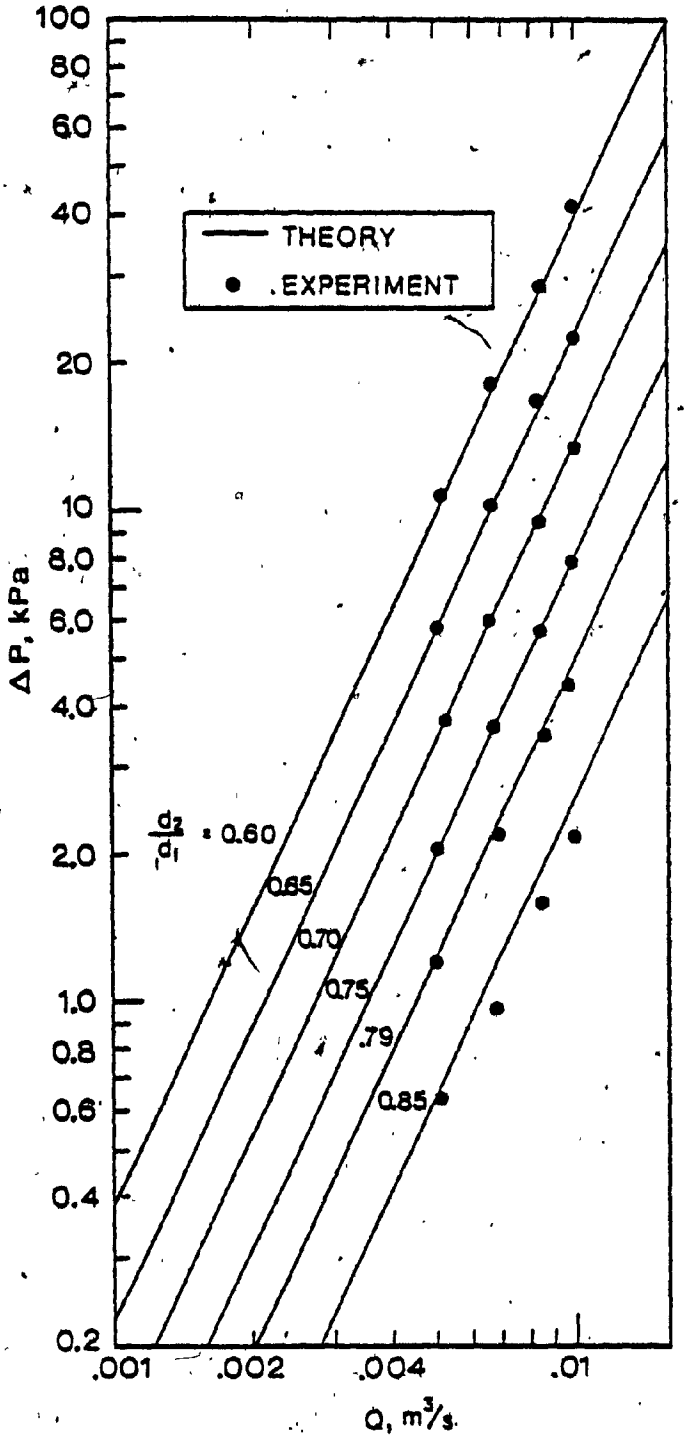

Figure 2-5. Comparison of Experiment and Theory for Orifice Alone

$\frac{d_2}{d_1}$	Flow $Q(m^3/s)$	Pressure Drop ΔP (kPa)	Experimental C^*_{v1}	Theoretical C^*_{v1}
0.60	.0052	10.82	.516	.531
	.0068	18.48	.517	
	.0087	28.89	.529	
	.0102	42.46	.511	
0.65	.0051	6.85	.637	.682
	.0069	10.54	.694	
	.0086	16.98	.682	
	.0102	24.28	.676	
0.70	.0053	3.87	.880	.880
	.0066	6.08	.871	
	.0085	9.87	.884	
	.0099	13.33	.886	
0.75	.0051	2.09	1.152	1.145
	.0068	3.71	1.153	
	.0086	5.77	1.170	
	.0099	7.91	1.150	
0.79	.0051	1.22	1.508	1.427
	.0069	2.25	1.502	
	.0087	3.57	1.504	
	.0098	4.51	1.508	
0.85	.0052	0.64	2.123	2.027
	.0069	0.99	2.265	
	.0086	1.60	2.221	
	.0099	2.18	2.190	

TABLE 2-1. Data for Orifice Alone

indicates that the loss coefficients associated with the orifice have been selected correctly.

Results from experiments and calculations from Equation 2.11 for the disc alone, are plotted in Figure 2-6. The data are also given in Table 2-2. Results are shown in terms of d_2/d_1 rather than d_3/d_1, recalling the governing overlap Equation 2.12. Since the overlap is constant there is a fixed relation between these ratios. Use of d_2/d_1 ratio permits the direct matching of the appropriate sizes when the orifice and the disc are used together. Results are in good agreement when the diameter ratio is large at 0.85, corresponding to a small flow passage. Results for the two smallest discs are close to each other and may be attributed to the large flow passage area that is not changing appreciably. The maximum discrepancy in flow coefficient C^*_{v2} is less than 20 percent. This may be attributed to the uncertainty in disc loss coefficients and to the approximation of the flow passage area.

The complete experimental results for the orifice and disc together are given in Table 2-3. For the assembled restrictions, the data may be presented more clearly by showing the relation between normalized flow coefficient C^*_{v3} and the diameter ratio. This is shown in Figure 2-7 for only one pipe flow at about 0.010 m^3/s. The largest discrepancy between experimental and theoretical flow

coefficient is about 8 percent and occurs when the diameter ratio is 0.79. The maximum value of the flow coefficient is about 0.870 at a diameter ratio of 0.75, close to that expected from theory. A very good overall agreement with theory can be observed.

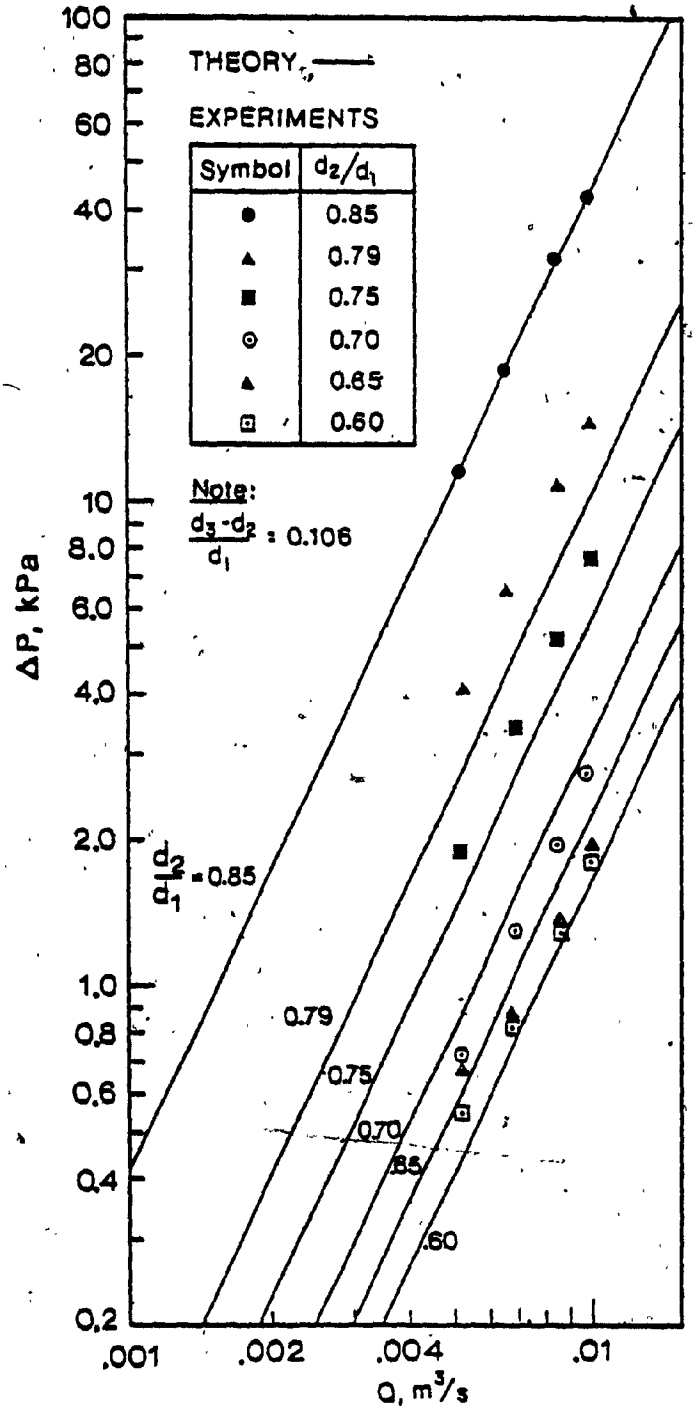

Figure 2-6. Comparison of Experiment and Theory for Disc Alone

$\frac{d_2}{d_1}$	Flow $Q(m^3/s)$	Pressure Drop ΔP (kPa)	Experimental C^*_{v2}	Theoretical C^*_{v2}
0.60	.0052	0.56	2.270	2.455
	.0068	0.84	2.424	
	.0087	1.32	2.474	
	.0100	1.83	2.415	
0.65	.0053	0.68	2.100	2.153
	.0069	0.85	2.445	
	.0086	1.36	2.409	
	.0099	1.94	2.322	
0.70	.0052	0.69	2.045	1.781
	.0070	1.30	2.006	
	.0085	1.95	1.989	
	.0098	2.71	1.945	
0.75	.0051	1.93	1.199	1.361
	.0069	3.48	1.208	
	.0085	5.33	1.203	
	.0100	7.77	1.172	
0.79	.0053	4.09	0.856	1.012
	.0068	6.66	0.861	
	.0086	10.86	0.853	
	.0100	14.85	0.848	
0.85	.0052	11.67	0.497	0.493
	.0066	18.88	0.496	
	.0085	32.21	0.489	
	.0099	43.07	0.493	

TABLE 2-2. Data for Disc Alone

$\frac{d_2}{d_1}$	Flow $Q(m^3/s)$	Pressure Drop ΔP (kPa)	Experimental C^*_{v3}	Theoretical C^*_{v3}
0.60	.0050	9.44	.532	.519
	.0067	17.73	.520	
	.0086	29.16	.520	
	.0100	40.20	.515	
0.65	.0052	6.41	.671	.650
	.0068	10.63	.681	
	.0085	16.43	.685	
	.0100	23.90	.668	
0.70	.0050	3.79	.839	.789
	.0068	6.90	.846	
	.0085	11.05	.835	
	.0100	15.41	.832	
0.75	.0051	3.60	.878	.876
	.0069	6.37	.893	
	.0083	9.49	.880	
	.0100	14.19	.867	
0.79	.0052	4.92	.766	.825
	.0067	8.23	.763	
	.0087	13.71	.768	
	.0098	17.64	.762	
0.85	.0052	13.01	.471	.479
	.0066	20.95	.471	
	.0086	35.68	.470	
	.0099	47.55	.469	

TABLE 2-3. Data for Orifice and Disc Together.

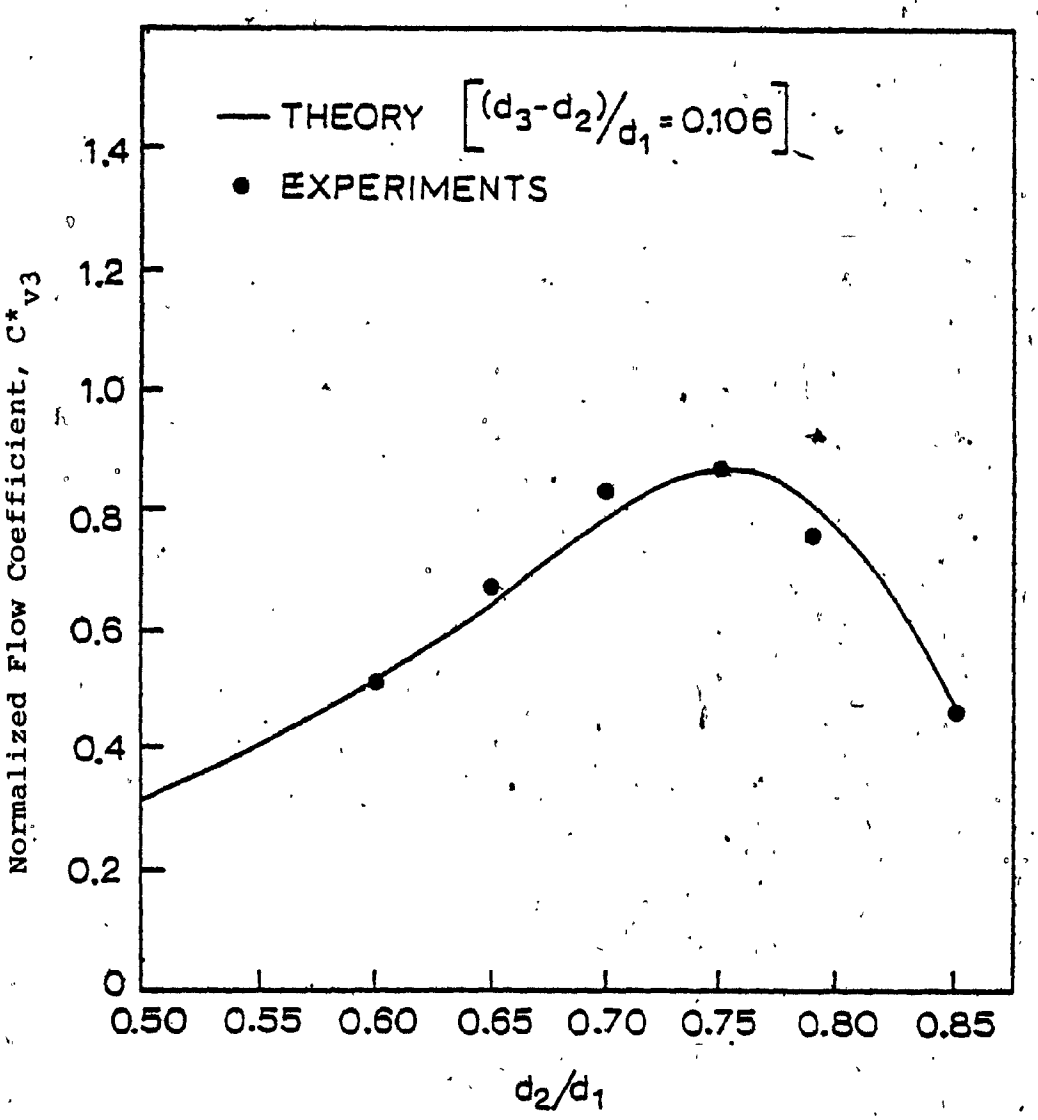

Figure 2-7. Comparison of Experiment and Theory for Orifice and Disc Assembly

CHAPTER 3

APPLICATION OF THE CONCEPT TO RITEPRO VALVES

3.1 Introduction

Two types of wafer swing-disc check valves are redesigned to improve their pressure drop characteristics. These valves are products of Ritepro Inc. (formerly Rite Manufacturing Ltd.) of Montreal. The hard seat seal check valve is for general industrial use. The soft seat seal type is used in fire protection service. Requirements for the latter valve type is a pressure drop less than 20.7 kPa when the pipe water velocity is 4.57 m/s. The first type of valve has no upper limit on the pressure drop, but is minimized for an improved loss characteristic. For both types of valves, diameter size range from 50-mm to 300-mm is considered.

Procedures to determine soft and hard seal valve dimensions using analytical equations predicting the pressure loss across the valves are presented. The concept developed from Chapter 2 determines the geometry of orifice and disc that minimizes the losses. Also, optimization of internal valve geometries, of disc pivot location and disc shape, further reduces the losses. Disc clearances are also considered in the final valve design.

Final soft and hard seal valve dimensions are tabulated with corresponding expected flow coefficients and pressure drops. Experiments are verified on 50-mm, 80-mm and 100-mm valve models. In addition, test results on soft seal valve prototypes from 50-mm to 300-mm are presented. All test results are below the 20.7 kPa pressure loss limit, except for the 50-mm soft seal valve. Also, for further design considerations, experiment shows that the hard seal valve pressure loss may be reduced beyond those of the soft seal valve.

3.2 Valve Sealing Arrangement and Design Objective

Ritepro Inc. manufactures wafer swing-disc check valves that consist of two types of valve sealing. First, the hard seat seal type, is shown in Figure 3-1a, with all important dimensions indicated. The valve dimensions will be fully explained appropriately. The sealing arrangement consists of the metal disc and the metal seat ring. As back-pressure is applied to the disc, metal-to-metal contact with the face of the metal seat ring is achieved for sealing. This type of valve is used in general industrial applications. The second type of valve, the soft seat seal valve, is shown in Figure 3-1b. All important valve dimensions are indicated in the figure. The sealing arrangement consists of the metal disc and an O-ring within a metal groove. As back-pressure is applied to the disc,

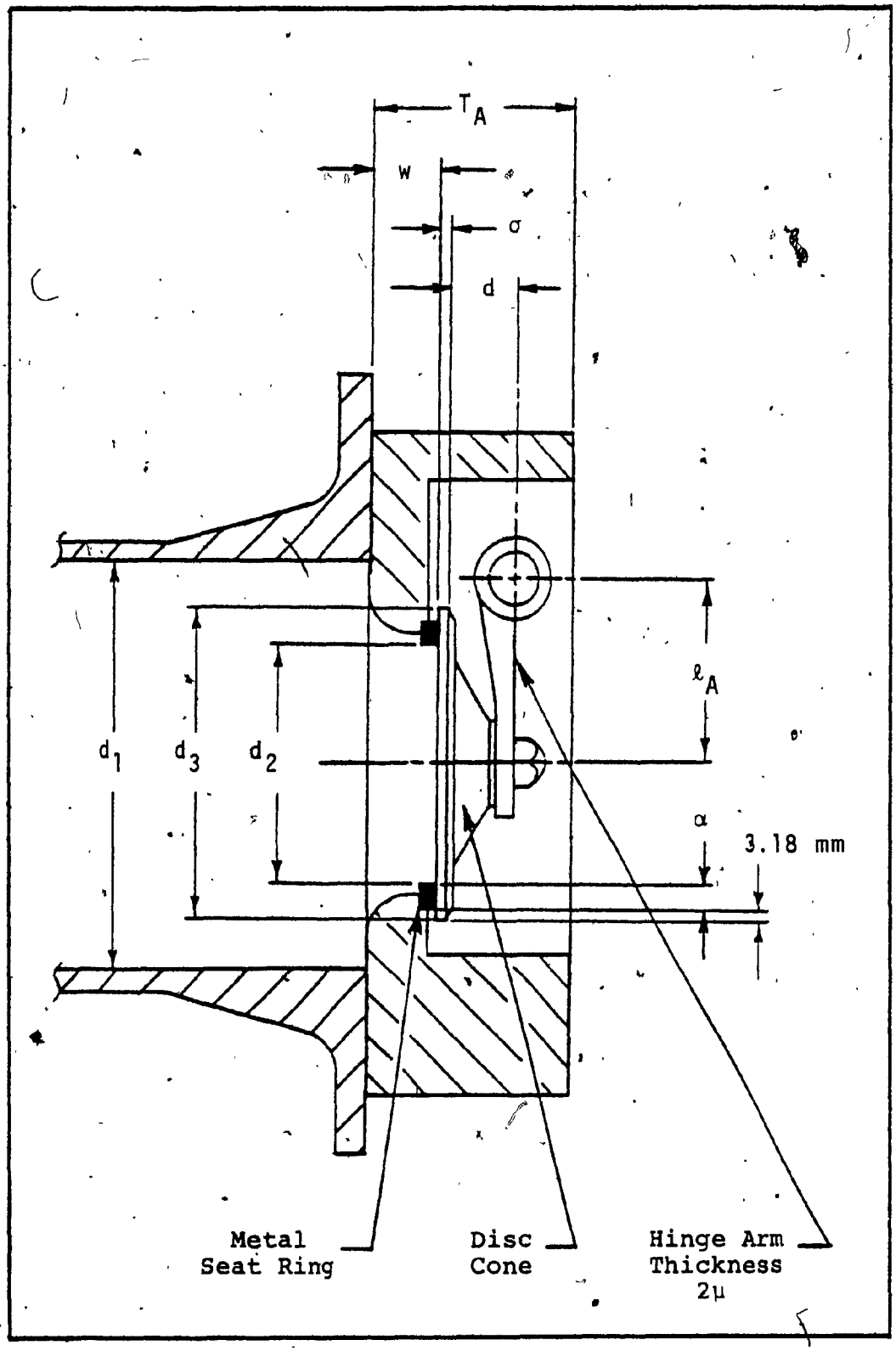

Figure 3-1a. Basic Design of Ritepro Wafer Valve (hard seat seal type)

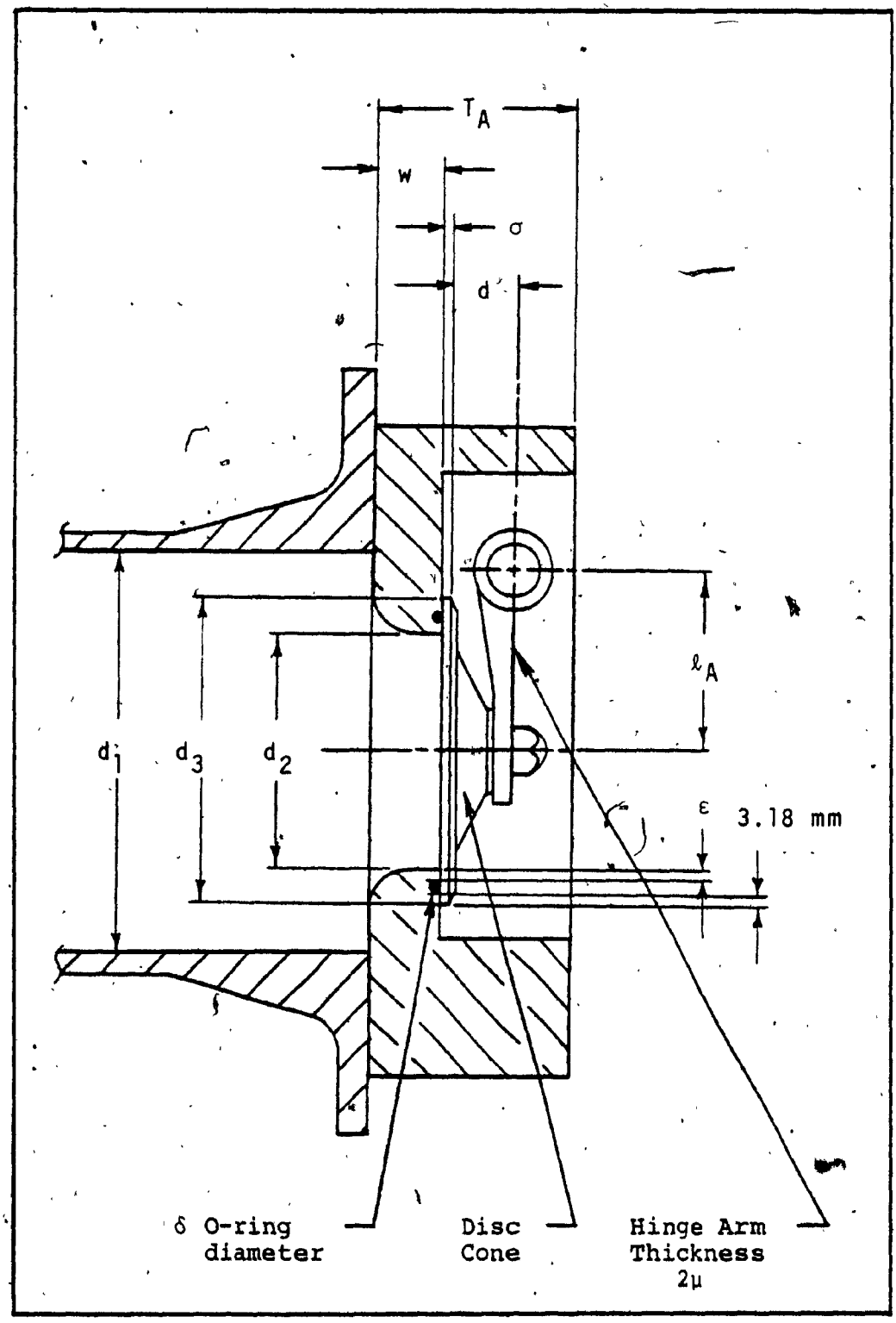

Figure 3-1b. Basic Design of Ritepro Wafer Valve (soft seat seal type)

the O-ring seal is compressed into the groove allowing the disc to make metal-to-metal contact which provides additional sealing. This type of valve is used in fire prevention systems.

The design objective is to minimize the pressure drop across the soft seal valve to a value less than 20.7 kPa when the pipe water flow velocity is 4.57 m/s in Schedule 40 pipe. This is one of the requirements outlined by the U.S. Underwriters' Laboratories [16] for check valves used in fire protection service. Ritepro desires that their soft seal valve type be approved for fire prevention applications in the United States.

The hard seal valve type used in general industrial applications has no upper limit on its pressure drop requirement. The pressure drop across this type of valve is minimized for the same 20.7 kPa objective to give the valve an improved loss characteristic as compared with its existing design.

Design constraint stipulated by Ritepro is that the exterior length of the valve body remains the same as in the existing design. That is, referring to Figure 3-1, valve body length T_A remains the same. This design constraint provides easy replacement with newly designed valves into existing piping arrangements already using Ritepro valves.

If the valve body length was increased, the disc would be allowed to open further. As described in Section 2.2.4, this effect would increase the flow passage area provided by the disc and the result would be a lower overall pressure drop for the valve. But, increasing of the valve body length defeats the desired compact and light-weight features. Valve body lengths are the same for both hard and soft seal check valves. These dimensions are tabulated in Table 3-1 and Table 3-2, respectively, for valve sizes from 50-mm to 300-mm.

Another constraint stipulated by Ritepro and by the American Petroleum Institude (API) [17] standards is the wall thickness of the orifice. Referring to Figure 3-1, the orifice thickness is represented by dimension w. This API thickness standard provides strength for the valve seat. For the soft seal valve, orifice thickness dimensions for different valve sizes are provided in Table 3-2. For the hard seal valve, referring to Figure 3-1a, orifice thickness w is considered to be the thickness of the orifice plus an additional thickness provided by the seat ring. This additional thickness is specified by the U.S. Underwriters' Laboratories [16] and states that the face of a metal seat ring must be raised at least 3.2-mm above adjacent portions of the valve body. Orifice thickness dimensions for the hard seal valves are given in Table 3-1 for different valve sizes.

The last design constraint is the amount of disc material that must overlap around the orifice when the valve is closed. This constraint is specified by Ritepro and by the U.S. Underwriters' Laboratories [16]. For the soft seal valve, referring to Figure 3-1b, the amount of disc material that must overlap around the orifice is given by:

$$d_3 - d_2 = 2(\varepsilon + \delta + 3.2) \qquad (3.1)$$

where d_2 and d_3 are respectively the orifice and disc diameters, ε is a dimension of the disc seating surface, and δ is the O-ring cross section diameter. All dimensions are in millimeters. Table 3-2 lists the dimensions for ε and δ for valve sizes from 50-mm to 300-mm. For the hard seal valve, referring to Figure 3-1a, the amount of disc material that must cover the orifice is given by:

$$d_3 - d_2 = 2(\alpha + 3.2) \qquad (3.2)$$

where α is the width of the seat ring face in millimeters. Table 3-1 lists the dimensions for α for the different valve sizes. These variable dimensions are chosen with cooperation from Ritepro.

From the sealing arrangement described and from the definition of valve overlap γ described in Section 2.2.4, the valve overlap for the soft and hard seal valve is:

$$\gamma = \frac{d_3 - d_2}{d_1} \qquad (3.3)$$

where d_1 is the pipe diameter. Tables 3-1 and 3-2 list valve overlaps, respectively, for the hard and soft seal valve types for the different valve sizes.

The hinge arm thickness and disc face thickness were considered in the valve design but their dimensions were not changed from existing values. From Figure 3-1, it can be seen that these dimensions are respectively 2μ and σ. The hinge arm thickness is required for arm strength due to bending at full valve opening. The disc face thickness is required for disc strength to prevent the disc from bending when seated. Both these strengths remain the work for Ritepro to evaluate and thus their dimensions remain the same. Only their influence on the valve pressure drop is considered. Dimensions for half the arm thickness μ and disc face thickness σ are both tabulated in Tables 3-1 and 3-2, respectively for the hard and soft seal valve types. Both valve types have the same arm thickness and disc face thickness.

3.3 Preliminary Concepts

3.3.1 Disc Full Opening Angle

The valve disc full opening angle θ_F is determined from the valve opening geometry represented in Figure 3-2. The axial view, Figure 3-2a, shows the flow passage of the pipe as a circle with diameter d_1 and the valve full opening within the passage as an ellipse with major diameter 2a and minor diameter 2b. The XY coordinate system is shown with respect to the pipe centre. Disc centre rise with respect to the pipe centre is c. The full valve opening of the disc will touch the pipe walls at two points, (p_1) and (p_2). Figure 3-2b illustrates the transverse view of full opening geometry. ℓ_A is the disc arm length and d is the disc depth.

The pipe and disc geometry is expressed respectively as:

$$x^2 + y^2 = (d_1/2)^2 \qquad (3.4a)$$

$$\frac{x^2}{a^2} + \frac{(y - c)^2}{b^2} = 1 \qquad (3.4b)$$

with major diameter:

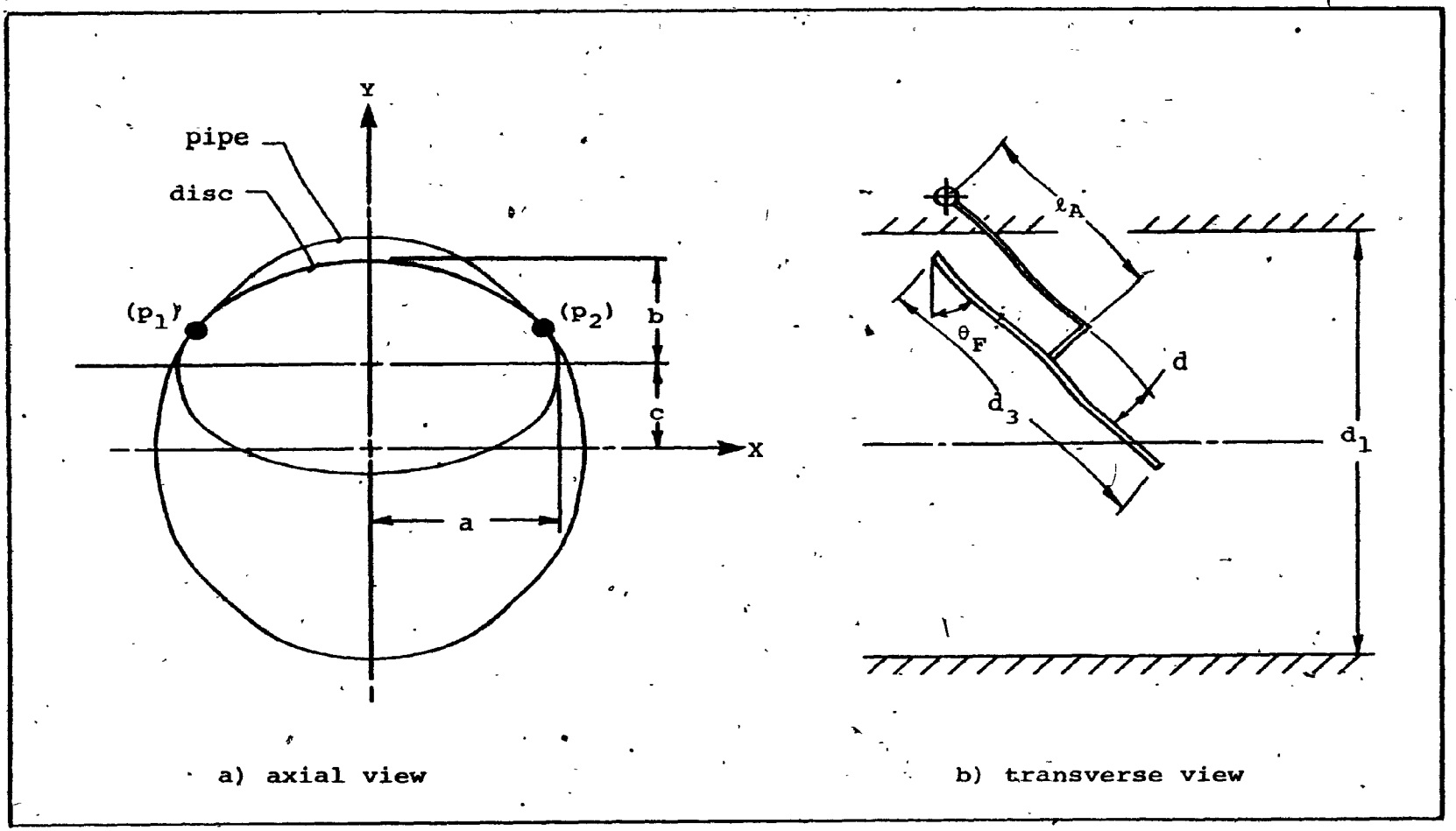

Figure 3-2. Disc Full Opening Geometry

$$2a = d_3 \tag{3.5a}$$

minor diameter:

$$2b = d_3 \cdot \cos\theta_F \tag{3.5b}$$

and rise:

$$c = \ell_A \cdot (1 - \cos\theta_F) - d \cdot \sin\theta_F \tag{3.5c}$$

For the disc to open fully, the disc will touch the pipe walls at two points, (p_1) and (p_2). Mathematically, this means the slopes of the pipe and disc must be equal at the points of intersection. The slopes derived from Equation 3.4 are:

$$\left(\frac{dx}{dy}\right)_{pipe} = -\frac{x}{y} \tag{3.6a}$$

$$\left(\frac{dx}{dy}\right)_{disc} = -\frac{b^2}{a^2} \cdot \frac{x}{y-c} \tag{3.6b}$$

Equating the slopes and solving for the two points of intersection gives:

$$y = \frac{\ell_A}{1 + \cos\theta_F} - \frac{d}{\sin\theta_F} \tag{3.7}$$

Substituting Equations 3.4a, 3.6, and 3.7 into the disc Equation 3.4b and solving for the disc full opening angle yields:

$$\theta_F = 2 \cdot \tan^{-1} \left[\frac{d + \frac{1}{2} \cdot (d_1^2 - d_3^2)^{\frac{1}{2}}}{\ell_A} \right] \qquad (3.8)$$

It will be shown later in Section 3.4 that as the disc opening increases, additional improvements in the pressure drop result.

3.3.2 Modification of Disc Flow Passage Area

The flow area described by Equation 2.9 is modified by asumming that the flow area provided by the disc is related to the projection in direction of flow by the disc, disc cone and hinge arm thickness, as shown in Figure 3-3. With these assumptions, the flow area A_4 provided by the disc assembly with respects to pipe area A_1, is:

$$\frac{A_4}{A_1} = 1 - \frac{A_3}{A_1} \cos\theta - \frac{A}{A_1} \qquad (3.9)$$

where A_3 is the disc area, and A is the area of the disc cone and hinge arm thickness projected into the flow path for disc opening angle θ.

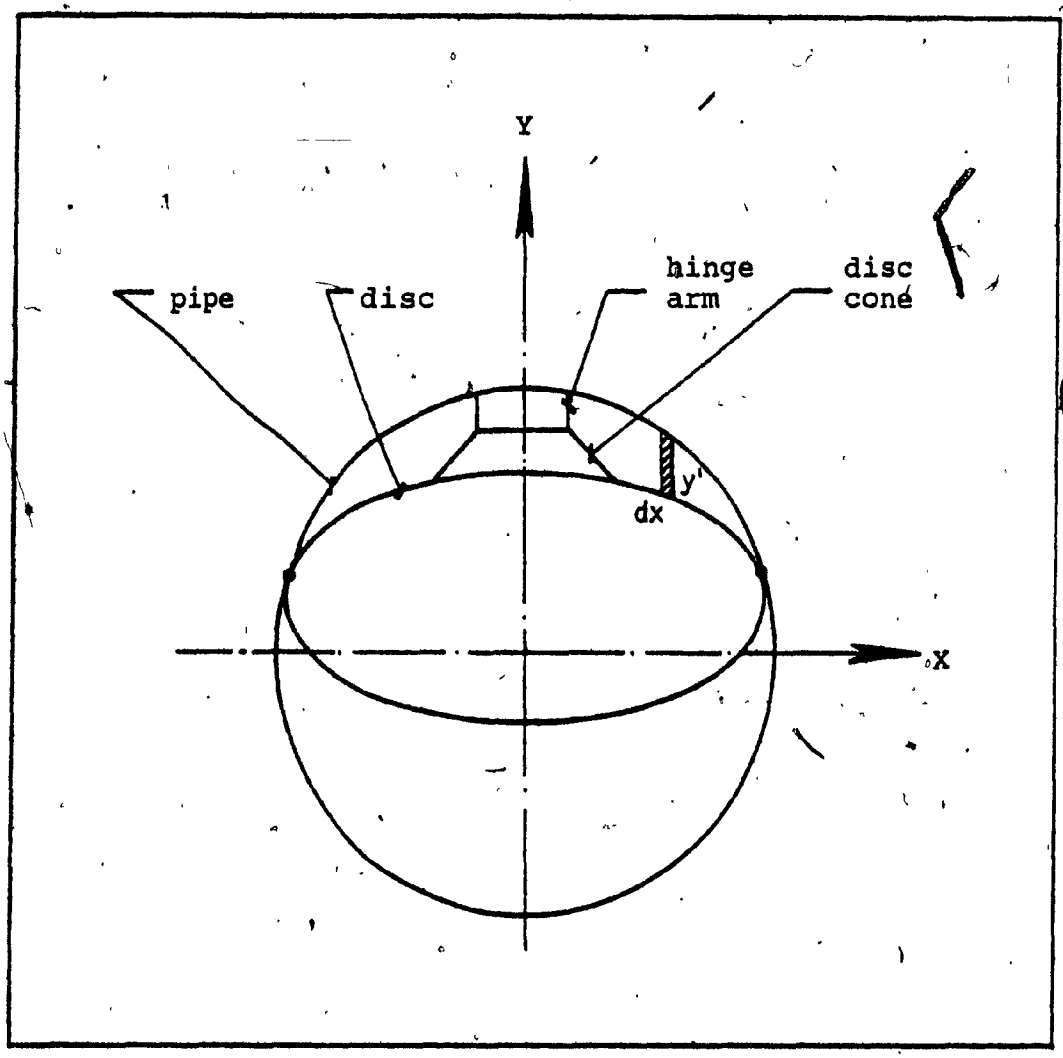

Figure 3-3. Flow Area Provided by Disc Assembly

From Figure 3-3, the projected area of the disc cone and hinge arm thickness is evaluated as:

$$A = 2 \cdot \int_0^{x'} y' \, dx \tag{3.10}$$

where x' is the limit of integration. The above integrand, y', is found from Equations 3.4 and 3.5 as:

$$y' = \left[\left(\frac{d_1}{2}\right)^2 - x^2\right]^{\frac{1}{2}} - \left[\left(\frac{d_3}{2}\right)^2 - x^2\right]^{\frac{1}{2}} \cdot \cos\theta - \ell_A \cdot (1 - \cos\theta) + d \cdot \sin\theta \tag{3.11}$$

where all variables and parameters were previously defined. Integrating Equation 3.10 with the integrand defined gives:

$$A = x \cdot \left[\left(\frac{d_1}{2}\right)^2 - x^2\right]^{\frac{1}{2}} + \left(\frac{d_1}{2}\right)^2 \cdot \sin^{-1}\left(\frac{2x}{d_1}\right) - \left(x \cdot \left[\left(\frac{d_3}{2}\right)^2 - x^2\right]^{\frac{1}{2}} + \left(\frac{d_3}{2}\right)^2 \cdot \sin^{-1}\left[\frac{2x}{d_3}\right]\right) \cdot \cos\theta - 2 \cdot \ell_A \cdot x \cdot (1 - \cos\theta) + 2 \cdot d \cdot x \cdot \sin\theta \Big|^{x=x'} \tag{3.12}$$

Limit of integration x' will be further discussed in Section 3.4. It will be shown that the pressure drop improves with a smaller integration limit.

3.3.3 Valve Flow Coefficients

The equations required to determine the valve flow coefficients for both soft and hard seat seal valves are the same as those developed from Chapter 2 with some modifications. The normalized flow coefficient associated with the orifice alone, is:

$$C_{v1}^{*} = \frac{(d_2/d_1)^2}{\sqrt{K_{L1} + ([d_2/d_1]^2 - 1)^2}} \qquad (2.8)$$

where K_{L1} is the entrance contraction loss coefficient of the orifice, and all other variables have been previously defined. Entrance loss coefficient K_{L1} for a well rounded entrance associated with the soft seal valve has been fully described in Section 2.2.3 with experimental verification. For the hard seal valve, referring to Figure 3-1a, the orifice consists of a well rounded entrance followed by a short square edged reduction of orifice diameter provided by the seat ring. Orifice diameter d_2 is considered to be the internal diameter of the seat ring. (The rounded entrance is followed by a 3.2-mm diameter reduction for removal and replacement of the seat ring.) The entrance loss K_{L1} associated with such shape of orifice is not known. It is assumed that the pipe diameter d_1 is followed by a sudden contraction provided by the orifice diameter d_2. The loss coefficient for sudden contraction as a function of

downstream to upstream diameter ratio, d_2/d_1 in this case, are known from Reference [14]. Diameter ratio d_2/d_1 for the hard seal valve sizes range from 0.75 to 0.83, as will be shown later in Section 3.4.4. Since experimental verification was not performed on the hard seal orifice and the diameter ratio range is small, it is sufficient to take an average entrance loss coefficient K_{L1} for all the valve sizes. The loss coefficient is associated with the higher of the two appropriate velocities. This conforms with the analysis presented in Section 2.2.2. Therefore, the entrance loss coefficient associated with the orifice for soft and hard seal valve types are, respectively:

$$K_{L1} = 0.05 \tag{2.7a}$$

$$K_{L1} = 0.15 \tag{3.13}$$

Equation 2.11a, and Equation 3.9 written in terms of the area's respective diameters, represents the normalized flow coefficient associated with the disc, is:

$$C^*_{v2} = \frac{Z}{\sqrt{K_{L3} + (Z - 1)^2}} \tag{2.11a}$$

where

$$Z = \frac{A_4}{A_1} = 1 - \left(\frac{d_3}{d_1}\right)^2 \cos\theta - \frac{4A}{\pi d_1^2} \qquad (3.14)$$

where all variables and parameters have been previously defined. To evaluate the disc flow coefficient for full disc opening, Equation 3.8 is used.

By assuming that the flow coefficients for the orifice and disc are unaffected when combined for the overall normalized flow coefficient of the valve, as described in Chapter 2, is:

$$C_{v3}^* = \frac{C_{v1}^* \cdot C_{v2}^*}{\sqrt{C_{v1}^{*2} + C_{v2}^{*2}}} \qquad (2.6)$$

The flow Q through the valve is related to the pressure drop ΔP across the valve by:

$$Q = C_{v3}^* \cdot A_1 \sqrt{2/\rho \cdot \Delta P} \qquad (3.15)$$

where ρ is the density of water.

3.4 Procedures to Redesign Ritepro Valves

3.4.1 Effects of Disc Pivot Location, Disc Cone Shape and Hinge Arm Thickness

The individual effects of the orifice and disc on the valve overall flow cofficient have been fully described in Chapter 2. Each effect is summarized in Figure 2-3 and shows that an optimal diameter ratio can be found resulting in the maximum overall flow coefficient and hence minimum pressure drop for the valve. As realized through the investigation, a higher overall flow coefficient can be achieved by reducing the valve overlap. The effect of valve overlap on the flow coefficient is summarized in Figure 2-4. Since valve overlaps were chosen in cooperation with Ritepro, as described in Section 3.2, reduction in overlap is at its specified limit and pressure drop improvement along this route is complete.

For a given valve overlap, the flow coefficient can be further improved by changing internal valve dimensions. Referring to Equation 2.11a and 3.14, the disc flow coefficient is increased as the disc flow passage area ratio increase. This is achieved by letting the disc angle θ open more and by reducing the disc cone and hinge arm area A.

The amount of disc cone and hinge arm area interfering in the flow passage, is expressed by Equation 3.12. For a given valve overlap, this interference area is at a minimum when the integration limit x' is minimum. The hinge arm thickness is not changed from existing Ritepro dimensions as discussed in Section 3.2. The disc cone shape can be streamlined to the flow and thus eliminated from the flow path. With these considerations, the interference area would be reduced to effects due only to the hinge arm thickness. Therefore, the integration limit x' becomes half the arm thickness.

By referring to Equation 3.8, the disc angle is permitted to open further by an increase in disc depth d and by shortening the hinge arm length ℓ_A. Changing these two dimensions is equivalent to determining the disc pivot location. From Figure 3-1, the pivot location is constrainted by the amount of valve material required to house the hinge pin.

To illustrate the design of Ritepro valves, the procedure is applied to a 100-mm soft seal valve. From Table 3-2, the valve overlap is 17.27%. The interference area from the disc cone shape has been eliminated from the flow path, giving the integration limit x' as 15.88-mm due only from the hinge arm thickness 2μ. The hinge arm length ℓ_A has been reduced to a physically feasible dimension of

54.76-mm that still provides sufficient valve material to house the hinge pin.

A plot of normalized overall flow coefficient with variations in disc depth is illustrated in Figure 3-4. This plot is for the valve touching the pipe walls. The applicable equations are from Section 3.3. With reference to the figure, the flow coefficient increases as the disc depth increases providing more disc opening. Providing more disc flow passage is equivalent to increasing the disc flow coefficient C^*_{v2} upwards. That is, referring to Figure 2-3, the curve representing the disc flow coefficient is shifted upwards while the orifice flow coefficient remains the same. This results in an increased overall valve flow coefficient and the least pressure drop occurs at larger diameter ratios, as shown in Figure 3-4. The limit to which the disc depth is increased and still provides sufficient valve material to house the hinge pin is 19.69-mm. Thus, point (B) is considered the maximum flow coefficient for the 100-mm soft seal valve with the above design dimensions.

If the disc depth is held at its maximum and the hinge arm length dimension is changed, a similar variation in flow coefficient versus diameter ratio results, as shown in Figure 3-4. The remainder of that figure will be discussed in the following section.

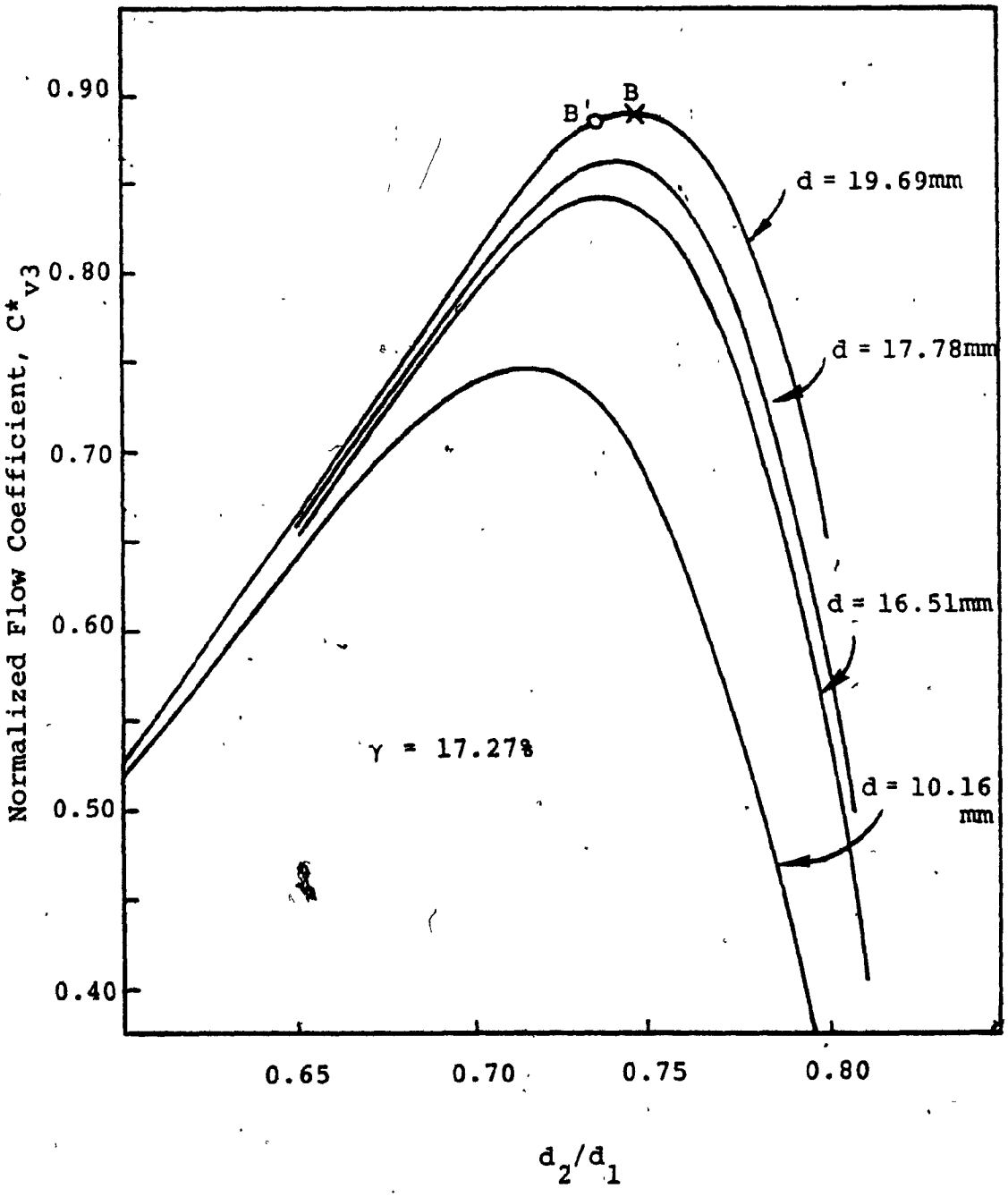

Figure 3-4. Effect of Disc Depth on Flow Coefficient

3.4.2 Pipe Bottom Clearance

Referring to Figure 3-5, the disc will swing open freely without hitting the edge of the downstream pipe if pipe bottom clearance η is provided. The disc diameter d_3 providing such a pipe bottom clearance will be derived in the following.

The following dimensions are from Figure 3-5:

$$u_1 = T_A - (w + \sigma + d) \tag{3.16a}$$

$$u_2 = \sigma + d \tag{3.16b}$$

$$u_3 = \ell_A + (d_1 - 2\eta)/2 \tag{3.16c}$$

where all dimensions have been previously defined. From geometry the unknown dimensions k_1 and k_2 are written as:

$$\frac{k_2}{u_1 + k_1} = \frac{u_2}{u_3} \tag{3.17}$$

$$k_2^2 = k_1^2 - u_2^2 \tag{3.18}$$

Combining Equations 3.17 and 3.18 and solving for the

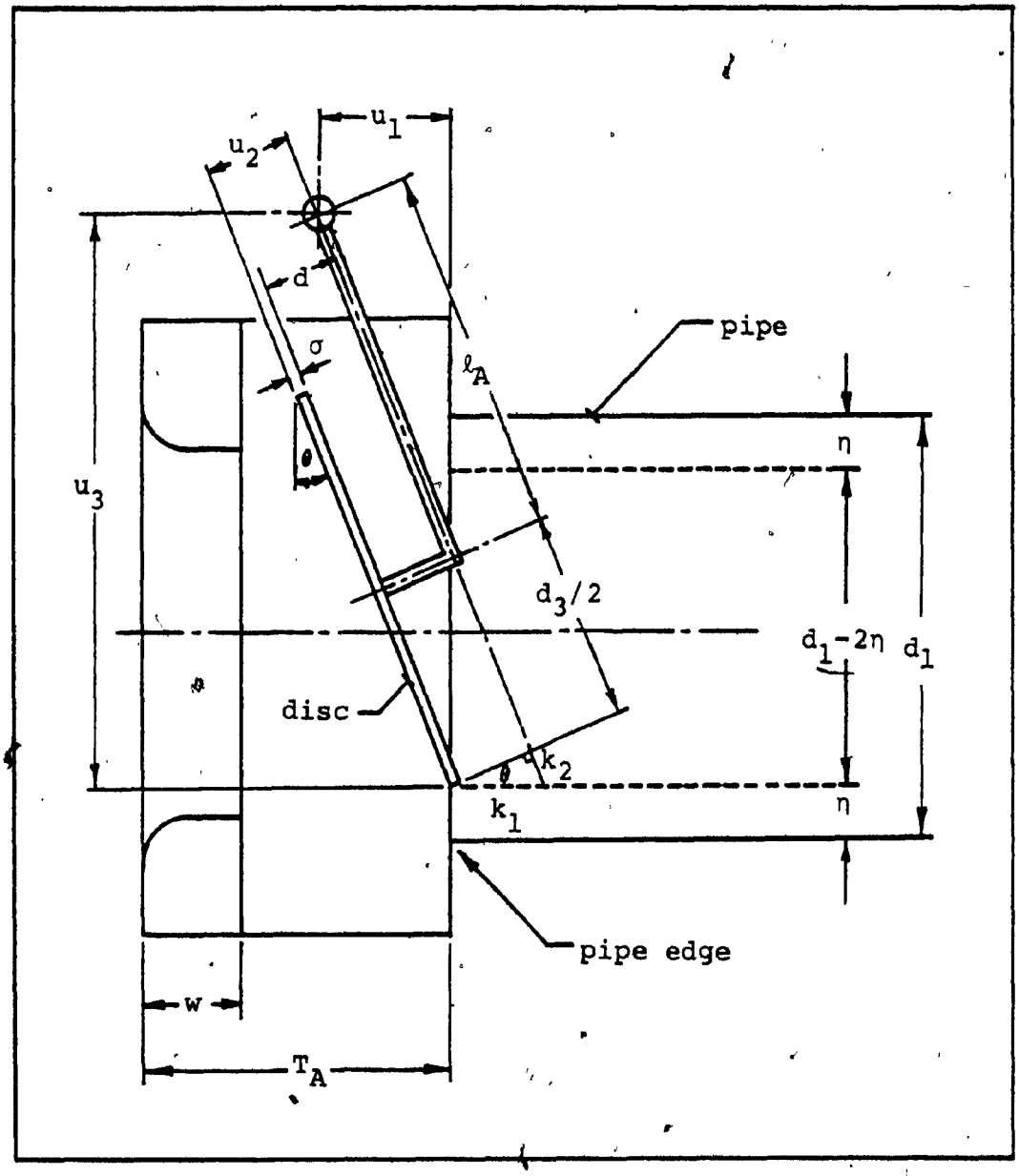

Figure 3-5. Disc to Pipe Bottom Edge Clearance

unknown (positive) dimensions give:

$$k_1 = \frac{u_1 \cdot u_2^2}{u_3^2 - u_2^2} + \left[\left(\frac{u_1 \cdot u_2^2}{u_3^2 - u_2^2}\right)^2 + u_2^2 \cdot \left(\frac{u_1^2 + u_3^2}{u_3^2 - u_2^2}\right)\right]^{\frac{1}{2}} \quad (3.19)$$

$$k_2 = (k_1^2 - u_2^2)^{\frac{1}{2}} \quad (3.20)$$

To find the disc diameter d_3 that provides the clearance η, Equation 3.8 is rearranged with the required dimensions to give:

$$d_3 \leq [(d_1 - 2\eta)^2 - 4(\ell_A \cdot \tan[\tfrac{\theta}{2}] - [\sigma + d])^2]^{\frac{1}{2}} \quad (3.21a)$$

where the disc is at opening:

$$\theta = \sin^{-1}\left(\frac{k_2}{k_1}\right) \quad (3.21b)$$

Figure 3-4 shows the effect of pipe bottom clearance η = 3.2-mm for the 100-mm valve as point (B'). The previously found maximum overall flow coefficient, point (B), cannot be used since its disc diameter does not provide the required clearance η. If point (B') was found to lie to the right of point (B), point (B) would be considered the best flow coefficient. Since point (B') lies to the left of point (B), point (B') is considered optimal lying on a boundary constraint. Point (B') is considered the maximum

flow coefficient for the 100-mm valve.

3.4.3 Pipe Wall Clearance

Another clearance limit in conjunction with the pipe bottom clearance is required for the final check valve design. This is the pipe wall clearance from the disc. For a disc hitting the pipe walls at two points (refer to Section 3.3.1) is both detrimental to the disc and to the proper operation of the check valve. Due to the dynamic flow forces acting against the valve disc, the disc swings open and is suddenly stopped when it hits the pipe walls. The dynamic forces at impact may bend the disc or the disc may wedge into the pipe walls. The damaging effect of a bent disc is improper sealing when the disc is seated. For a disc wedged into the pipe walls, the disc does not close when it is required to obstruct reverse flow. Thus, the disc opening must decrease to angle θ_N for a required wall clearance λ. This is provided by the anti-wedging nut as shown in Figure 3-1, or by the stopper web as shown in Figure 2-1.

The wall clearance allowing the disc to clear the pipe walls, requires the anti-wedging nut to limit the opening of the disc to angle:

$$\theta_N = 2 \cdot \tan^{-1} \left[\frac{(d + \tfrac{1}{2} ([d_1 - 2\lambda]^2 - d_3^2)^{\frac{1}{2}}}{\ell_A} \right] \qquad (3.22)$$

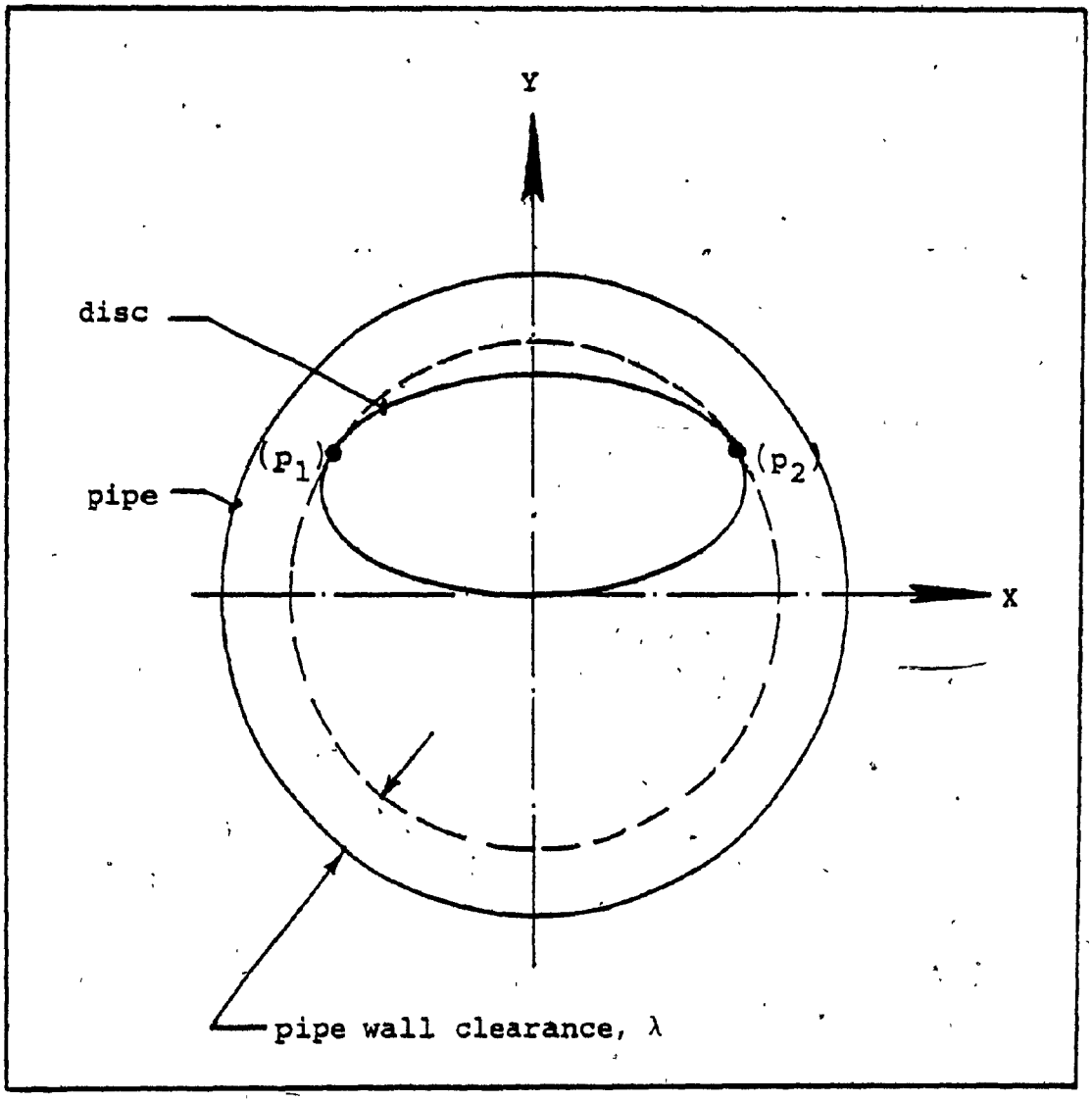

Figure 3-6. Disc to Pipe Wall Clearance

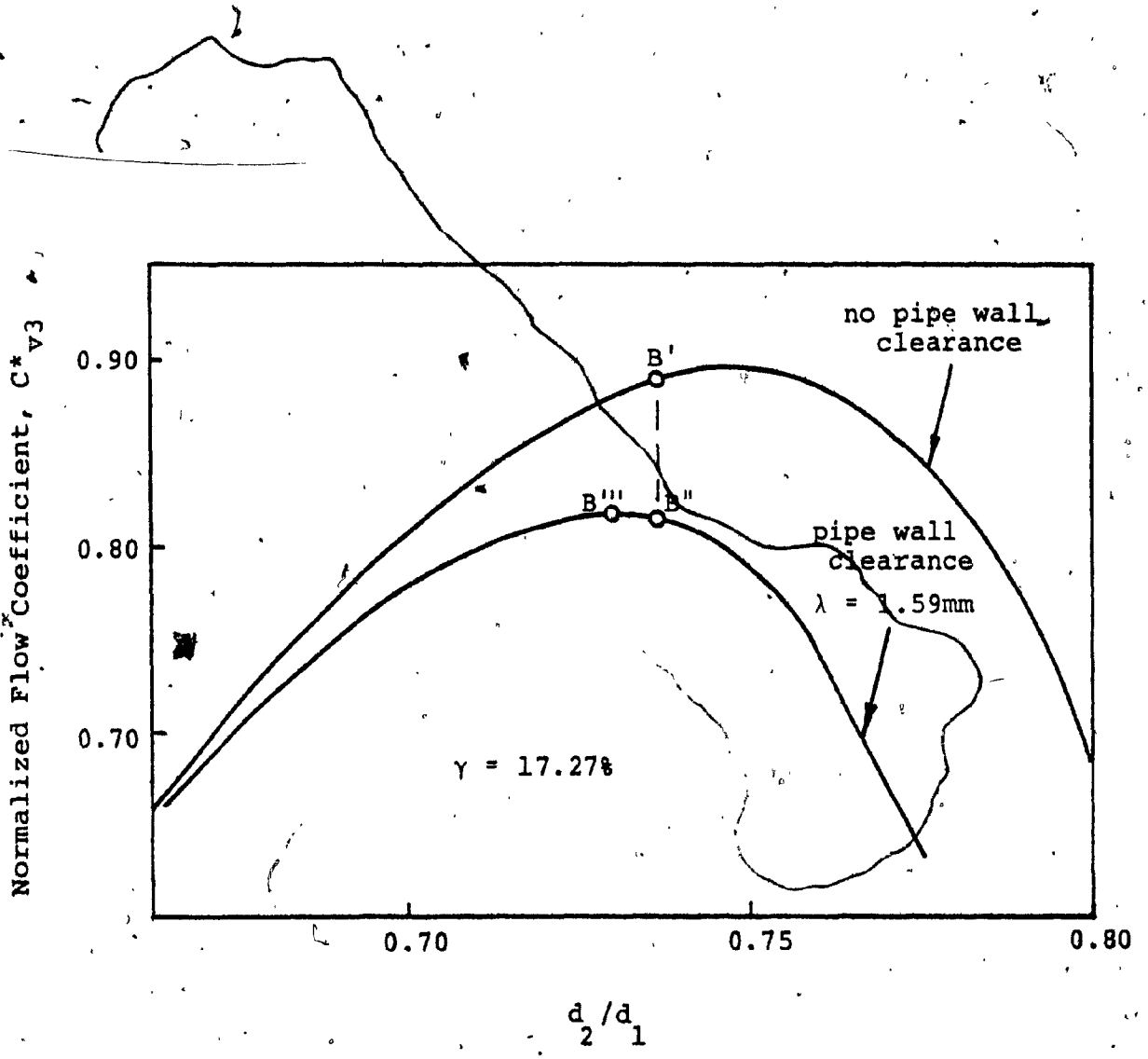

Figure 3-7. Effect of Anti-Wedging Wall Clearance on Flow Coefficient

where all variables were previously defined. Equation 3.22 is the same as Equation 3.8 except the pipe diameter has been reduced by 2λ giving a λ clearance for the two points (p_1) and (p_2) of the disc that would have touched the pipe walls, as shown in Figure 3.6.

The effect of pipe wall clearance, λ = 1.59-mm, is shown in Figure 3-7 for the 100-mm valve. The best flow coefficient, point (B'), found in the previous section for the disc hitting the pipe walls, has shifted down to point (B'') affected by the wall clearance. Point (B'') can now be slightly shifted to point (B''') giving the best flow coefficient C^*_{v3} for a 100-mm wafer check valve of the soft seal type with pipe bottom and wall clearances.

3.4.4 Design Dimensions

Table 3-1 and Table 3-2 present design dimensions for the redesigned hard and soft seal valves, respectively. All soft seal valve sizes and only the 50-mm hard seal valve are redesigned according to the presented procedure, as applied to the 100-mm soft seal valve; the remainder of hard seal valve sizes are not. Separate sets of valve body, disc, and hinge arm dimensions for both soft and hard seal valves were considered not feasible by both Ritepro and the author.

Valve Size (mm)	d_1 (mm)	T_A (mm)	w (mm)	μ (mm)	σ (mm)	d (mm)	ℓ_A (mm)	α (mm)	γ (°)	d_2 (mm)	d_3 (mm)	θ_F (deg)	θ_N (deg)	η (mm)	λ (mm)
50	52.50	44.5	11.05	9.53	1.59	12.07	28.57	1.19	16.63	39.52	48.26	76.2	70	>2.5	.80
65	62.71	47.6	11.05	11.13	1.59	17.09	35.71	1.58	15.19	49.15	58.67	76.5	71	~2.3	1.02
80	77.93	50.8	12.82	12.70	3.17	16.79	42.55	1.58	12.22	61.60	71.12	75.1	70.5	~2.5	1.02
100	102.26	57.2	15.88	15.88	3.17	19.69	54.76	2.38	10.87	81.86	92.96	73.6	69	>3.2	1.59
125	128.19	63.5	16.66	19.05	4.76	21.77	66.68	2.38	8.67	104.47	115.57	73.2	68.8	~5.1	1.59
150	154.05	69.9	17.86	20.65	4.76	24.59	82.55	2.38	7.21	124.79	135.89	72.8	69.6	~6.4	1.59
200	202.72	73.0	20.57	22.23	4.76	20.39	105.56	3.18	6.26	162.05	174.75	68.4	66	>11.1	1.59
250	254.51	79.4	22.23	23.83	4.76	31.75	130.81	3.18	4.99	210.82	223.52	70.6	68.6	>12.7	1.59
300	303.23	85.7	23.83	31.75	4.76	27.00	156.21	3.18	4.19	247.04	259.74	67.9	64.7	>19.1	3.18

Table 3-1. Design Dimensions for Hard Seal Valves

Valve Size (mm)	d_1 (mm)	T_A (mm)	w (mm)	μ (mm)	σ (mm)	d (mm)	ℓ_A (mm)	δ (mm)	ε (mm)	γ (°)	d_2 (mm)	d_3 (mm)	θ_P (deg)	θ_N (deg)	η (mm)	λ (mm)
50	52.50	44.5	7.87	9.53	1.59	15.24	28.57	1.78	1.85	25.92	37.19	50.80	74.9	70	≈2.0	.80
65	62.71	47.6	11.05	11.13	1.59	17.09	35.71	1.78	1.85	21.73	45.03	58.67	76.5	71	≈2.3	1.02
80	77.93	50.8	12.82	12.70	3.17	16.79	42.55	2.62	2.03	20.08	55.47	71.12	75.1	70.5	≈2.5	1.02
100	102.26	57.2	15.88	15.88	3.17	19.69	54.76	3.53	2.13	17.27	75.31	92.96	73.6	69	>3.2	1.59
125	128.19	63.5	16.66	19.05	4.76	21.77	66.68	3.53	2.92	15.02	96.32	115.57	73.2	68.8	≈5.1	1.59
150	154.05	69.9	17.86	20.65	4.76	24.59	82.55	3.53	2.92	12.50	116.64	135.89	72.8	69.6	≈6.4	1.59
200	202.72	73.0	20.57	22.23	4.76	20.39	105.56	3.53	3.05	9.62	155.24	174.75	68.4	66	>11.1	1.59
250	254.51	79.4	72.23	23.83	4.76	31.75	130.81	7.99	3.18	10.48	196.85	223.52	70.6	68.6	>12.7	1.59
300	303.23	85.7	23.83	31.75	4.76	27.00	156.21	7.99	3.51	9.01	232.41	259.74	67.9	64.7	>19.1	3.18

Table 3-2. Design Dimensions for Soft Seal Valves

Valve Size (mm)	SOFT SEAL VALVES					RITEPRO [18] Existing Valves		SOFT SEAL VALVES		HARD SEAL VALVES				
	Full Opening (θ_F)			Limited Opening (θ_M)		Applicable to Valve Sizes soft (80 to 300) hard (50 to 300)		PRODUCTION PROTOTYPE [19]		Full Opening (θ_F)			Limited Opening (θ_M)	
	Analysis		Experimental	Analysis		Experimental				Analysis		Experimental	Analysis		Experimental
	C^*_{v3}	ΔP (kPa)	ΔP (kPa)	C^*_{v3}	ΔP (kPa)	ΔP (kPa)		C^*_{v3}	ΔP (kPa)	C^*_{v3}	ΔP (kPa)	ΔP (kPa)	C^*_{v3}	ΔP (kPa)	ΔP (kPa)
50	0.760	18.06	19.44	0.695	21.58	26.27	0.677	22.75	0.669	23.30	0.841	14.75	13.44	0.771	17.51	19.44
65	0.829	15.17		0.765	17.86		0.623	26.89	0.791	16.69	0.921	12.27		0.835	14.96	
80	0.816	15.65	14.89	0.771	17.51		0.586	30.34	0.797	16.41	0.951	11.51	9.86	0.882	13.38	
100	0.888	13.24	14.00	0.798	16.34	17.65	0.600	28.96	0.807	16.00	0.969	11.10	15.17	0.855	14.20	18.82
125	1.015	10.14		0.938	11.86		0.520	38.61	0.935	11.93	1.014	10.14		0.937	11.86	
150	0.978	10.89		0.935	11.93		0.462	48.95	0.872	13.72	1.019	10.07		0.971	11.10	
200	0.983	10.82		0.948	11.58		0.502	41.37	0.831	15.10	0.962	11.24		0.930	12.07	
250	1.027	9.86		0.996	10.48		0.607	28.27	0.820	15.51	1.063	9.24		1.029	9.86	
300	0.985	10.76		0.939	11.86		0.550	34.47	0.845	14.62	1.146	7.93		1.074	9.03	

Note 1: ΔP values correspond to flow velocity $v_1 = 4.57$ m/s in Schedule 40 pipe.

Note 2: number in square bracket refers to reference.

Table 3-3. Pressure Loss Values for Optimally Designed Valves

Overall normalized flow cofficient C^*_{v3} maximization is towards the larger of the two types of valve overlap. The soft seal valve overlap is larger. The disc and hinge arm dimensions found from sizes 65-mm to 300-mm for soft seal valves are also used for the hard seal valves. This results in the same disc opening and the same pipe bottom and wall clearances for both types of valves. Since disc sizes found for the soft seal valve are also used for the corresponding hard seal valve sizes, the orifice diameter for the latter type of valve is simply found from its overlap specification. The 50-mm valve required different design dimensions for both soft and hard seal valves to meet the 20.7 kPa pressure drop requirement.

Analytical overall flow coefficient C^*_{v3} and the related pressure drop ΔP at a water flow velocity of 4.57 m/s in Schedule 40 pipe are presented in Table 3-3, corresponding to the valve design dimensions from Tables 3-1 and 3-2. Values are given for both disc full opening θ_F and disc anti-wedging nut opening θ_N. All theoretical pressure drops are below the 20.7 kPa limit, except for the 50-mm soft seal valve at its limited opening.

Table 3-3 also lists the pressure drop of existing Ritepro valves at 4.57 m/s in Schedule 40 pipe. These values are taken from Underwriters' Laboratories of Canada [18] listing of Ritepro valves. The stated pressure

drop values apply to soft seal valve sizes from 80-mm to 300-mm, and to hard seal valve sizes from 50-mm to 300-mm. It can be seen from Table 3-3 that the new valve design at their limited opening has expected pressure drops well below existing Ritepro valves.

The remainder of Table 3-3, the experimental values, will be discussed in the following sections.

3.5 Experimental Verification of Valve Design

3.5.1 Test Results

The test arrangement and procedure to verify the Ritepro valve designs are presented in Appendix C. Experimental values are established only for small valve sizes of 50-mm, 80-mm and 100-mm. This is considered sufficient since it is more difficult to achieve a pressure drop below the critical 20.7 kPa at 4.57 m/s for small valves. In other words, success with small valve sizes guarantees success with larger valves.

The test results for the soft seal valves are shown in Figure 3-8. All pressure drops at 4.57 m/s are interpolated from the test points as shown in Figure 3-8, except for the 100-mm valve at its limited opening which is extrapolated. These experimental values are also tabulated

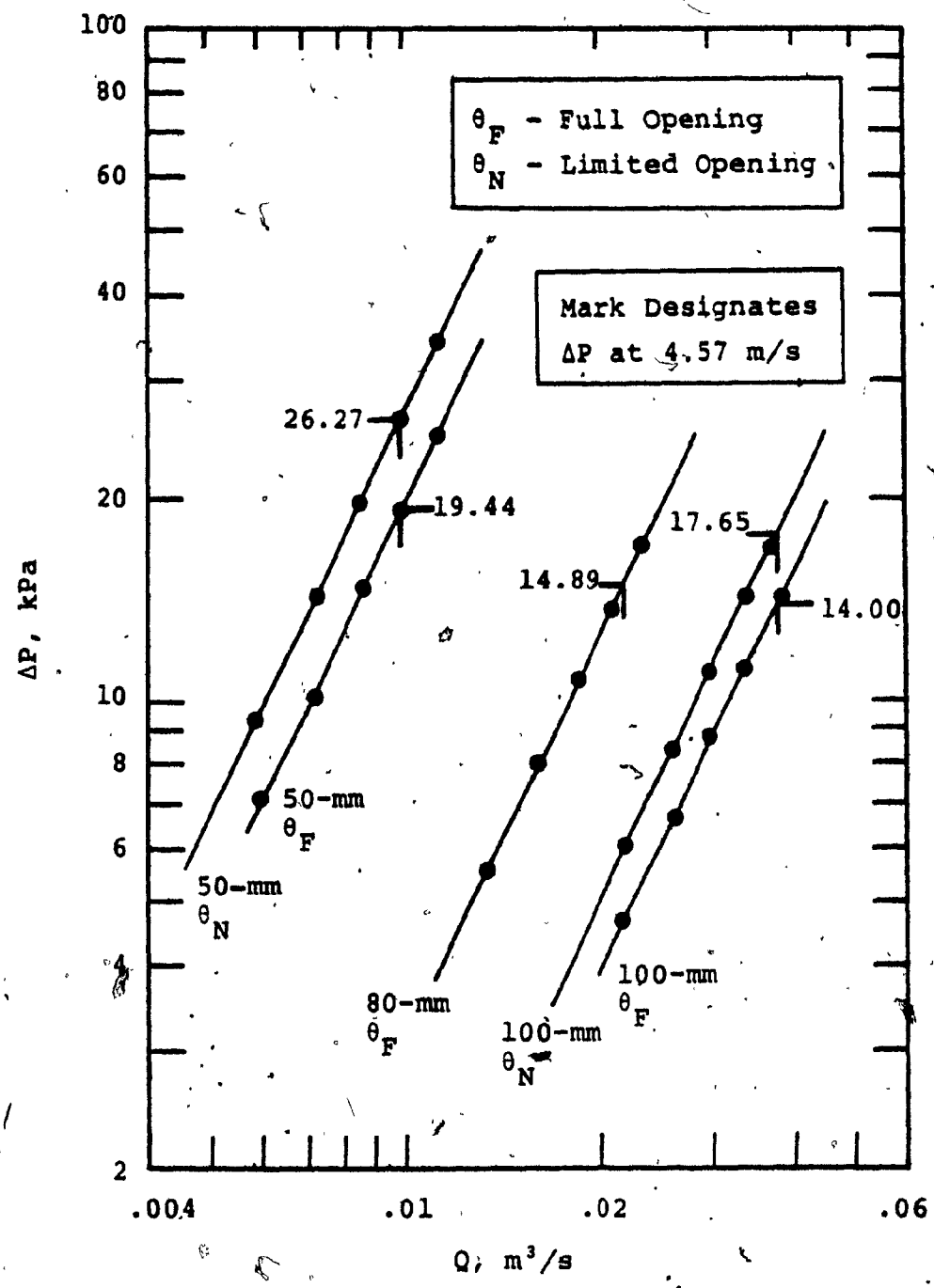

Figure 3-8. Test Results for 50-mm, 80-mm and 100-mm Soft Seal Valves

in Table 3-3 for comparison with their theoretical values.

Experimental pressure drop values for the three soft seal valve sizes at full opening are in close agreement with their theoretical values. The maximum difference with respect to theoretical values is approximately 18 percent, occurring for the 50-mm valve. The results suggest that the loss coefficients selected in Section 3.3.3 for the valve are correct.

The experimental pressure drop value for the 50-mm soft seal valve at its limited opening is 22 percent greater than the expected value, while that of the 100-mm valve is in closer agreement at 8 percent greater than the calculated value. This discrepancy may be attributed to the choice of entrance contraction loss coefficient for the disc, Equation 2.10a, where the coefficient was chosen constant to be 0.1. Theoretical values would be in better agreement with experimental values if the loss coefficient was determined as a function of disc angle.

Test results for the hard seal valves are plotted in Figure 3-9. Also shown in the figure are experimental results for the 100-mm valve in which the original hard seal orifice consisted of a step, was replaced by a smooth orifice of the same diameter. Interpolated or extrapolated pressure drops at 4.57 m/s are shown in Figure 3-9 and are

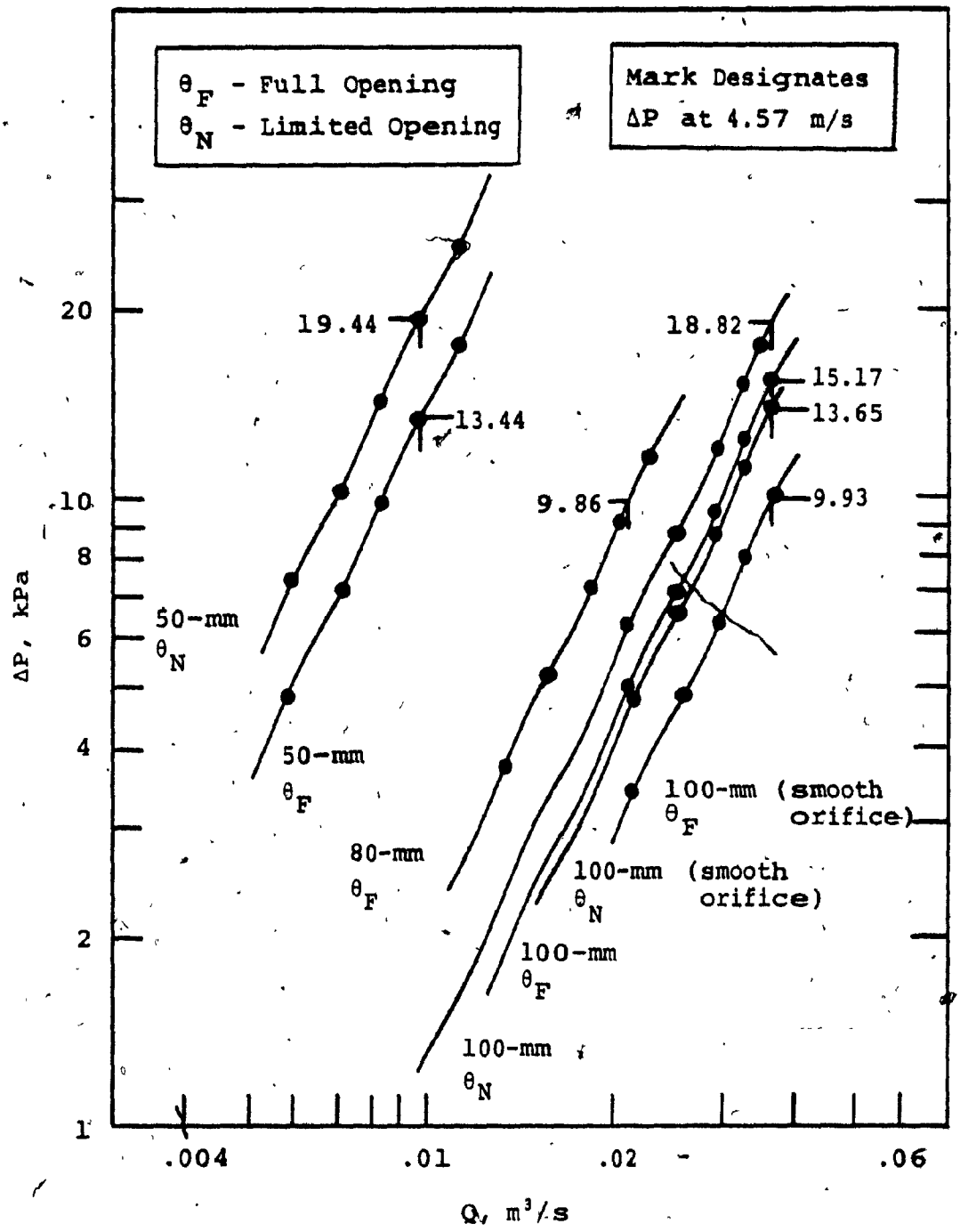

Figure 3-9. Test Results for 50-mm, 80-mm and 100-mm Hard Seal Valves

tabulated in Table 3-3.

The pressure drop results for the 50-mm and 80-mm valves at their full open position are, respectively, 9 percent and 14 percent less than their expected values. The pressure drop for the 100-mm valve is 37 percent greater than the expected value. Results obtained for the soft seal valves at full opening suggest that both loss coefficients selected for the orifice and disc entrance had been chosen correctly. Since the 80-mm and 100-mm soft and hard seal valves have identical disc diameters, discrepancy in results for hard seal valves is attributed to the choice of entrance loss for the hard seal orifice with a step. The assumption that constant entrance loss $K_{L1} = 0.15$, from Section 3.3.3, does not fully describe the orifice loss. For better agreement between experiment and theory, more experiments are required to determine the effect of the orifice with the step.

The pressure drop results for the 50-mm and 100-mm hard seal valves at their limited opening are, respectively, 11 percent and 33 percent greater than their expected values. The first reason for the large difference is due to the choice of orifice entrance loss. The discrepancy is compounded by not knowing the entrance loss coefficient for the disc as a function of disc angle.

Except for the 50-mm soft seal valve at its limited opening, all valves tested are below the 20.7 kPa critical limit. This was expected from theory and proven by experiment. Although the 100-mm hard seal valve performance at its limited opening is 33 percent above its expected value, it can be assumed that all other untested valves with this similar percentage increase in expected pressure drop, would also be below the 20.7 kPa limit.

To investigate further possible pressure drop improvements for hard seal valves, experiments were performed on the 100-mm valve by replacing the orifice with a step by a smooth orifice of the same diameter. That is, with a smooth orifice diameter equivalent to the seat ring internal diameter. Referring to Figure 3-9, the pressure drops are:

OPENING (100-mm valve)	ORIFICE WITH STEP ΔP (kPa)	SMOOTH ORIFICE ΔP (kPa)
θ_F	15.17	9.93
θ_N	18.82	13.65

It is clearly seen that the valve with a smooth orifice at its limited opening (13.65 kPa) has a pressure drop even less than the valve with a step in the orifice at its full opening (15.17 kPa). If the hard seal valve would

incorporate a smooth orifice, the pressure drop would be greatly improved. Their pressure drop would be ensured to be much less than that of the soft seal valve.

3.5.2 Evaluation of Production Prototype

On the basis of the optimal sizing table for soft seal valves, Table 3-2, a whole new line of Ritepro wafer check valves was designed. An actual production prototype of the 100-mm soft seal valve was built using the production tooling. The valve picture is shown in Figure 3-10. Figure 3-11 shows the experimental pressure drop versus flow characteristic of the valve. The plot indicates a pressure loss of 15.44 kPa at 4.57 m/s which is in close agreement with the value predicted by both the analysis (16.34 kPa) and by the experiment (17.65 kPa) with the preliminary valve model (see Table 3-3).

For further evaluation, production prototypes of the new line of Ritepro soft seal valves from 50-mm to 300-mm has been built and then tested by the Hydraulics Laboratory at the Natural Research Council of Canada (NRC) [19]. These pressure drop values tested for 4.57 m/s in Schedule 40 pipe are listed in Table 3-3. All valves are built according to dimensions given in Table 3-2, except for the 50-mm soft seal valve for which the valve body length T_A had been increased to permit the disc to open further.

As seen from Table 3-3, all pressure drops are below the 20.7 kPa limit except for the 50-mm valve. Although the 50-mm valve does not meet the pressure drop requirement, increasing of its body length has decreased its pressure loss value by 11 percent from 26.27 kPa to 23.30 kPa. The pressure drop for valve sizes from 65-mm to 125-mm are less than 7 percent as compared to the analytical values. The 100-mm valve, measured at 16.00 kPa is 4 percent above our prototype test at 15.44 kPa and 9 percent below the test rig value at 17.65 kPa. Both prototype test results being below the valve model value may be attributed to the difficulty in measuring and locking of the hinge arm exactly at its limited opening for the test.

For the valve sizes from 150-mm to 300-mm, although all pressure drops are well below the 20.7 kPa limit, their test results are not in good agreement with their expected values. The largest difference is 48 percent greater than the expected pressure drop value, occurring for the 250-mm valve. This discrepancy, as discussed in Section 3.5.1, is attributed to no adequate knowledge of the disc entrance loss coefficient as a function of disc angle.

As a final result of the presented work, the pressure drop for all newly designed valves is well below existing Ritepro valves loss values (applicable only for sizes 80-mm to 300-mm).

Figure 3-10. Picture of Optimized 100-mm Soft Seal Valve

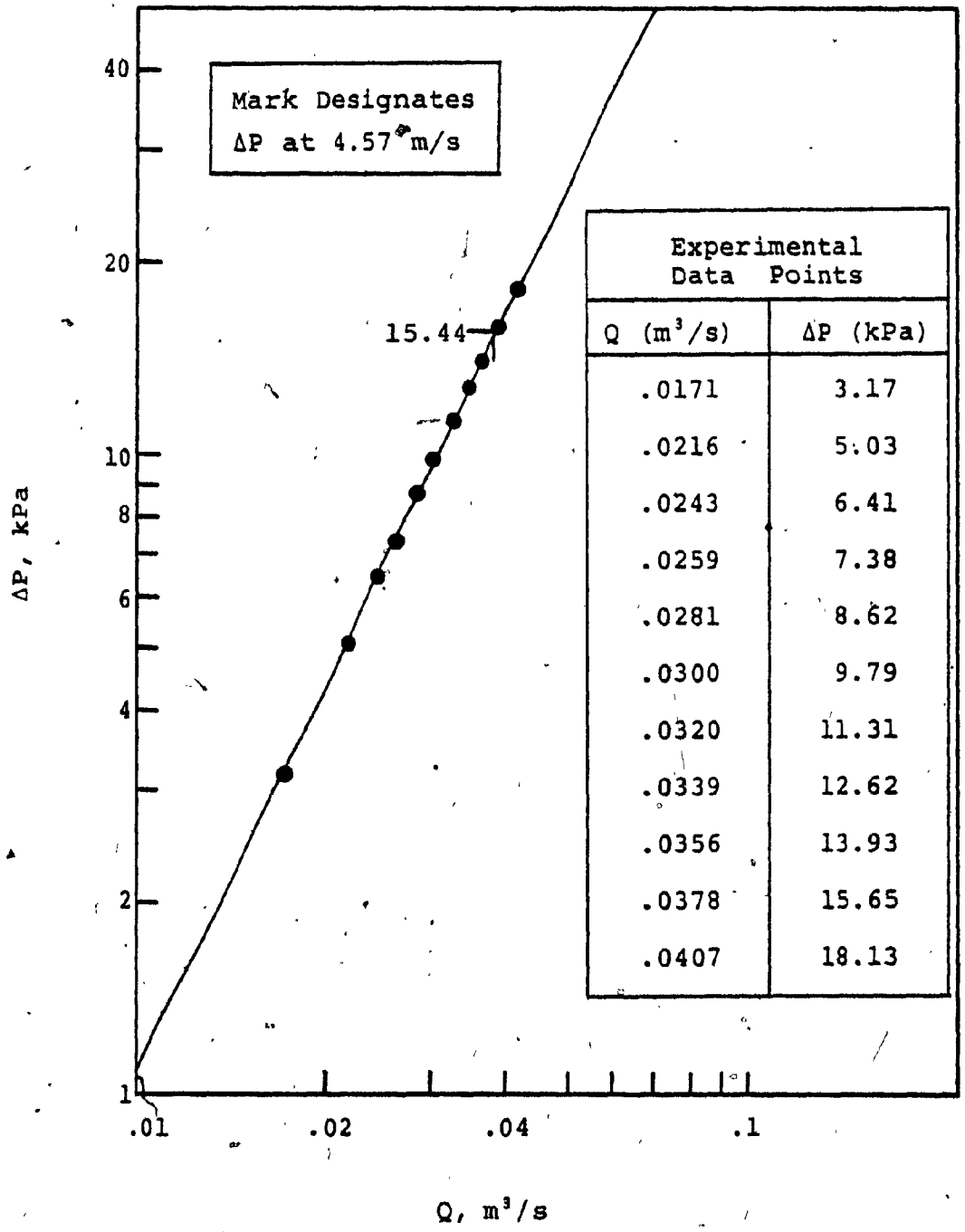

Experimental Data Points	
Q (m^3/s)	ΔP (kPa)
.0171	3.17
.0216	5.03
.0243	6.41
.0259	7.38
.0281	8.62
.0300	9.79
.0320	11.31
.0339	12.62
.0356	13.93
.0378	15.65
.0407	18.13

Figure 3-11. Pressure Drop vs Flow Characteristic of Optimized 100-mm Soft Seal Valve

CHAPTER 4

VALVE MECHANISM DYNAMICS

4.1 Introduction

A hydro-pneumatic mechanism acting as a combination spring and damper is described. This mechanism when combined with the swing-disc check valve provides a control for valve closing speed and non-slam action. Modelling of the system dynamics relates the angular position of the valve disc to an input torque. This torque represents the fluid forces acting against the disc shaft. Computer simulation and experimental confirmation of the check valve mechanism dynamics has been researched by Svoboda and Lee [8], Lee [9], and Lee, Svoboda and Kwok [10] in conjunction with this project. Their work covering the valve mechanism dynamics is summarized here for coherence of the present research. This hydro-pneumatic mechanism incorporated with a swing-disc check valve is computer simulated under transient pipe flow conditions in Chapter 6.

4.2 Hydro-Pneumatic Valve Mechanism Analysis

4.2.1 Valve Description

A schematic drawing of the hydro-pneumatic spring-damper check valve is shown in Figure 4-1. The

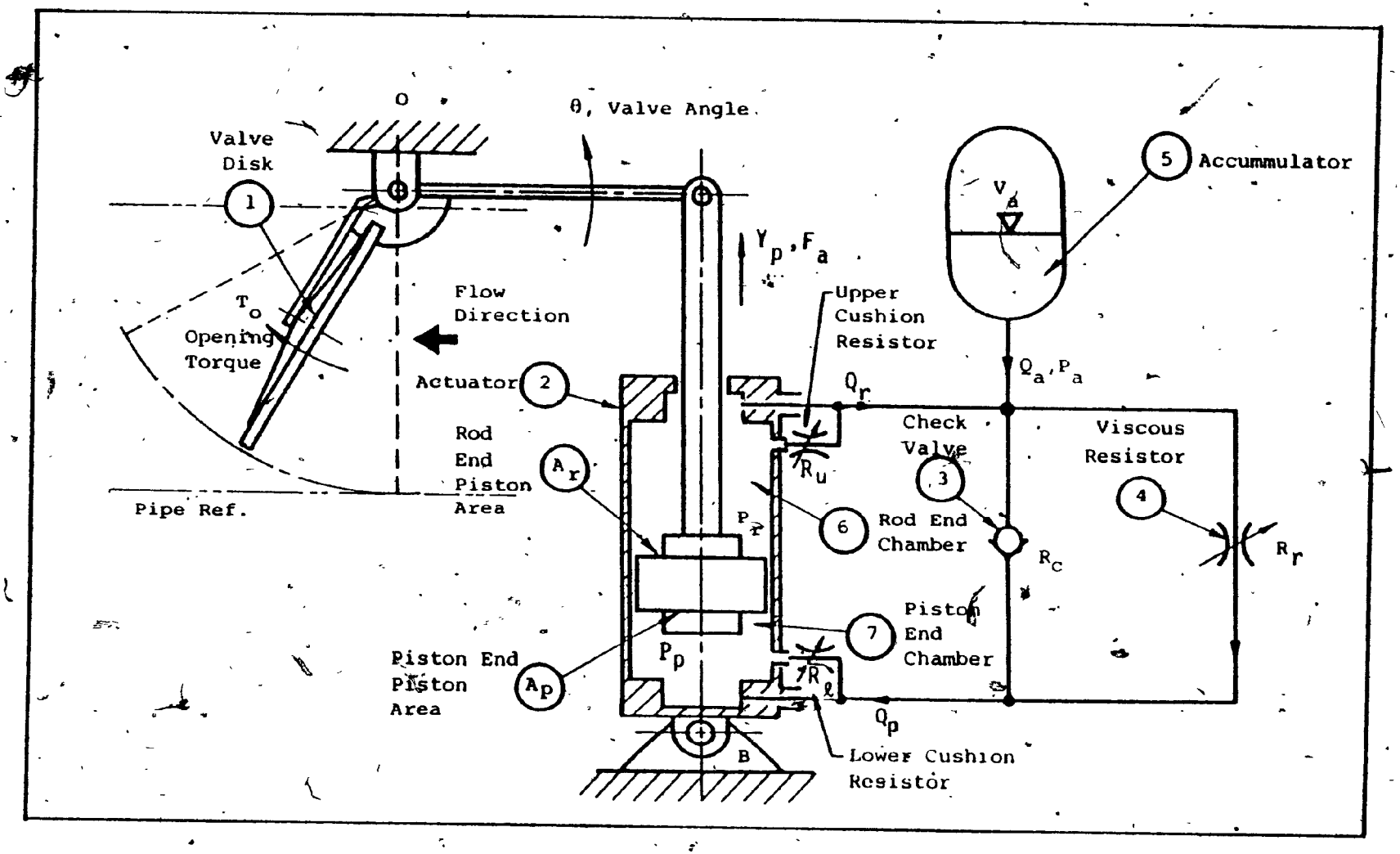

Figure 4-1. Schematic Diagram of Hydro-Pneumatic Spring-Damper Valve [9]

spring like force F_a that tends to keep the valve closed is due to the force difference within actuator (2). That is, pressure P_p acting on piston end area A_p results in greater force than pressure P_r acting on rod end area A_r. The initial spring force depends on the precharged pressure of accumulator (5).

Opening torque T_o about the pivot pin is due to the flow forces against the valve disc (1). As the opening torque exceeds the closing torque created by the spring force about pivot point (O), the disc angle θ would swing open and the piston would retract by the displacement Y_p. Hence, flow Q_p through the check valve (3) from piston chamber (7) supplies flow Q_r to rod chamber (6). Due to the difference in actuator chamber volumes, excess flow Q_a charges the accumulator. In this way, the spring force increases further to oppose the opening torque as the accumulator gas volume V_a compresses, and pressure P_a increases. As the valve disc approaches its fully opened position, adjustment of the lower cushion resistor, R_ℓ acts as a damper to reduce slamming of the disc against the downstream pipe walls.

During valve opening the accumulator increases its stored energy. During valve closing, there are two processes to be considered. The first case, is when the opening torque is reduced below that of the closing torque.

However, the water flow tends to keep the valve open. Hence, the pervailing differential force across the piston will cause the valve disc to close. In the second case, reverse flow within the pipe is considered. Flow forces against the valve disc drive the disc to close. This forces the piston to extend and the diffential force across the piston will resist the disc driving force. In both cases, stored oil is discharged from the accumulator via the adjustable needle valve R_r. Thus, variable viscous damping is obtained during closure. Also, slamming of the valve disc against the valve seat during closing can be further dampened by adjusting the actuator upper cushion resistor R_u.

4.2.2 Valve Modelling

The mathematics representing the hydro-pneumatic valve mechanism is summarized here. Full derivation leading to these simplified equations are developed in Reference [9]. Figure 4-1 describes the operations of the hydro-pneumatic spring-damper valve components. Figure 4-2 shows the actual valve arrangement. A simplified kinematic diagram of the actuator piston travel is shown in Figure 4-3. Referring to these figures, the valve dynamics can be described by the following equations:

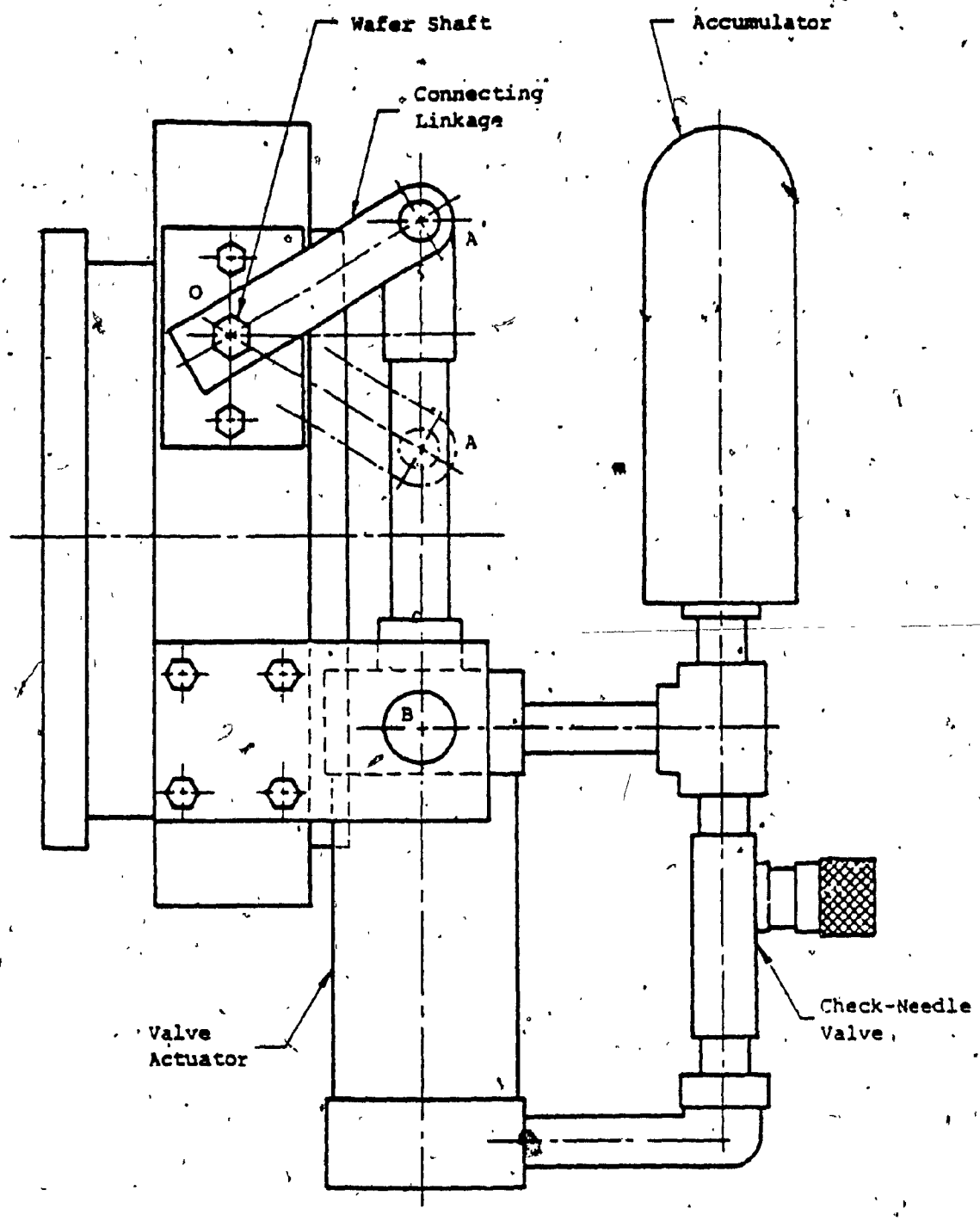

Figure 4-2. Hydro-Pneumatic Spring-Damper Valve Actual Arrangement [9]

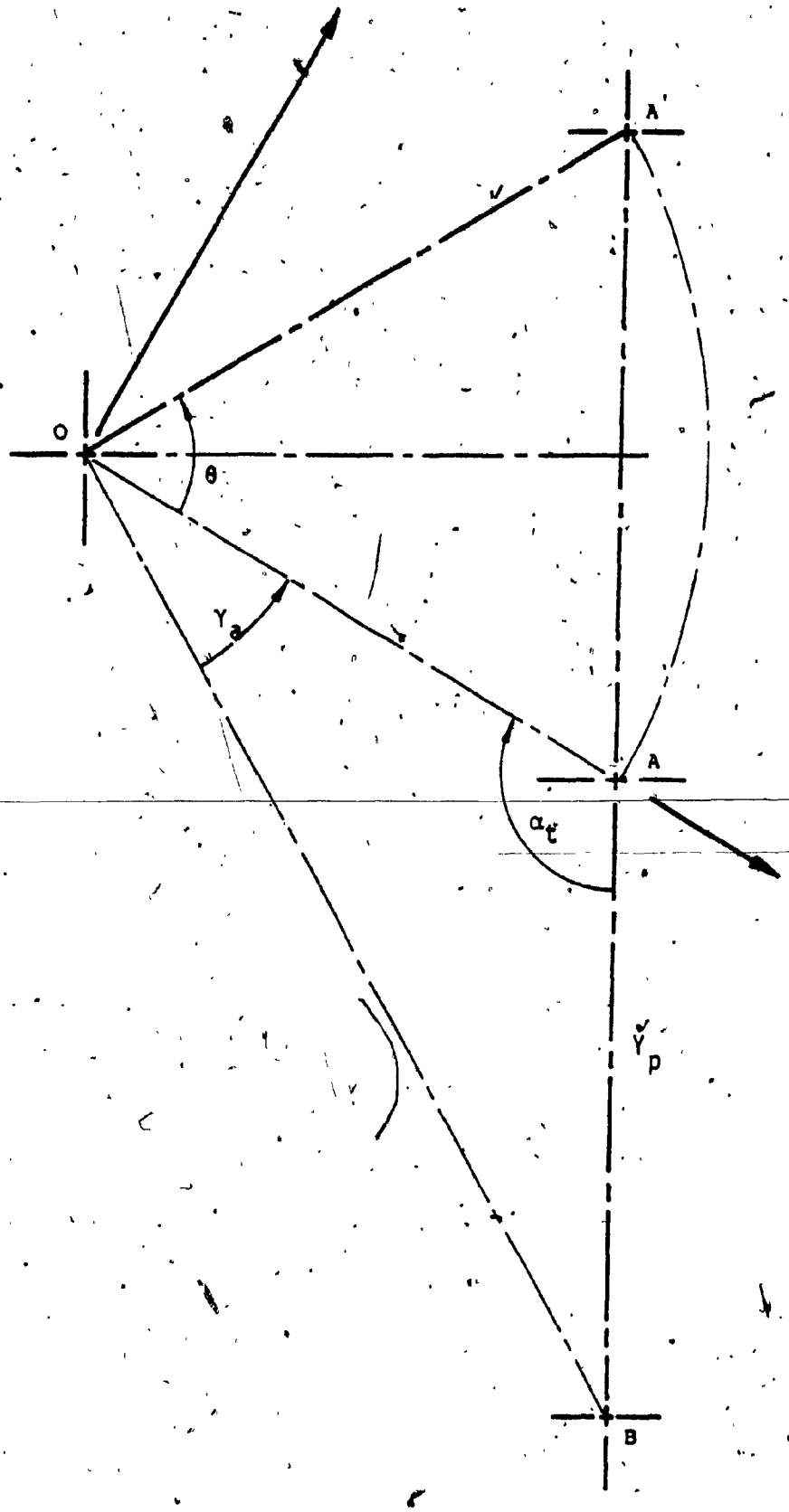

Figure 4-3. Kinematics of Hydraulic Spring-Damper Type Valve [9]

Cylinder hydraulic force:

$$F_a = P_p \cdot A_p - P_r \cdot A_r \qquad (4.1)$$

Cylinder hydraulic torque:

$$T_{cy} = F_a \cdot \overline{OA} \cdot \sin\alpha_t \qquad (4.2)$$

where $\overline{OA}$ is the torque lever.

Torque angle:

$$\alpha_t = \cos^{-1} \frac{Y_p^2 + \overline{OA}^2 - \overline{OB}^2}{2 \cdot Y_p \cdot \overline{OA}} \qquad (4.3)$$

where $\overline{OB}$ is the reference pivot distance.

Actuator displacement:

$$Y_p = [\overline{OA}^2 + \overline{OB}^2 - 2 \cdot \overline{OA} \cdot \overline{OB} \cdot \cos(\gamma_a + \theta)]^{\frac{1}{2}} \qquad (4.4)$$

where γ_a is a kinematic angle.

Actuator velocity:

$$\dot{Y}_p = \overline{OA} \cdot \overline{OB} \cdot \sin(\gamma_a + \theta) \cdot \omega / Y_p \qquad (4.5)$$

Valve angular velocity:

$$\omega = \frac{1}{I_m} \int_0^t (T_{cy} - T_o)\, dt + \omega_o \qquad (4.6)$$

where I_m is the valve mechanism inertia.

Valve angle:

$$\theta = \int_0^t \omega\, dt + \theta_o \; ; \quad \theta_{min} \leq \theta \leq \theta_{max} \qquad (4.7)$$

where θ_{min} and θ_{max} is the disc angle at the fully closed and fully opened valve position, respectively.

Accumulator flow rate:

$$Q_a = Q_p - Q_r \qquad (4.8)$$

Cylinder flow rate:

$$Q_r = \dot{Y}_p \cdot A_r \qquad (4.9)$$

$$Q_p = \dot{Y}_p \cdot A_p \qquad (4.10)$$

Accumulator gas volume:

$$V_a = \int_0^t Q_a\, dt + V_{ao} \qquad (4.11)$$

Accumulator isothermal pressure:

$$P_a = \frac{P_{ao} \cdot V_{ao}}{V_a} - P_{atm} \quad ; \quad (4.12)$$

where P_{ao} and V_{ao} is the accumulator precharged pressure and volume, respectively, and P_{atm} is the atmospheric pressure.

Cylinder pressures:

$$P_r = P_a \quad (4.13)$$

$$P_p = P_r - R_r \cdot Q_p^2 \quad ; \quad \text{if } (\dot{Y}_p > 0) \text{ and } (Y_p < Y_{uc}) \quad (4.14a)$$

$$P_p = P_r - (R_u + R_r) \cdot Q_p^2 \quad ; \quad \text{if } (\dot{Y}_p > 0) \text{ and } (Y_p > Y_{uc}) \quad (4.14b)$$

$$P_p = P_r + R_c \cdot Q_p^2 \quad ; \quad \text{if } (\dot{Y}_p < 0) \text{ and } (Y_p > Y_{\ell c}) \quad (4.14c)$$

$$P_p = P_r + (R_\ell + R_c) \cdot Q_p^2 \quad ; \quad \text{if } (\dot{Y}_p \leq 0) \text{ and } (Y_p > Y_{\ell c}) \quad (4.14d)$$

where Y_{uc} and $Y_{\ell c}$ is the actuator upper and lower cushion limits, respectively.

The system parameters for a 200-mm valve are:

A_r	$= 2.374 \times 10^{-3} m^2$	A_p	$= 3.161 \times 10^{-3} m^2$
R_c	$= 4 \times 10^{12} \frac{N-s}{m^8}$	R_r	$= 13 \times 10^{12} \frac{N-s}{m^8}$
I_m	$= .101$ kg-m^2	γ_a	$= 0.588$ rad
θ_{min}	$= 0.0$ rad	θ_{max}	$= 1.047$ rad
$\overline{OA}$	$= 101.6$ mm	$\overline{OB}$	$= 198.4$ mm
R_u	$= 26 \times 10^{12} \frac{N-s}{m^8}$	R_ℓ	$= 21 \times 10^{12} \frac{N-s}{m^8}$
Y_{uc}	$= 209.6$ mm	$Y_{\ell c}$	$= 146.1$ mm
V_{ao}	$= 492 \times 10^{-6} m^3$	P_{ao}	$= 1.034$ MPa, abs
θ_o	$= 1.047$ rad	ω_o	$= 0.0$ rad/sec

4.3 Experimental Verification of Valve Model

4.3.1 Test Arrangement

The purpose of the test stand shown in the picture of Figure 4-4 is to subject the valve mechanism to specified disc shaft torque inputs. The test results thus evaluate the analytical valve mechanism model. The test arrangement shown schematically in Figure 4-5, consists of an

Figure 4-4. Pictorial View of Valve Mechanism Test Stand

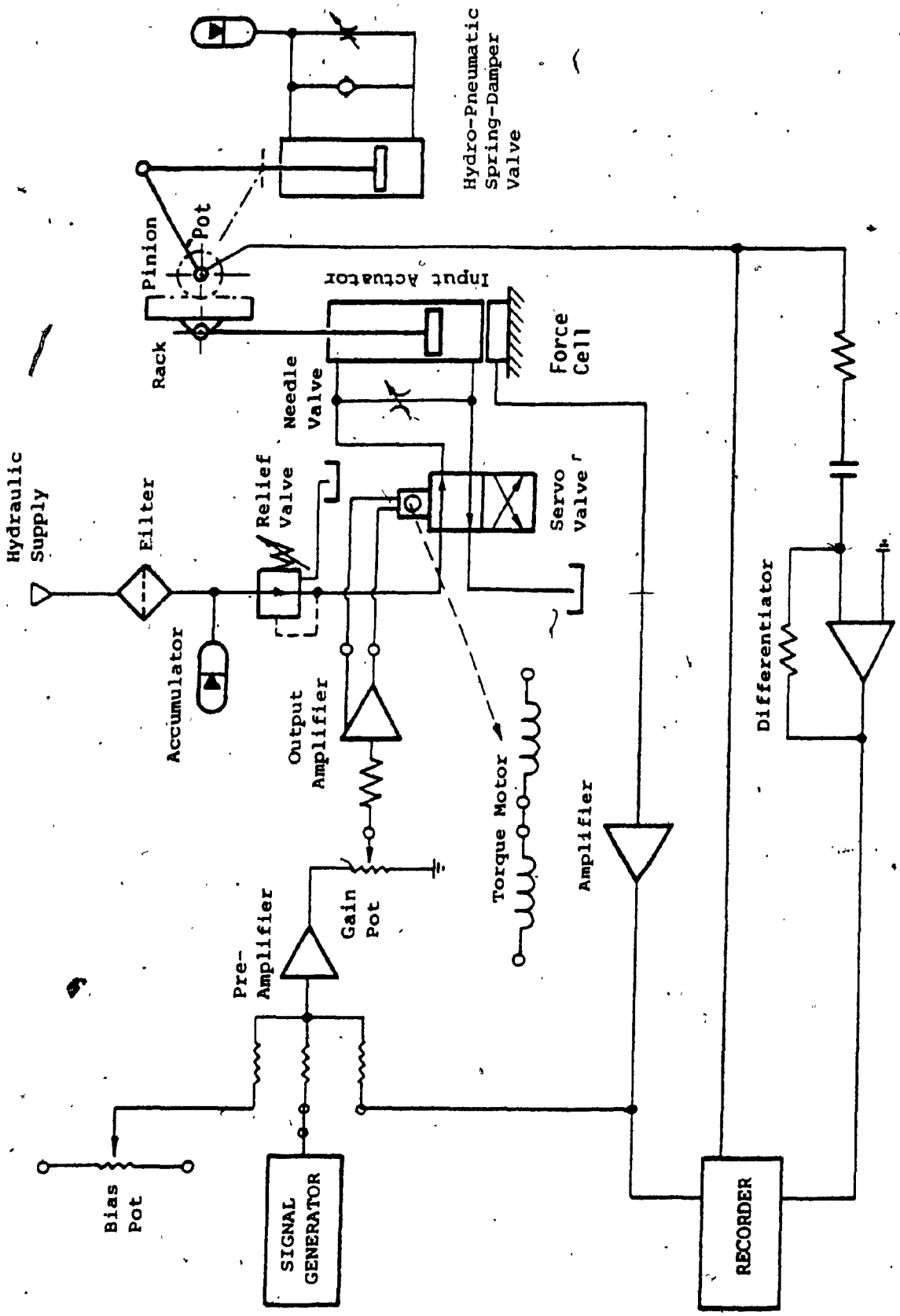

Figure 4-5. Schematics of Valve Mechanism Test Stand [9]

electro-hydraulic linear input actuator equiped with a closed-loop force control. The linear actuator force is then converted into valve disc shaft torque input by a rack-and-pinion mechanism. The disc position is monitored by a potentiometer mounted on the disc shaft. Additional equipment is a signal generator for torque input, and a two-channel X-Y recorder for measuring the input torque and disc position output. A differentiation circuit serves for calculating the disc velocity signal. The test stand was designed for an 200-mm valve size.

4.3.2 Simulation vs. Experimental Results

Figure 4-6 compares an example of the model simulated to that of the experimental valve response. The valve is a 200-mm hydro-pneumatic spring-damper type. The valve model was simulated using MIMIC, a digital computer simulation language. The input was a square wave with an amplitude of 113 N-m, a period of 10 seconds, and a 50% duty cycle. The plot indicates good correlation between the simulation and experimental results. The major deviations are:

- Slower response of the experimental hardware, which is due to the fact that the inertia and the friction of additional mechanical parts of the test rig are not implemented in the simulation model.

- Experimental velocity readings are oscillatory due to small oscillations in the displacement signal. The displacement oscillations resulted from stiction in the mechanical components. These oscillations are within the bandwidth of the differentiator and hence are accentuated.

Since the results provide good correlation, it is concluded that the equations describing the hydro-pneumatic spring-damper valve are adequate.

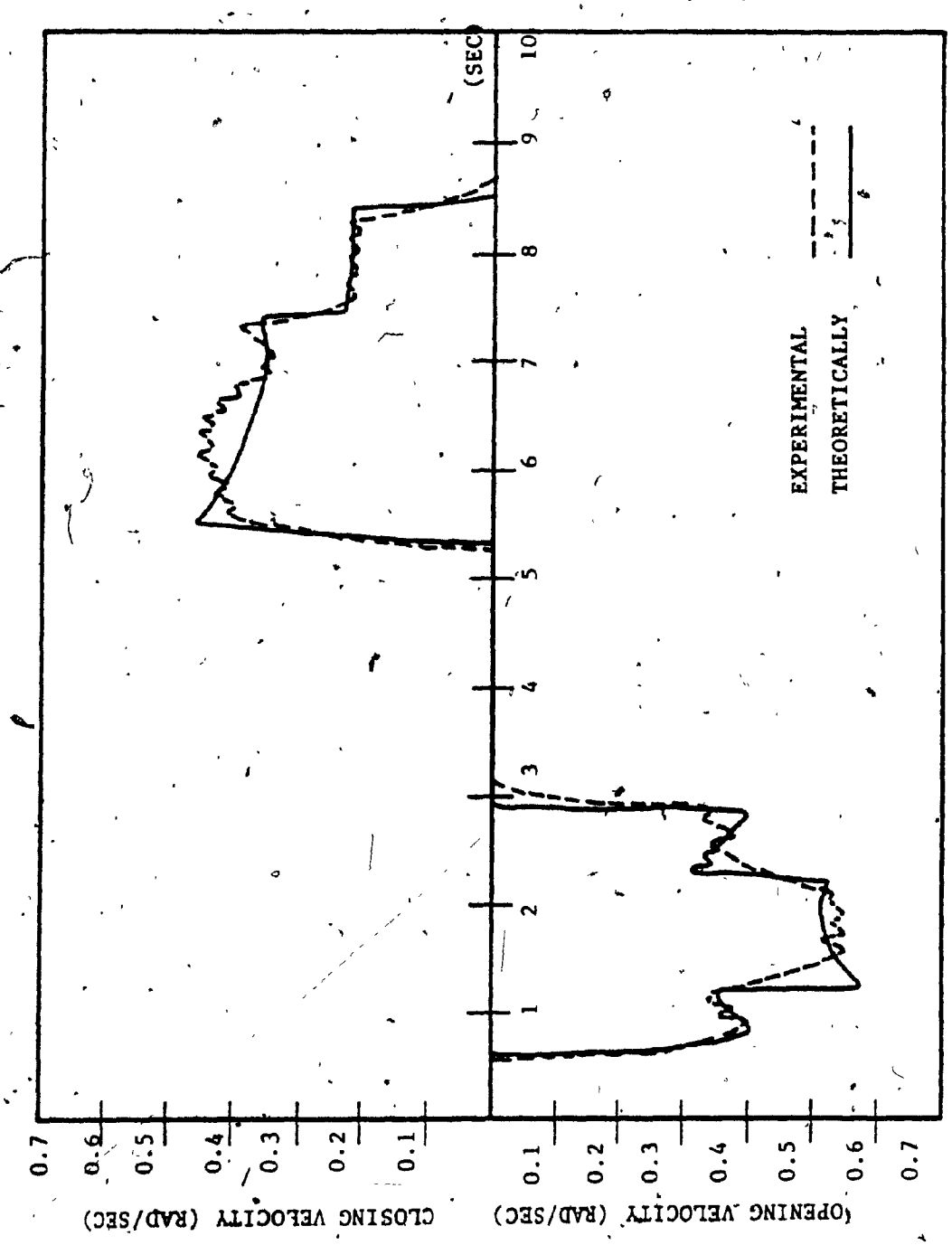

Figure 4-6. Comparison of Typical Response of Hydraulic Spring-Damper Valve [9]

CHAPTER 5

CHECK VALVE FLOW CHARACTERISTICS

5.1 Introduction

In steady-flow conditions, the pressure drop across the check valve and the fluid forces acting against the valve disc, are related to the fluid flow through the valve. This is true for all combinations of valve flow rates and disc openings. In unsteady-flow conditions, the valve flow; fluid forces, upstream and downstream pressure adjacent to the valve, as well as the disc position, are assumed to be related to their equivalent steady-state conditions at each instant of time [13][20]. These unique steady-state conditions are the flow characteristics of the valve.

In this chapter, the check valve flow characteristics are described by a normalized flow coefficient and by a normal drag coefficient. The flow coefficient describes the pressure drop across the valve. The drag coefficient describes the fluid flow forces acting in the direction normal to the disc. Both coefficients are experimentally determined for forward and reverse steady pipe flows and at various angular positions of the disc. These coefficients together with their describing equations, apply to any size of wafer swing-disc check valve.

5.2 Theoretical Valve Torque and Pressure Drop

5.2.1 Disc Shaft Torque

Figure 5-1 shows the important parameters for the unsteady-flow condition through a check valve. Due to the fluid forces acting against the valve disc, a torque T_o is created which acts on the disc-shaft forcing the disc to swing with angular velocity ω. The relative uniform fluid velocity v_R with respect to the angular velocity of the disc for forward and reverse flow, respectively, are given by:

$$v_R = v_2^* - \ell_A \cdot \omega \cdot \cos\theta \qquad (5.1)$$

$$v_R = v_1^* - \ell_A \cdot \omega \cdot \cos\theta \qquad (5.2)$$

where ℓ_A is the hinge arm length and θ is the disc opening angle.

For forward flow the fluid velocity is given by:

$$v_2^* = Q_v/A_2 \qquad (5.3)$$

where Q_v is the flow through the valve and A_2 is the orifice area.

For reverse flow the fluid velocity is given by:

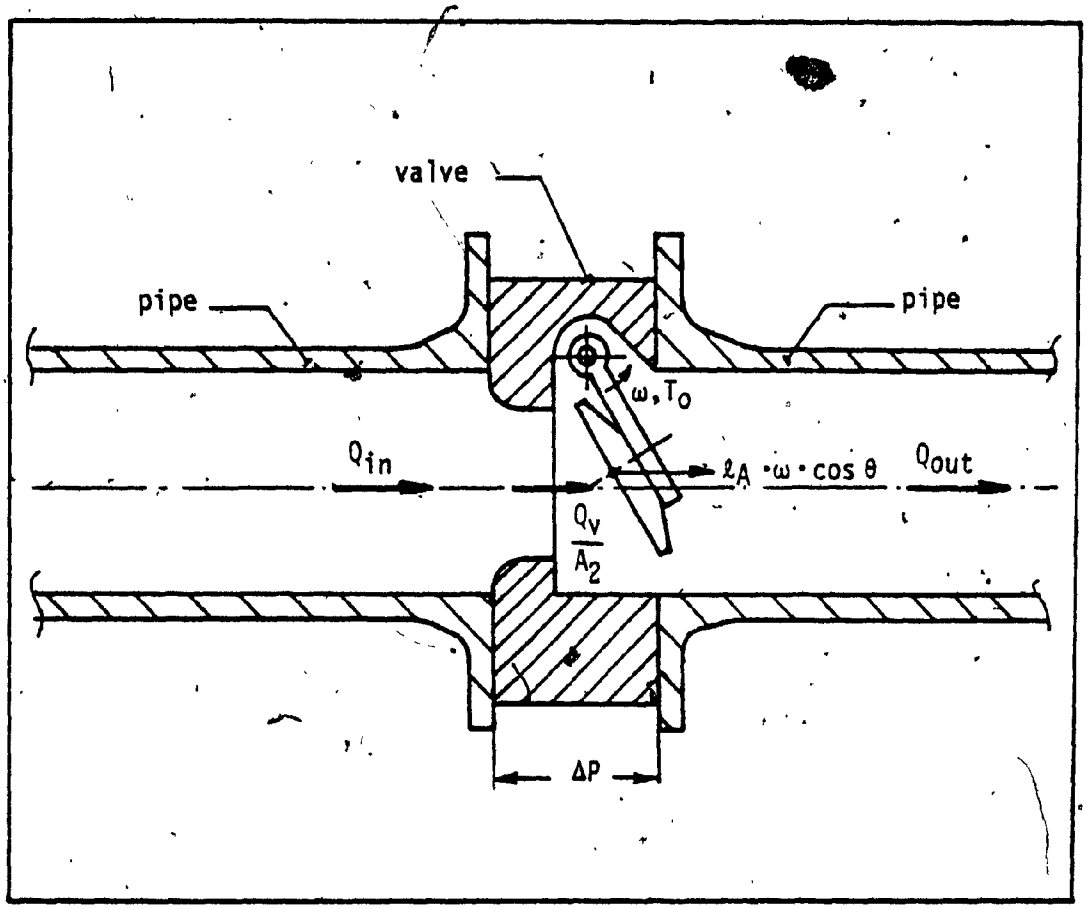

Figure 5-1. Unsteady-Flow Through a Check Valve

$$v_1^* = Q_v / A_1 \qquad (5.4)$$

where A_1 is the pipe area.

The flow force is acting normal to the disc centre and is expressed in terms of the normal drag coefficient C_{ND} as:

$$F_c = \frac{1}{2} \cdot \rho \cdot C_{ND} \cdot A_3 \cdot v_R \cdot |v_R| \qquad (5.5)$$

where A_3 is the disc area and ρ is the density of water. Hence, from Equation 5.5, the fluid torque acting on the disc shaft, for any size of wafer swing-disc check valve is given by:

$$T_o = F_c \cdot \ell_A \qquad (5.6)$$

For complete description of the fluid torque acting on the valve disc, the normal drag coefficient must be determined as a function of disc angle and pipe flow Reynolds number. This coefficient is evaluated under steady-flow conditions. Since the fluid torque on the disc is related to the differential pressure across the valve, the definition of a normal drag coefficient conveniently avoids determining the pressure distribution around the disc and the location of the pressure centre.

5.2.2 Valve Pressure Drop

Concepts developed from Chapters 2 and 3 are used to define the pressure drop across the valve for any position of disc opening and valve size, and for both forward and reverse flow conditions. With reference to Figure 5-1, the flow rate Q_v through the check valve is related to the pressure drop ΔP across the valve by:

$$Q_v = C^*_{v3} \cdot A_1 \cdot \sqrt{2/\rho \cdot \Delta P} \qquad (5.7)$$

The overall flow coefficient for the valve is given by:

$$C^*_{v3} = \frac{C^*_{v1} \cdot C^*_{v2}}{\sqrt{C^{*\,2}_{v1} + C^{*\,2}_{v2}}} \qquad (2.6)$$

where the flow coefficient of the orifice alone is:

$$C^*_{v1} = \frac{(d_2/d_1)^2}{\sqrt{K_{L1} + ([d_2/d_1]^2 - 1)^2}} \qquad (2.8)$$

and the flow coefficient of the disc alone is:

$$C^*_{v2} = \frac{Z}{\sqrt{K_{L3} + (Z - 1)^2}} \qquad (2.11a)$$

where

$$Z = 1 - \left(\frac{d_3}{d_1}\right)^2 \cos\theta - \frac{4A}{\pi d_1^2} \qquad (3.14)$$

The symbols in the above equations are defined in the Nomenclature.

The entrance loss K_{L1} for the orifice and K_{L3} for the disc must be determined for the forward and reverse flow conditions. Also, the entrance loss for the disc must be determined as a function of disc opening and pipe flow Reynolds number. These coefficients are evaluated under steady-flow conditions.

5.3 Experimental Valve Flow Characteristics

5.3.1 Coefficient Representation of Valve Characteristics

The test set-up and procedure to determine the pressure drop across the valve and the flow forces against the valve disc are presented in Appendix D. By applying Equations 5.1, 5.3, 5.5 and 5.6 to the forward flow force measurements, the drag coefficient C_{ND} normal to the disc is evaluated and presented in Figure 5-2. Similarly, applying the equations mentioned in Section 5.2.2 to the forward flow pressure drop measurements results in determining of the normalized flow coefficient C_{v3}^* as presented in Figure 5-3. Both coefficients are shown versus Reynolds number

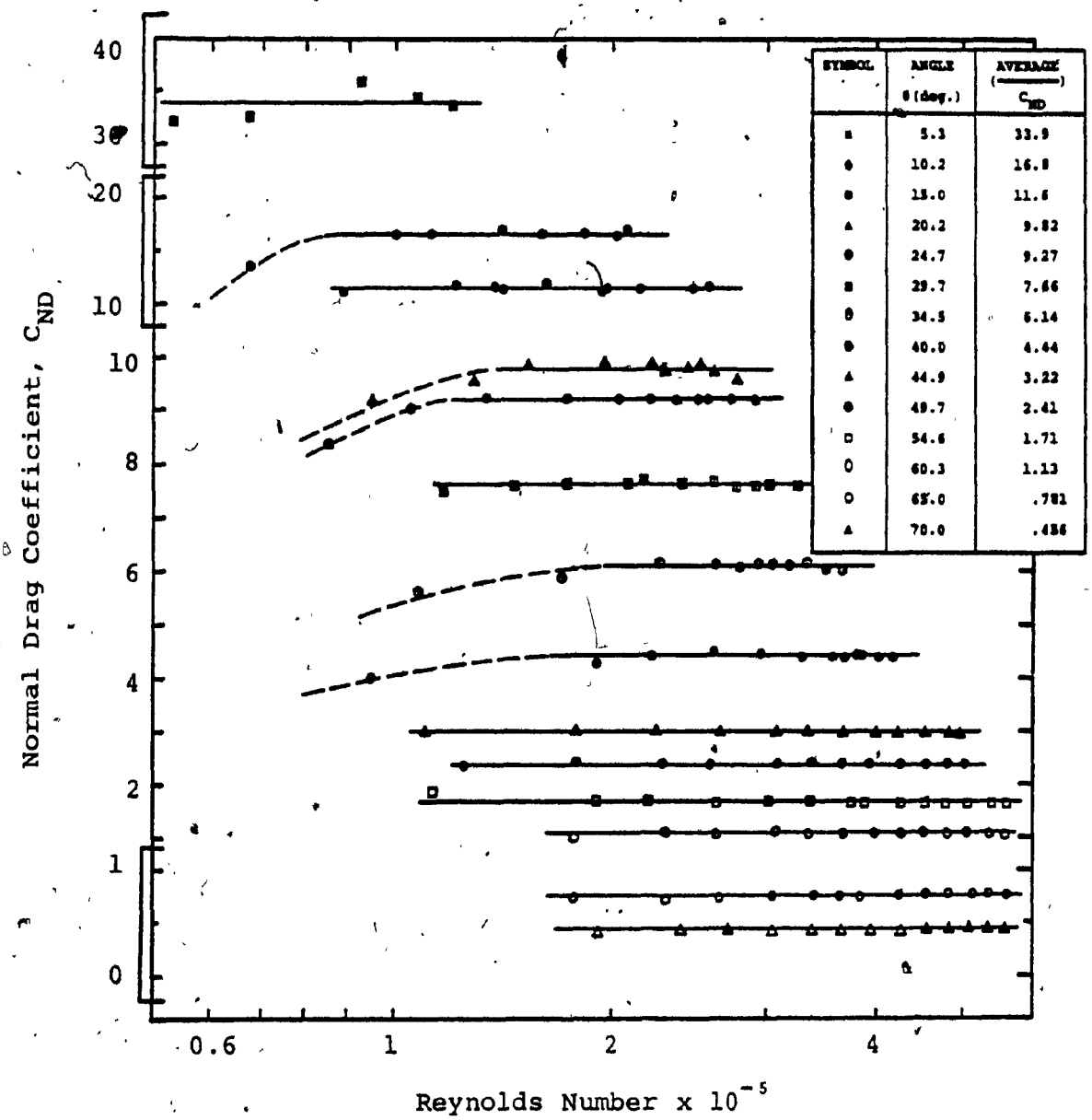

Figure 5-2. Disc Drag Coefficient for Forward Flow

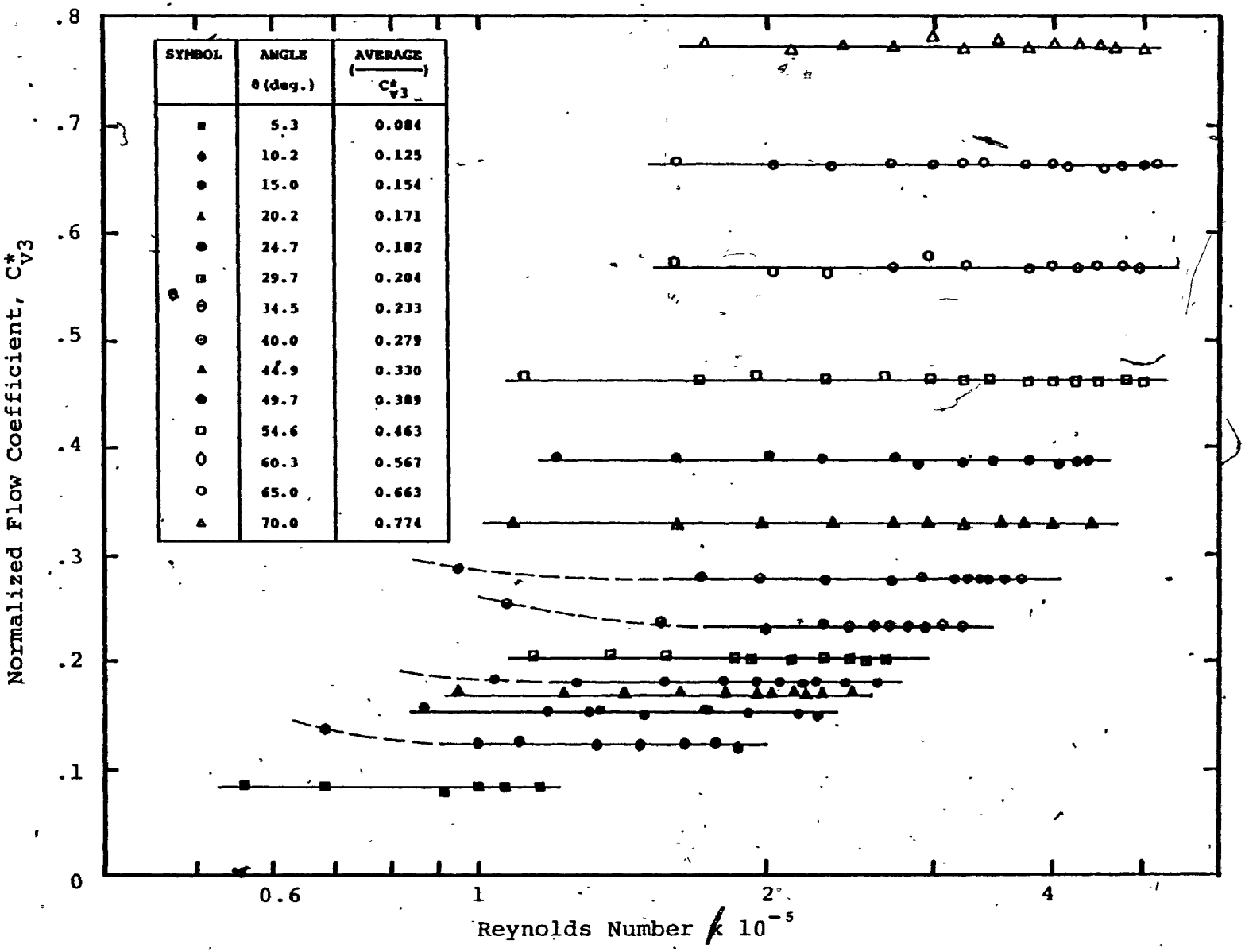

Figure 5-3. Valve Flow Coefficients for Forward Flow

calculated with respect to the pipe fluid flow velocity and for various disc angle positions.

With reference to Figures 5-2 and 5-3, the solid lines show average values for the data points where the coefficient changes negligibly with the Reynolds number. Data points at lower Reynolds number deviate from the average coefficients and may be caused by a change in the characteristics of the wake behind the disc. This effect is not studied and the average coefficients are assumed at these regions. This assumption is justified by the fact that a check valve opens rapidly and only stays in the low flow region for a short period of time. At low Reynolds number the experimental data deviate from the pressure drop and force calculations using the average coefficients. The maximum deviation is 20 percent with respect to the pressure drop and force measurements.

Figure 5-2 shows the drag coefficient plots. With reference to the figure, the drag coefficient is seen to increase as the valve opening decreases. This behavoir indicates an increase in flow force against the disc with a decrease in valve opening. Figure 5-3 show plots of the valve flow coefficient. Since the flow force against the disc is related to the pressure drop across the valve, the plots in the figure show a decrease in flow coefficient with smaller valve openings. Smaller valve coefficients indicate

an increase in valve pressure drop.

Substituting the experimental force data for reverse flow in Equation 5.2 and Equations 5.4 to 5.6 give the drag coefficient C_{ND} as shown in Figure 5-4. Similarly, the valve flow coefficient C^*_{v3} shown in Figure 5-5 is calculated with the experimental pressure drop data substituted in the equations described in Section 5.2.2. Both the drag and the flow coefficient figures are shown versus pipe flow Reynolds number for various disc angles. The solid lines passing through the data points is the average coefficient.

Referring to Figure 5-4, data points above 40 degrees at low Reynolds number deviate from the average drag coefficients. This effect of the deviation is not reflected in the corresponding flow coefficients shown in Figure 5-5, and may be due to the fact that the orifice downstream from the disc affects the wake behind the disc. At low Reynolds number the experimental force measurements deviate from the forces calculated using the average drag coefficients. These deviations are less than 20 percent.

The plots in both figures show that for disc angles between 15 degrees and 25 degrees, both the drag coefficient and the flow coefficient do not change much with disc angle. This is mainly due to the small change in the projected area of the disc within this disc opening range. However, for

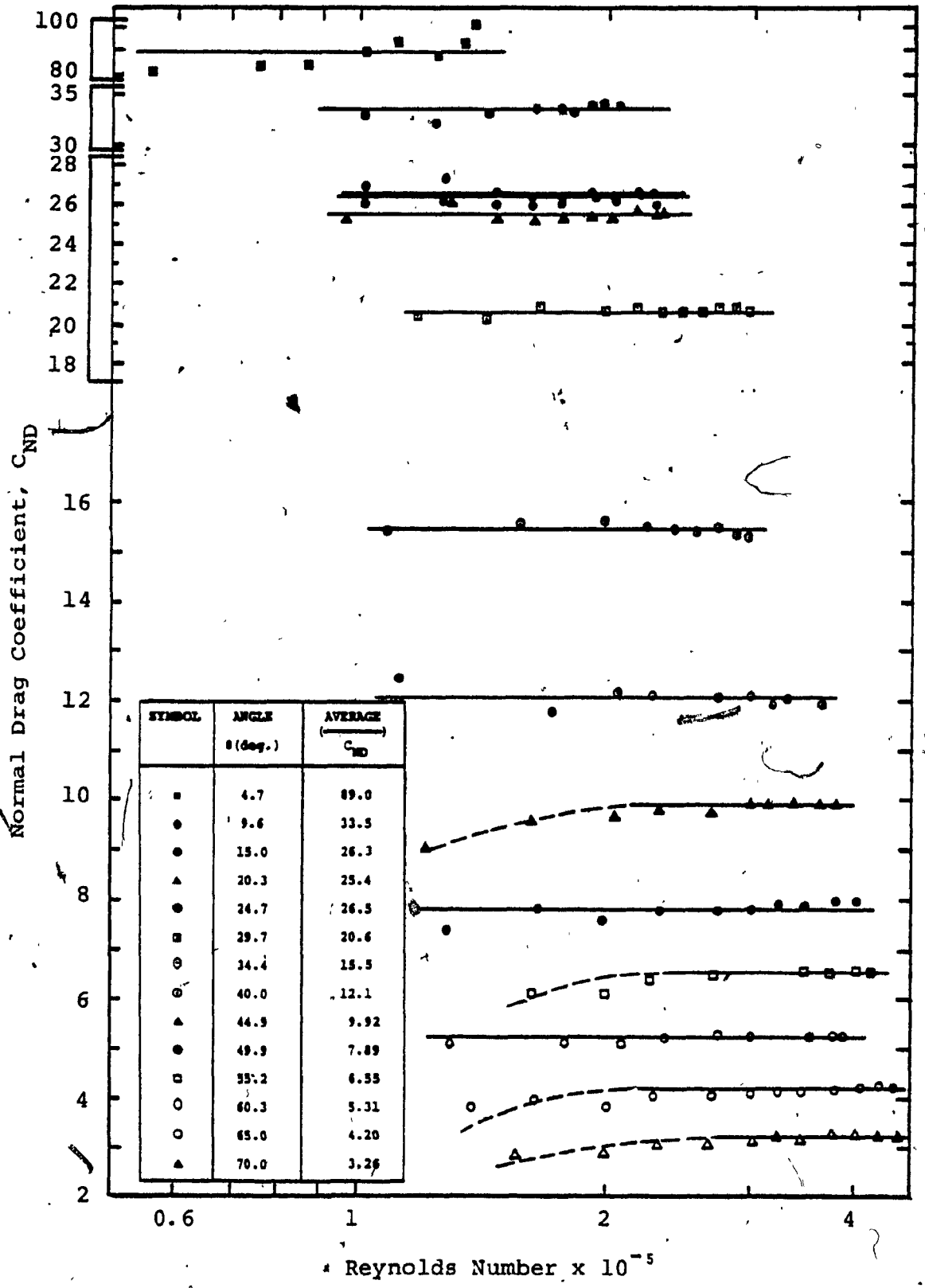

Figure 5-4. Disc Drag Coefficient for Reverse Flow

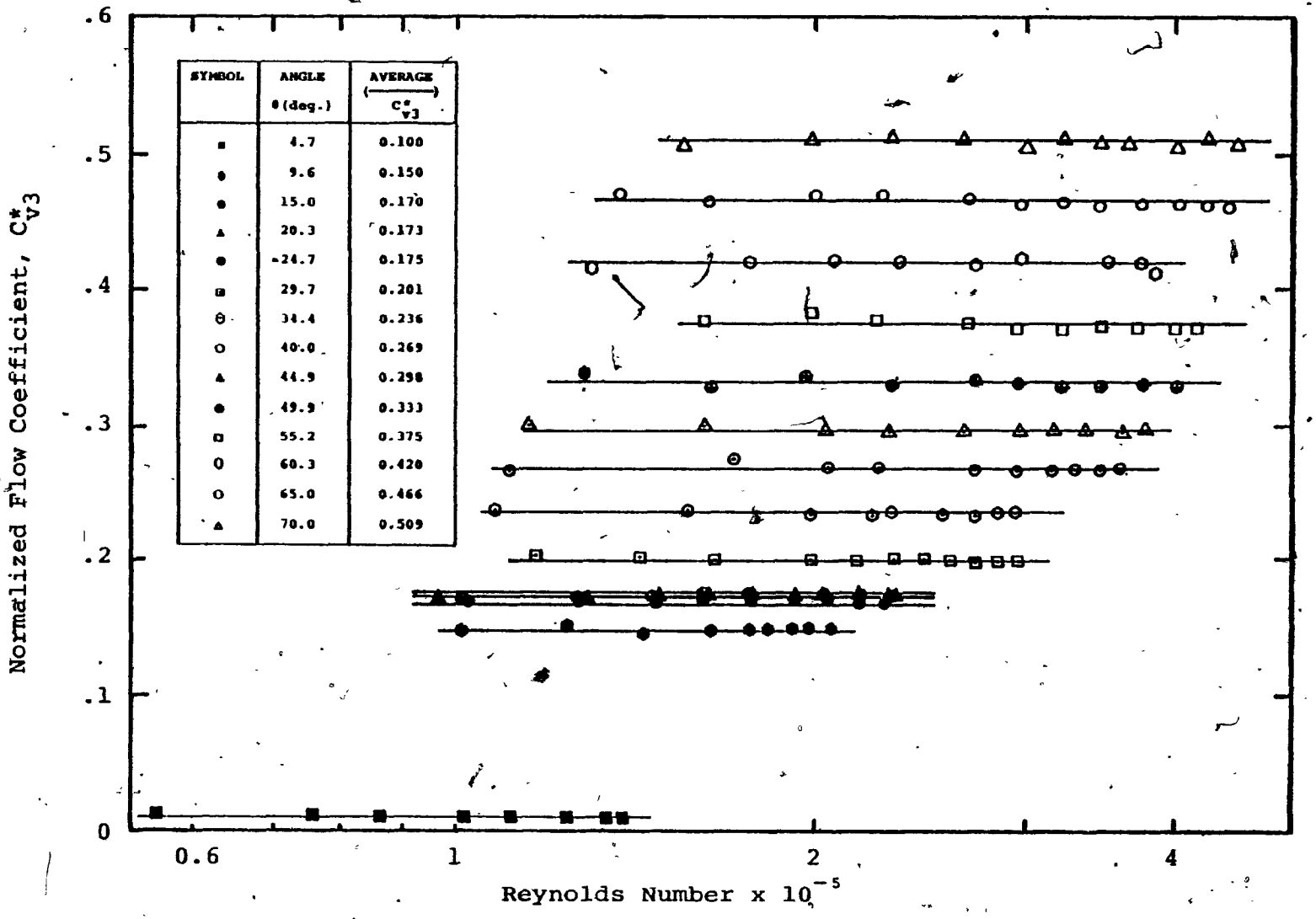

Figure 5-5. Valve Flow Coefficients for Reverse Flow

disc openings below 15 degrees the magnitude of the flow coefficient again decreases indicating an increase in valve pressure drop. Similarly, for angles below 15 degrees the magnitude of the drag coefficient again increases indicating an increase in flow forces against the disc.

5.3.2 Preparation of the Coefficient Values for Use in the Dynamic Simulation

The experimental forward flow coefficient C^*_{v1} for a well rounded orifice was found to be 1.010. Experimental results show that this coefficient changes negligibly within the range of Reynolds number tested from 1.37×10^5 to 4.87×10^5. Substituting C^*_{v1} in Equation 2.8 gives the entrance loss to the orifice as:

$$K_{L1} = 0.078 \qquad (5.8)$$

The valve overall flow coefficient C^*_{v3} for forward flow conditions is replotted in Figure 5-6 as a function of disc angle θ. By utilizing the coefficients C^*_{v1} and C^*_{v3}, the flow coefficient C^*_{v2} contributed by the disc is calculated from Equation 2.6 and is plotted in Figure 5-6. For angles less than 40 degrees, calculations indicate that the orifice contributes less than 10 percent to the total valve pressure loss, and that the valve pressure drop may be assumed to be primarily due to the disc.

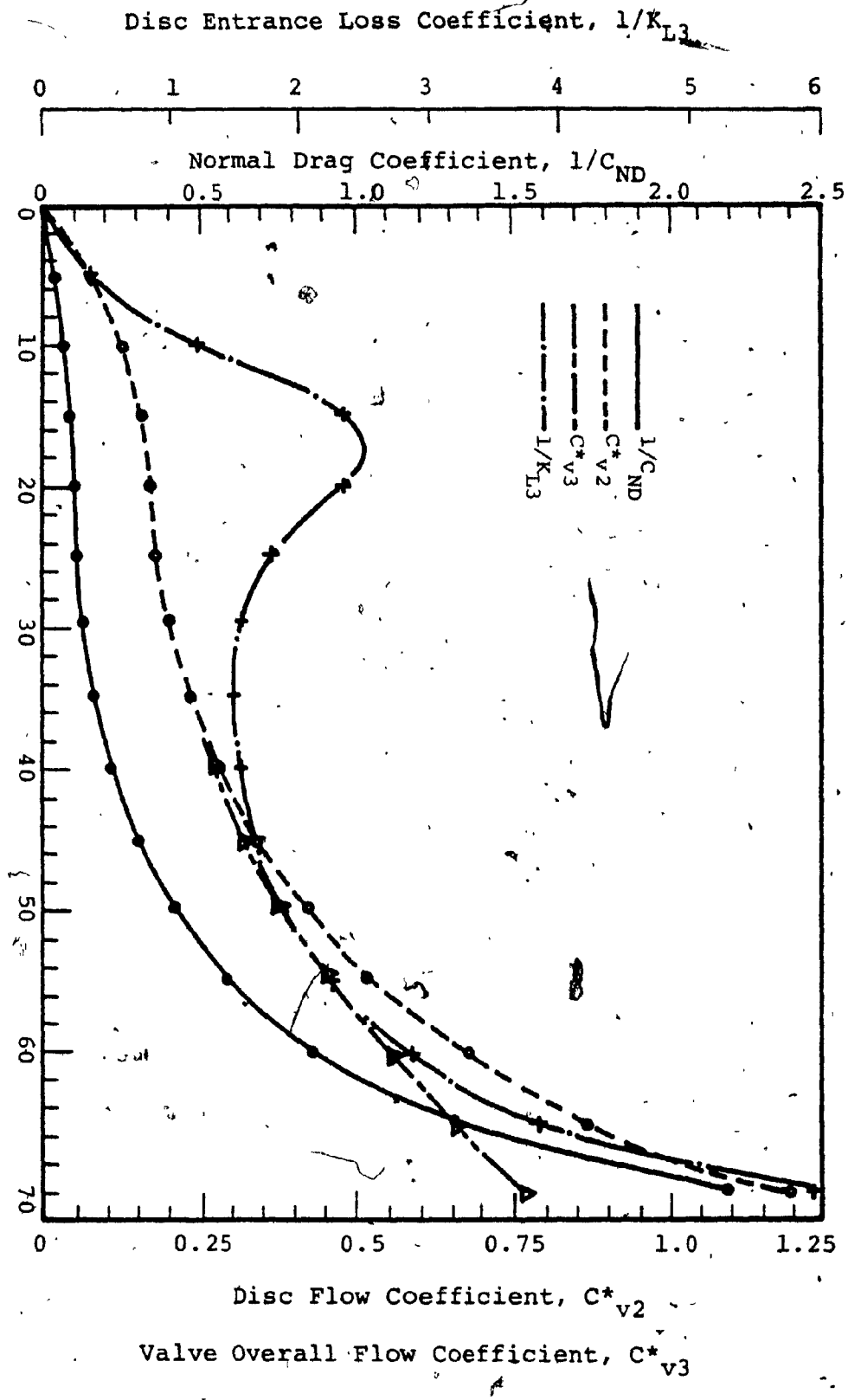

Figure 5-6. Valve Coefficients vs Disc Opening; Forward Flow

The entrance loss coefficient K_{L3} for the disc is calculated by substituting C^*_{v2} in Equation 2.11a and 3.14. The reciprocal of K_{L3} is plotted in Figure 5-6 versus the disc angle. The discrete data are rendered continuous by employing the natural cubic spline method of interpolation, as shown in Appendix [H]. The continuous representation of K_{L3} is suitable for computer simulation, and will be applied in Chapter 6.

Referring to Figure 5-6, for angles above 35 degrees the inverse of the entrance loss coefficient increases in a quadratic fashion as the disc angle increases. This indicates the entrance loss coefficient K_{L3} decreases as the disc opens more and disturbs the flow less. For angles less than 35 degrees, $1/K_{L3}$ no longer varies in a quadratic fashion. This deviation from the quadratic variation is attributed to the changes in disc shape disturbing the flow path. The reciprocal of the entrance loss, as the disc angle decreases from 35 degrees until the valve is completely closed, increases to a local maxima and then decreases to zero at valve closure. When the valve is closed, $1/K_{L3} = 0.0$ indicates an infinite value for the entrance loss K_{L3} since the flow through the valve is completely blocked.

Figure 5-6 shows a plot of the reciprocal of the drag coefficient C_{ND}. This coefficient has been determined from

Section 5.3.1. With reference to the figure, $1/C_{ND}$ decreases monotonically with the decrease in disc opening. This indicates the flow forces against the disc increases as the disc closes. When the valve is completely closed, the force on the disc is dependent on the static pressures across the disc. The flow coefficient C^*_{v2} contributed by the disc varies with disc opening in a similar fashion as compared to the drag coefficient $1/C_{ND}$. As the disc angle decreases, the flow coefficient C^*_{v2} decreases indicating an increase in pressure drop across the disc. This similarity in variation between the disc flow coefficient and the disc drag coefficient results from the fact that the pressure drop across the disc is related to the force on the disc.

For reverse flow, the orifice flow coefficient C^*_{v1} is found experimentally to be 0.593. Substituting this value in Equation 2.8 gives an orifice entrance loss of:

$$K_{L1} = 0.63 \qquad (5.9)$$

Figure 5-7 shows a plot of the valve overall flow coefficient C^*_{v3} found from Section 5.3.1, and the flow coefficient C^*_{v2} contributed by the disc, for reverse flow conditions. The coefficients are shown for various positions of disc angles tested. C^*_{v2} is calculated from experimental pressure drop measurements similar to the procedure applied to the forward flow coefficients previously described. Pressure loss calculations using the

orifice flow coefficient and the disc flow coefficient indicate that for disc openings below 30 degrees, the valve pressure drop is primarily due to the disc since the loss contributed by the orifice is less than 10 percent.

Following a similar procedure as applied to the forward flow data, the entrance loss coefficient K_{L3} to the disc is calculated and rendered continuous by the natural cubic spline method of interpolation. The reciprocal of K_{L3} is shown plotted in Figure 5-7. For disc openings greater than 50 degrees, $1/K_{L3}$ increases in a quadratic fashion with the increase in disc angle. For openings less than 50 degrees, the reciprocal of the loss coefficient fluctuates and deviates from the quadratic variation with the increase in disc angle. This change from the quadratic variation with disc angle, as previously reasoned for the forward flow disc entrance loss, is attributed to the changing disc projected shape disturbing the flow path.

On Figure 5-7 is also plotted the reciprocal of the drag coefficient C_{ND} found from the previous section. The continuous representation of this coefficient is made by the natural cubic spline method of interpolation. As noticed in the forward flow description of the drag coefficient $1/C_{ND}$ and the flow coefficient C^*_{v2} contributed by the disc, these two coefficients for reverse flow also vary in a similar fashion with the increase in disc opening.

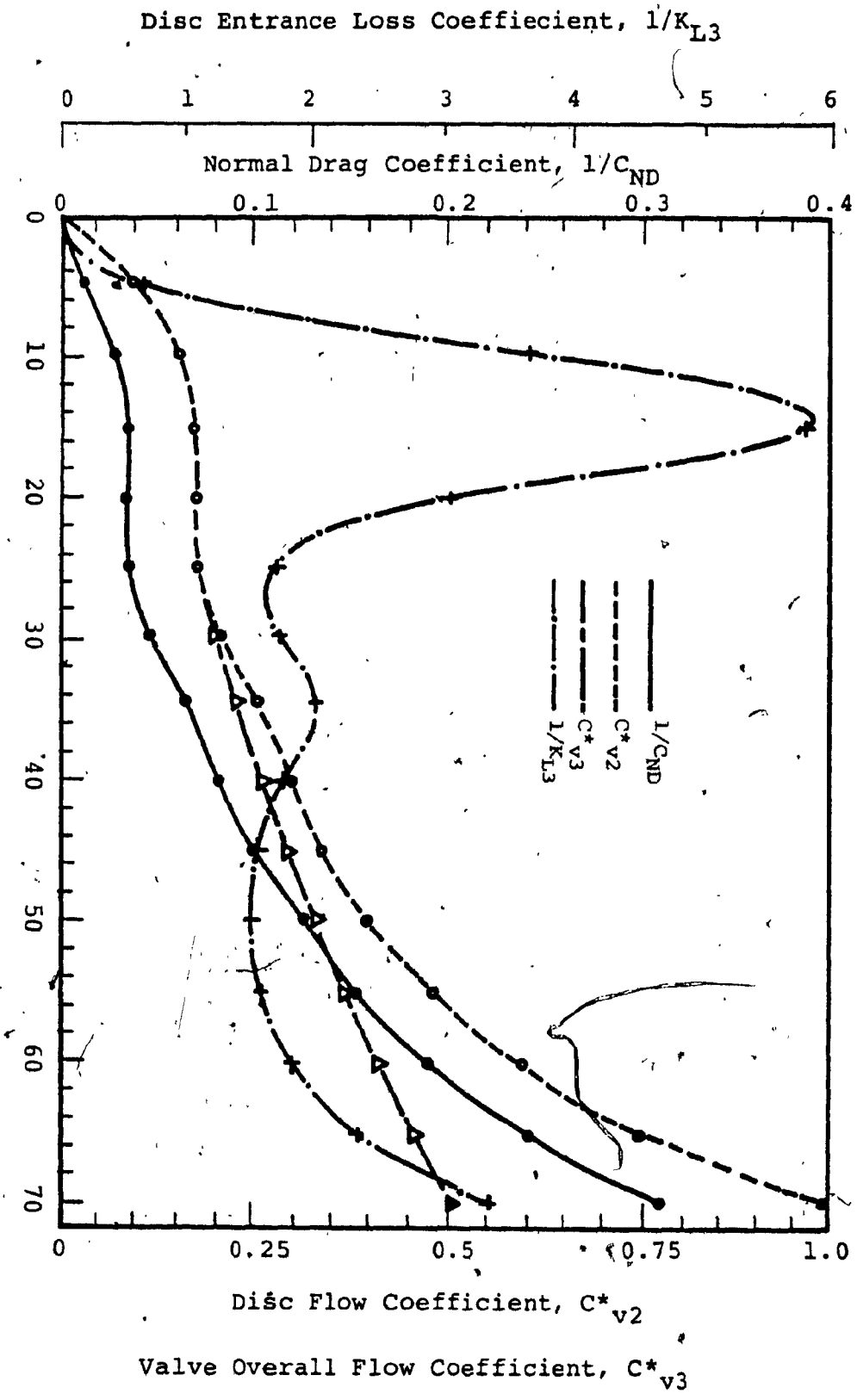

Figure 5-7. Valve Coefficients vs Disc Opening; Reverse Flow

CHAPTER 6

UNSTEADY PIPE FLOW AND CHECK VALVE RESPONSE

6.1 Introduction

As mentioned earlier, the main function of the check valve is to provide an infinite resistance to reverse flow. In addition to the primary function, performance requirements for the check valve are rapid response and non-slam action. Slow valve response can be due to friction inherent in the valve moving parts, inertia of the moving parts, fluid damping, as well as damping provided to control the speed of valve closure. The adverse effect of a slow valve closure is the result of reverse flow. Reverse flow results in flow forces* which cause the undamped valve to close rapidly. The sudden stoppage of this reverse flow converts all the kinetic energy into large waterhammer pressures. Valve closure before reverse flow develops, reduces waterhammer phenomena. When a non-slamming mechanism is employed in the final stage of the valve closure, the reverse flow decelerates gradually thus reducing waterhammer effects. For each particular valve and pipe system arrangement, a compromise is required between the maximum amount of reverse flow and the disc impact force upon closure producing the slam effect.

In this chapter, a piping system containing the hydro-pneumatic spring-damper check valve, described in Chapter 4, is analysed. A dynamic simulation of the check valve and piping system is carried out on a digital computer. The response of the check valve due to the spring-damper mechanism and its effects on waterhammer transients are evaluated.

The pipeline fluid transients are approximated by modelling the pipe system using the lumped-parameter method. The pipe length is divided into sections where the fluid inertia, fluid capacitance and pipe elasticity, and shear stress between the fluid and pipe walls are lumped. The check valve with the moving disc is considered as a lumped variable resistance component.

The preliminary studies of this chapter has been published by Hong and Svoboda [21].

6.2 Lumped-Parameter Modelling of Transient Pipe Flow

6.2.1 Fluid Circuit Modelling and System Equations

The pipe system is modelled by the method of lumped-parameters [22]. To illustrate this method, consider the piping arrangement shown in Figure 6-1a. The system consists of a constant head reservoir and a variable flow

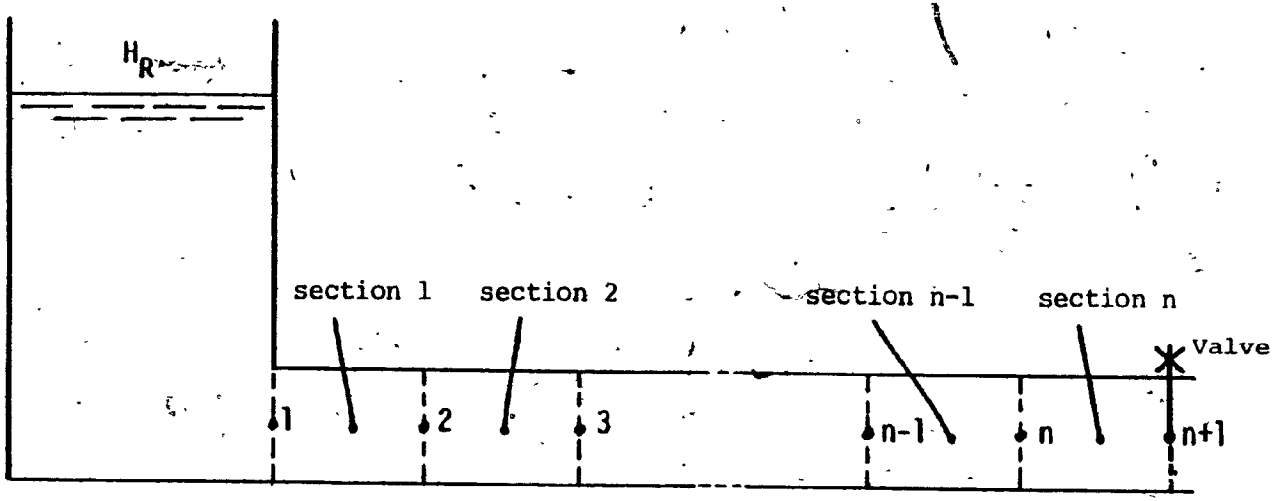

a) System Schematic

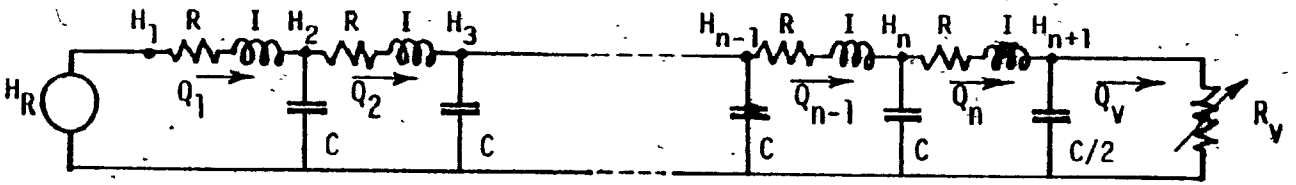

b) Circuit Diagram

Figure 6-1. Illustration of Lumper-Parameter Method

control valve placed at extreme ends of a straight pipe. In the lumped-parameter method, the pipe is divided into n-sections of equal lengths, where the fluid inertia and pipe friction are lumped. At the ends of each section corresponding nodal points represent the pressure head at these locations. Thus, for n-sections result in n+1 nodes where the fluid capacitance and pipe elasticity are lumped.

The circuit representing the pipeline system is shown in Figure 6-1b. Between each consecutive node a lumped resistance R and fluid inertance I represent, respectively, the friction losses and the fluid inertia in the corresponding sections. At each interior node a capacitance C connects the node to ground. C represents the sum of half the capacitance of adjacent lumps. At extreme ends of the pipe are inserted capacitance value C/2. The constant head reservoir is represented by a constant potential source H_R. Consequently, the capacitance inserted at node number 1 is irrelevent and ignored. At the other extreme pipe end the flow control valve is represented by a lumped variable resistance R_v.

With reference to Figure 6-1b, the coupled non-linear differential equations relating the pressure head H at each interior node to the flow rate Q through each section, are given by:

$$\frac{dH_i}{dt} = \frac{1}{C}(Q_{i-1} - Q_i) \quad ; \quad i = 2,3,\ldots,n \tag{6.1}$$

$$\frac{dQ_i}{dt} = \frac{1}{I}(H_i - H_{i+1} - R \cdot Q_i^2) \quad ; \quad i = 1,2,\ldots,n \tag{6.2}$$

At both ends of the pipe, one of the two variables, H or Q, must be known. At the resevoir, the boundary condition is given by:

$$H_1 = H_R \tag{6.3}$$

and at the valve connection, the boundary condition is given by:

$$Q_v = H_{n+1}^{\frac{1}{2}} / R_v \tag{6.4}$$

$$\frac{dH_{n+1}}{dt} = \frac{2}{C}(Q_n - Q_v) \tag{6.5}$$

6.2.2 Evaluation of the Lumped Parameters

Considering a single pipe section as shown in Figure 6-2, the force balance on the fluid of length L/n within the pipe of diameter d_1 is given by:

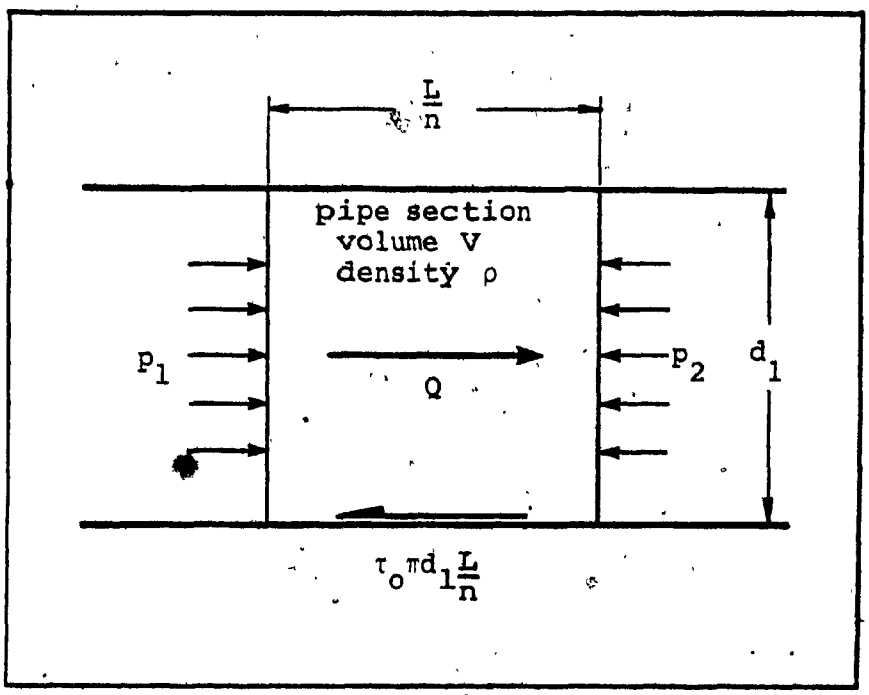

Figure 6-2. Interaction of Forces on a Single Fluid-Pipe Section

$$P_1A_1 - P_2A_1 - \tau_o \pi d_1 \frac{L}{n} = \rho \frac{L}{n} \cdot \frac{dQ}{dt} \qquad (6.6)$$

where A_1 is the pipe area, ρ is the fluid density, and τ_o is the shear stress between the fluid and pipe walls. The first two terms on the left hand side of Equation 6.6 represent the force due to the pressure difference across the fluid section. The third term represents the resistance force due to pipe friction. The term on the right hand of the equation is the fluid inertia force.

For turbulent flow the shear stress expressed in terms of the Darcy-Weisbach friction factor f is given by [13]:

$$\tau_o = \frac{f\rho Q^2}{8A_1^2} \qquad (6.7)$$

This friction loss term for steady-flow calculations will be considered valid, also, for transient flow calculations [23].

Since $P = \rho gH$, where g is the acceleration due to gravity, and substituting Equation 6.7 in Equation 6.6 and rearranging, gives:

$$H_1 - H_2 - RQ^2 = I \frac{dQ}{dt} \tag{6.8}$$

where the pipe friction and fluid inertia, for a single pipe section, are given respectively by:

$$R = \frac{f\,L}{2\,g\,d_1\,A_1^2\,n} \tag{6.9}$$

$$I = \frac{L}{g\,A_1\,n} \tag{6.10}$$

The capacitance of the pipe sections is derived from the fluid continuity equation. Referring to Figure 6-2, the fluid mass m within the control volume V is:

$$m = \rho V \tag{6.11}$$

Differentiating this equation with respect to time gives:

$$\frac{dm}{dt} = \rho \frac{dV}{dt} + V \frac{d\rho}{dt} \tag{6.12}$$

The term on the left hand side represents the change in fluid mass within the control volume. The first term on the

right hand side represents the elasticity of the pipe material, and the second term represents the compressibility of the contained fluid. Dividing both sides of Equation 6.12 by the fluid density ρ, and considering the fluid flow in and out of the control volume, the net change in flow within the pipe section is given by:

$$\Delta Q = \frac{dV}{dt} + \frac{V}{\rho} \cdot \frac{d\rho}{dt} \tag{6.13}$$

The elasticity of the pipe may be relevant along its sectioned length L/n and along its diameter d_1. If the pipe, for example, is only flexible along its diameter, the change in pipe area A_1 with pipe pressure P is [23]:

$$\frac{1}{A_1} \cdot \frac{dA_1}{dt} = \frac{d_1}{eE} \cdot \frac{dP}{dt} \tag{6.14}$$

where e is the pipe wall thickness and E is the Young's modulus of elasticity of the pipe material.

Since volume $V = LA_1/n$ and since the sectioned length L/n is constant, the change in pipe volume containing the fluid due to the change in pipe area caused by elasticity is:

$$\frac{dV}{dt} = \frac{L}{n} \cdot \frac{dA_1}{dt} \qquad (6.15)$$

The definition of the bulk modulus of elasticity β for a fluid is given by:

$$\beta = \rho \frac{dP}{d\rho} \qquad (6.16)$$

Since $P = \rho g H$, and substituting Equations 6.14 to 6.16 in Equation 6.13 and rearranging, gives:

$$\Delta Q = C \frac{dH}{dt} \qquad (6.17)$$

where the capacitance C of the pipe section is given by:

$$C = \frac{g A_1 L}{c_o^2 n} \qquad (6.18)$$

and c_o is the pressure wave propagation speed for the fluid, which is given by:

$$c_o = \sqrt{\frac{\beta/\rho}{1 + \frac{\beta d_1}{eE}}} \qquad (6.19)$$

Equation 6.19 indicates that the speed of pressure wave propagation is dependent on both the fluid property and pipe material property. This in turn affects the fluid capacitance given by Equation 6.18. In the subject of waterhammer given in the Bibliograhy, different allowances, such as pipe axial and transverse stress strain relations, for the pipe flexibilty are considered. For all cases, pipe elasticity affects the wavespeed. For a rigid pipe, Young's modulus of elasticity E is considered infinite, and Equation 6.19 reduces to its simplest form given by:

$$c_o = \sqrt{\frac{\beta}{\rho}} \qquad (6.20)$$

in which the speed of wave propagation is only dependent on the fluid property.

As mentioned earlier, nodal capacitance values are equal to the sum of half the capacitance values of adjacent lumps. Equations 6.18 to 6.20, however, shows that the wavespeed, and hence the capacitance of adjacent pipe sections are of different magnitudes due to the change in fluid density along the pipeline. The magnitude of the density change, however, is negligibly small [20], and the wavespeed and capacitances of all the sections are assumed equal.

6.2.3 Step Response of Pipeline Model

As the number of sections representing the fluid system is increased, the behavior of the model approaches that of the actual system. The increase in the number of sections would result in better approximation of the propagation wavespeed and the model would respond to a wider frequency range of input. The solution of the model, in this case, would require a larger number of coupled equations to describe the system. Consequently, a smaller integration step size is required. Furthermore, conventional methods of integration would be inadequate since the system becomes very stiff. Although the actual system is of infinite order, the lumped-parameter method must describe the system with a finite number of sections. This means the solution by the method of lumped-parameters, only approximates the true solution.

To illustrate the solution by the method of lumped-parameters, the piping system of Figure 6-1 is simulated on a digital computer. The pipe length, pipe diameter, and friction factor of the piping system are, respectively, $L = 600$ m, $d_1 = 202.7$ mm and $f = 0.02$. The pressure wave propagation speed c_o is taken to be 1200 m/s, and the pipe is assumed to be rigid. The resevoir head H_R is initially set at 150 m of water. The reservoir head is then suddenly raised to 300 m of water at 1 second. Throughout the

simulation the valve is kept closed in order to observe the waterhammer wave propagation and pressure surges at the valve end.

The pressure surges at the valve end are shown in Figure 6-3. Three plots are shown in the figure. These are for the lumped-parameter method using 5 and 10 pipe sections, and for comparison, using the method of characteristics [23] with 10 sections. A fourth-order Runge-Kutta integration method is used to solve the coupled differential equations for the lumped-parameter method.

The plot depicted by the method of characteristics show that the pressure disturbance initiated at the reservoir end is not felt at the valve until 0.5 seconds later. This time period corresponds to the value of L/c_o. The decaying head oscillation, due to pipe friction, as the pressure wave travels back and forth along the pipe length has a period of 2 seconds, corresponding to the value of $4L/c_o$. The peaks of the head oscillation are approximately flat.

The plots obtained using the lumped-parameter method with 5 and 10 sections, show that the head at the valve begins to rise appreciably after 0.3 and 0.4 seconds, respectively, after the reservoir head disturbance. The period of pressure wave oscillation is approximately $4L/c_o$

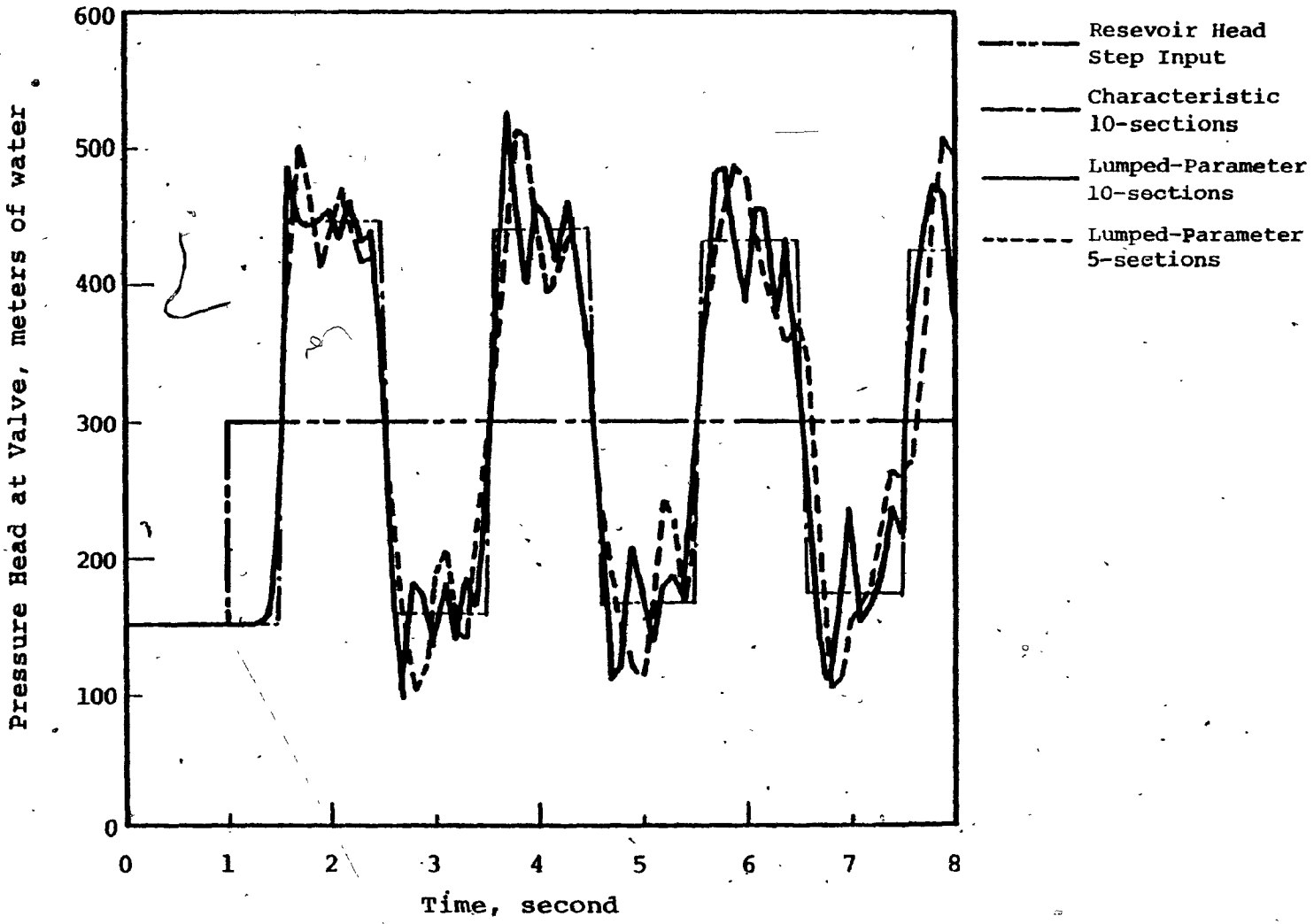

Figure 6-3. Response Comparison of Lumped-Parameter Method to the Method of Characteristics

seconds, for both cases. The plots also show some oscillations superimposed on the peaks. These oscillations tend to increase when the number of sections representing the pipeline is increased.

The figure shows that the three plots are decaying with time. This is due to the energy loss caused by the pipe friction. Furthermore, the response of the lumped-parameter model is expected to approach that of the characteristic method as the number of sections representing the pipe is increased. This conclusion demonstrates the advantage of the characteristic method in dealing with waterhammer transients in simple pipeline systems. However, when the check valve dynamic transients need to be considered, the characteristic method tends to be more difficult to implement.

6.3 Check Valve and Pipeline Transient Response

6.3.1 System Description

In order to observe the dynamic behavior of a check valve when the flow in the pipe is unsteady, the check valve is placed in a piping system as shown in Figure 6-4a. Both pipes adjacent to the valve are 600 m long with an inside diameter of 202.7 mm and a friction factor of 0.02. The pressure wave propagation speed is 1200 m/s. The check

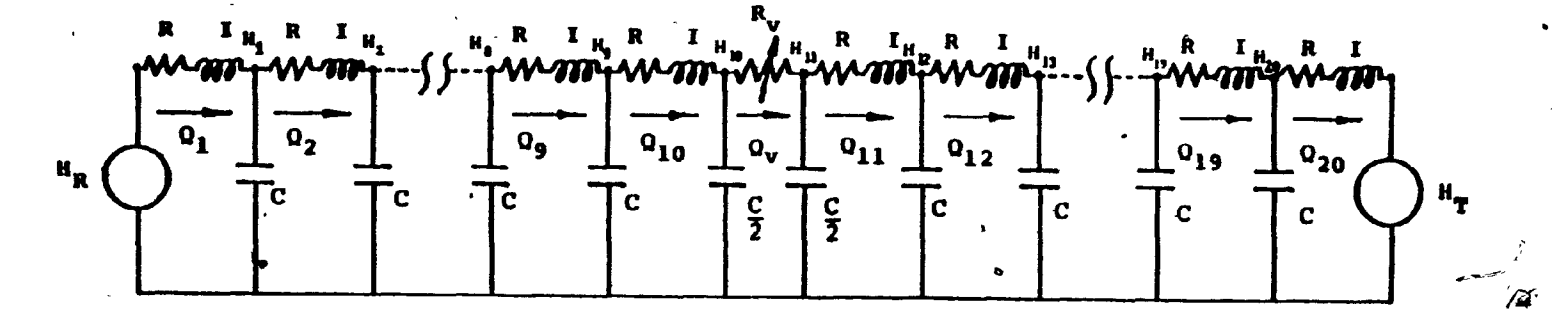

b) Circuit Diagram

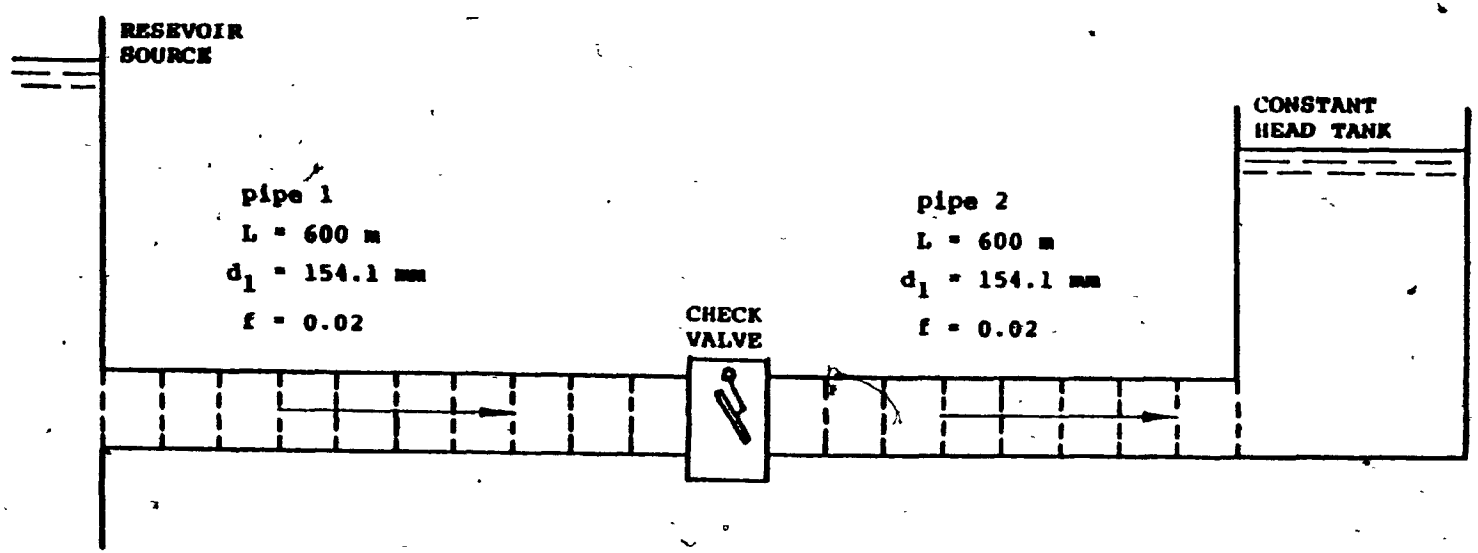

a) System Schematic

Figure 6-4. Check Valve and Pipeline System Simulation Example

valve is 200-mm in size, and is equiped with the hydro-pneumatic spring and damper mechanism described in Chapter 4. For this particular valve, the orifice diameter, disc diameter, hinge arm length, hinge arm thickness, and disc pivot are, respectively:

$$d_2 = 165.1 \text{ mm}$$
$$d_3 = 181.0 \text{ mm}$$
$$\ell_A = 114.3 \text{ mm}$$
$$2\mu = 44.5 \text{ mm}$$
$$d = 18.7 \text{ mm}$$

These design dimensions are described in Chapter 3.

The simulation of the pipeline and check valve system makes use of the studies presented from Chapters 4 and 5, and from the preceeding part of Chapter 6. The information flow between the variables studied are presented in the block diagram of Figure 6-5. With reference to the figure, the hydro-pneumatic spring-damper check valve described in Chapter 4 is mathematically modelled. Dynamics of the valve requires an input torque T_o and the resulting output is the valve disc opening angle θ and disc angular velocity ω. Then, from the disc angle information, the check valve flow coefficient C^*_{v3} and the drag coefficient C_{ND} representing the valve characteristics are calculated from Chapter 5. Knowing the valve pressure drop ΔP and the flow coefficient,

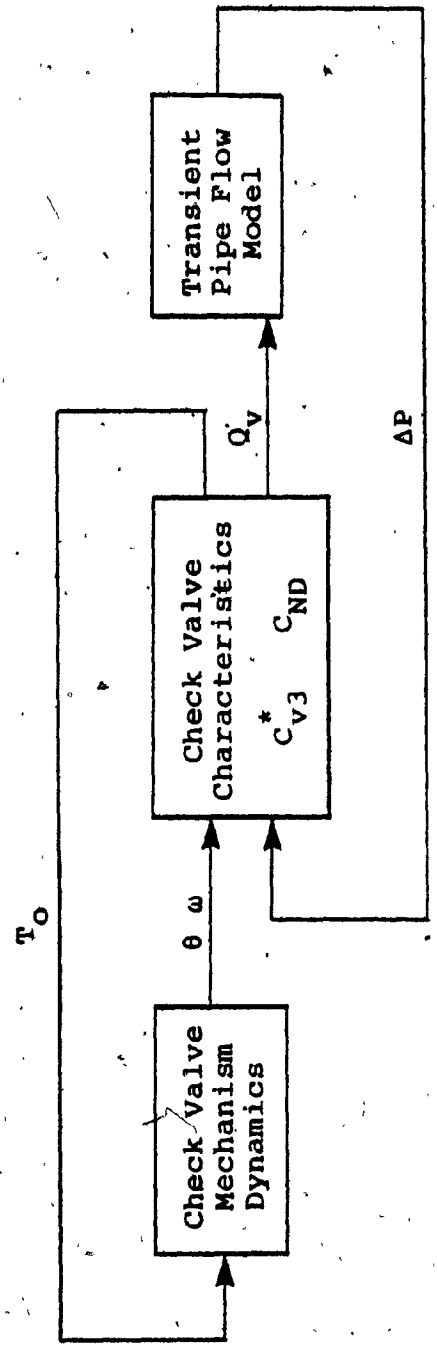

Figure 6-5. Block Diagram of Variables Studied: Information Flow.

the flow Q_v through the valve is calculated. The flow torque T_o created at the disc arm is then calculated by knowing the valve flow and drag coefficient, and the first information loop in the block diagram is closed. Finally, the valve flow provides the boundary condition neccessary for the lumped-parameter method of Chapter 6 to determine the transient pressure head ΔH (or ΔP) across the valve. Thus, the solution of valve pressure drop ΔP provides information for the valve characteristics and the second loop in the information flow is closed. The required software to simulate the system shown in Figure 6-4a as described by the block diagram of Figure 6-5 is listed in Appendix [H].

The equivalent circuit representing the system to be simulated is shown in Figure 6-4b. The fluid head at the reservoir and at the tank is H_R and H_T, respectively. The system is modelled using 10 sections for each of the pipe lengths. The check valve is represented by a variable resistance R_v. The two capacitances directly adjacent to the valve do not include the compressibility of the fluid contained within the valve. This is because the assumption stated in Section 5.1 implies that the fluid inertance and compressibility effects are neglected at the valve.

The speed of valve closure depends on the accumulator precharged pressure and on the amount of damping provided by

the viscous resistor. These two components are shown in Figure 4-1. The accumulator is precharged at 1.034 MPa according to the valve manufacturer's recommendations [24]. When the valve disc is fully opened at 60 degrees, the accumulator pressure reaches 1.235 MPa. From Chapter 5, the valve flow characteristics are determined for this disc opening. Also, from Chapter 5, the pressure drop across the valve and the flow force against the disc may be determined for any flow rate through the valve. Thus, using the force balance equation on the valve disc, the steady pipe flow required to keep the valve opened, is calculated to be 0.153 m^3/s, and the difference in reservoir to tank head required to sustain this flow is 137 m of water. In the simulation, this difference is set at 150 m of water yielding a steady-flow of 0.160 m^3/s. Thus, if the flow rate drops by 4.4 percent, the disc will start to close as early as possible to prevent reverse flow from developing. Furthermore, to obtain quick valve closure, the viscous resistor is set to a low damping value of 1.284×10^{13} $N\text{-}s/m^8$ [9].

6.3.2 Results of the Check Valve and Pipeline Simulation

At the beginning of the simulation the fluid heads at the reservoir and at the tank are 150 m of water, and the check valve is fully closed. Transient pipe flow is initiated by a ramp head rise at the reservoir. The

resulting fluid flow causes the check valve to open. When the valve is completely opened, the flow is allowed to settle before the fluid head at the reservoir is droped by a ramp decrease. The resulting fluid deceleration causes the valve to close. During both the check valve opening and closing sequence, the transient flow from the reservoir and from the tank, as well as the transient flow and pressure at the valve are observed. Also, the dynamic behavior of the check valve and its effects on the waterhammer pressures are observed.

a. **Opening Sequence**

Due to the ramp head rise of 150 m of water at the reservoir, as shown in Figure 6-6 beginning at 1.0 second until 1.5 second, the immediate lump of fluid in the first pipe is compressed and accelerated. A compression pressure wave starts toward the valve, causing successive lumps of fluid along the pipe to flow with corresponding head rises. Because the input head at the reservoir is a ramp function, the propagation wave is a succession of superimposed smaller pressure waves.

For the purpose of simplicity, assume for the moment the valve is already opened to some angle. Thus, when the compression wave reaches the tank, the head adjacent to the tank causes an unbalance and tank flow starts. The time for

the wave from the reservoir to reach the tank is $(L+L)/c_o$ seconds. From the simulation result this wave time is increased slightly since the valve requires a minimum cracking pressure to open. Also, because the method of lumped-parameters is an approximation, this wave time is, in turn decreased slightly. Referring to Figure 6-6, $(L+L)/c_o$ equals to 1.0 second, which corresponds to the time from the initial reservoir flow at 1.0 second to the beginning of the tank flow at 2.0 second.

Once the compression wave reaches the tank, it is fully reflected as an expansion wave. This expansion wave travels back upstream along the pipe, tending to decrease the head and increase the flow along its path. From the moment of reflection this expansion wave reaches the reservoir in another $(L+L)/c_o$ seconds. And upon reaching the reservoir the expansion wave is fully reflected as a compression wave and a new cycle begins. For a system with two reservoirs, its flow cycle time is $2(L+L)/c_o$ seconds. This is approximately the flow cycle time of 2 second for the reservoir and tank as shown in Figure 6-6.

Directly upstream from the check valve the head and flow, shown in Figure 6-7, begins to rise L/c_o seconds after the initial reservoir unbalance. This time corresponds to 0.5 second as shown in the figure. The incoming compression wave is fully reflected at the closed valve. This reflected

wave remain as a compression wave travelling back upstream towards the reservoir, and is superimposed on the original incoming wave as an additional head rise. If the valve remains closed for all time, the pipeline response would be similar to the response of Section 6.2.3.

Increasing fluid compression causes the valve head to rise further until the valve cracks open. When the valve opens the head is slightly relieved as fluid flows through. This causes a small expansion wave to be reflected in the upstream direction. Since the check valve opened quickly, the maximum head at the valve is approximately equal to the reservoir head. The check valve does not cause any significant waterhammer pressures.

Flow into the second pipe compresses the immediate lump of fluid and causes the head to rise. The head and flow directly upstream and downstream from the valve oscillate synchronously. This is because for a given flow rate the valve pressure drop is uniquely defined by its valve characteristics. This synchronous oscillation is seen in the comparison between Figures 6-7 and 6-8. The head oscillations are at a period of $2(L+L)/c_o$ seconds. Since the valve is located between the two pipes of equal length and diameter, the valve flow cycle time is half the frequency of the reservoirs. This frequency is $(L+L)/c_o$ seconds.

The cracking pressure head across the valve is 33.1 m of water for an accumulator precharged pressure at 1.2351 MPa. Figure 6-9 shows the pressure head across the valve and the flow through the valve. The cracking pressure is not indicated on the graph because the digital output at this time was an intermediate print-out. Once the valve cracks open, the pressure head drops and flow is related by the steady-flow coefficient C^*_{v3}.

The disc position and velocity response are shown in Figure 6-10. The initial opening velocity is not shown in the figure because the digital output at the time was an intermediate print-out. The first negative disc velocity indicates the pressure relief upstream from the valve when the disc first cracked open.

With increasing fluid flow the disc opens further and oscillates in response to the valve flow. These oscillations are clearly seen in the disc velocity response. A negative disc velocity indicates the hydro-pneumatic spring is driving the disc, while a positive velocity indicates the fluid flow is the driving force.

As the disc position approaches 48 degrees (at approximately 4.8 second), the lower cushion significantly reduces the disc velocity. Thus, the hydro-pneumatic spring and lower cushion acts as damper and limits the final disc

impact force and avoids damage to the opening check valve.

b. Closing Sequence

By reducing the reservoir head by 200 m of water, as shown in Figure 6-6 from 15 to 15.5 seconds, the disc starts to close when the valve flow decreases just under normal steady-flow. The negative velocity response in Figure 6-10 indicates that the hydro-pneumatic spring forces the disc to close.

In the simulation result the low viscous resistance provides quick disc response to the slowly decelerating valve flow. A comparison between the valve flow given in Figure 6-9 and the disc velocity from Figure 6-10 indicates that the disc velocity oscillates in phase (approximately 1 cps) with the flow. In other words, the disc is seen to be floating with the flow. At small disc openings, below 7 degees (above 20.5 second), the hydro-pneumatic spring force is small. The increasing disc velocity starts to decrease before the flow increases. This is because the forward flow forces are sufficient to balance the small spring force. Since the disc is moving with the flow, the disc closes at the instant the valve flow decelerates to zero. The valve closure time in Figure 6-10 corresponds to when the valve flow reaches zero, as shown in Figure 6-9.

When the disc reaches 12 degrees, the upper cushion acting as an additional damper for the final stage of disc closure, is provided to slow the speed of valve closure to reduce the disc impact force on its seat. Figure 6-10 indicates a change in the disc velocity at approximately 20 seconds (at 12 degrees) due to the cushion resistance. The figure does not indicate any significant disc velocity lag with respect to the valve flow given in Figure 6-9. When there is no reverse flow through the valve, as in this case study, damping provided by the upper cushion is not required.

Reopening of the valve after closure occurs if the head across the disc oscillate with an amplitude exceeding the cracking pressure. This bouncing effect of the disc is seen only once as indicated in the disc velocity and valve flow response shown in Figures 6-9 and 6-10, respectively. The time corresponding to the disc bounce occurs at 22.5 seconds. Disc bouncing does not occur again since the head across the disc never exceeds the cracking pressure.

During valve closure the head directly upstream and downstream from the valve oscillate synchronously at a period of $2(L+L)/c_o$ seconds. This is shown in the comparison between Figures 6-7 and 6-8. After valve closure, each pipe upstream and downstream from the valve become separate systems. The heads adjacent to the valve

oscillate at $4L/c_o$ seconds. From the figures, this cycle time corresponds to 2 seconds. The magnitude of these head oscillations are not severe since the valve closed at the instant the valve flow decelerated to zero. Also, reverse flow into the reservoir and tank, shown in Figure 6-6, are not severe due to the quick valve closure. With time, the pipe friction will eventually dampen all fluctuations and the piping system will come to rest.

6.4 Check Valve Effect on Waterhammer Pressures

For the particular case study described in the previous section, the viscous restrictor was set to a low damping value which provided quick valve response to the decelerating flow. The simulation results showed that the system flow decreased slowly. This allows the disc to respond quickly and move with the flow. The disc readjustes its position to the new flow and causes minor throttling of the valve flow. This response is desirable since the disc reached its seat at the instant the flow decelerated to zero, which resulted in minimum waterhammer pressures.

For the same piping system described in Section 6.3, consider as an illustrative example, that reverse flow has developed through the valve. For this situation, the reverse flow forces will urge the disc to close rapidly because of the low viscous resistance. Since the disc is

moving with the flow, the check valve causes minor throttling of the flow. When the closing disc reaches the stage where the upper cushion comes into effect, the disc velocity is suddenly reduced. This causes the reverse flow to experience, as in the case of a partial instantaneous valve closure, a sudden change in valve resistance. This sudden change in valve resistance requires the flow to readjust to the new resistance, and hence the flow is throttled. This results in compression waterhammer pressures downstream from the valve and expansion waterhammer pressures upstream from the valve. Because the upper cushion is in effect, the check valve moves slowly in response to the flow and gradually throttles the flow to zero to reduce the waterhammer pressures upon closure. For this case, water column separation may develop upstream from the valve. This discussion concurs with Krane and Cho [5].

Consider again the same piping system of Section 6.3, but with the viscous restrictor having a high damping value. A large viscous resistance causes the disc to close slowly permitting reverse flow to occur. For this case, the disc lags and moves slowly with the reverse flow and gradually throttles the flow. When the upper cushion comes into effect, additional damping is provided. The flow is throttled more slowly as compared to the previous case with a result in less waterhammer pressures but allowing more reverse flow to pass through the valve.

For the two cases considered, with reverse flow established, a compromise is required between the maximum amount of permissible reverse flow and the maximum disc impact force (velocity) upon closure. The most desired performance from the check valve is valve closure at the instant the flow decelerates to zero.

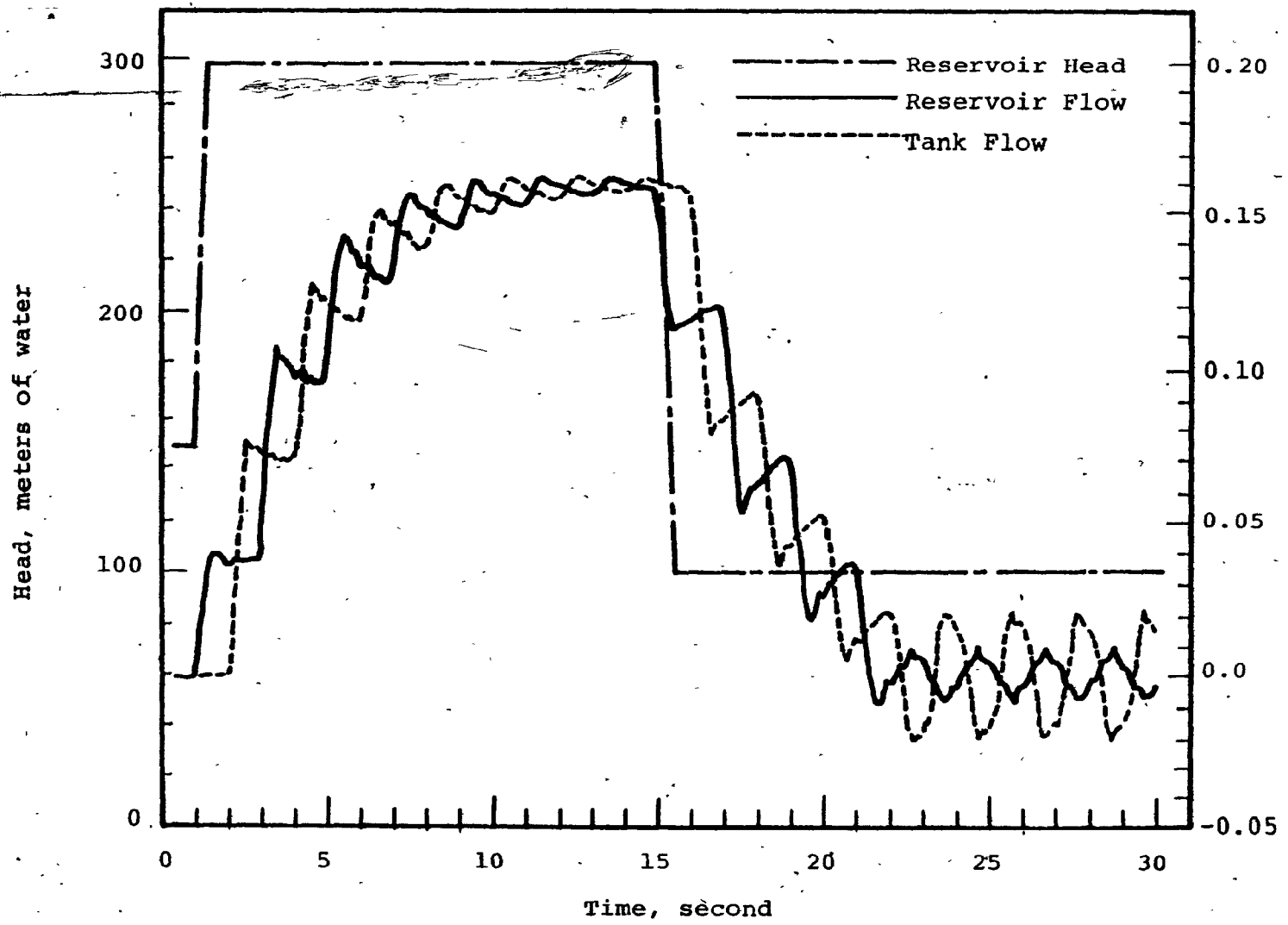

Figure 6-6. Resevoir Head and Flow and Tank Flow vs Time

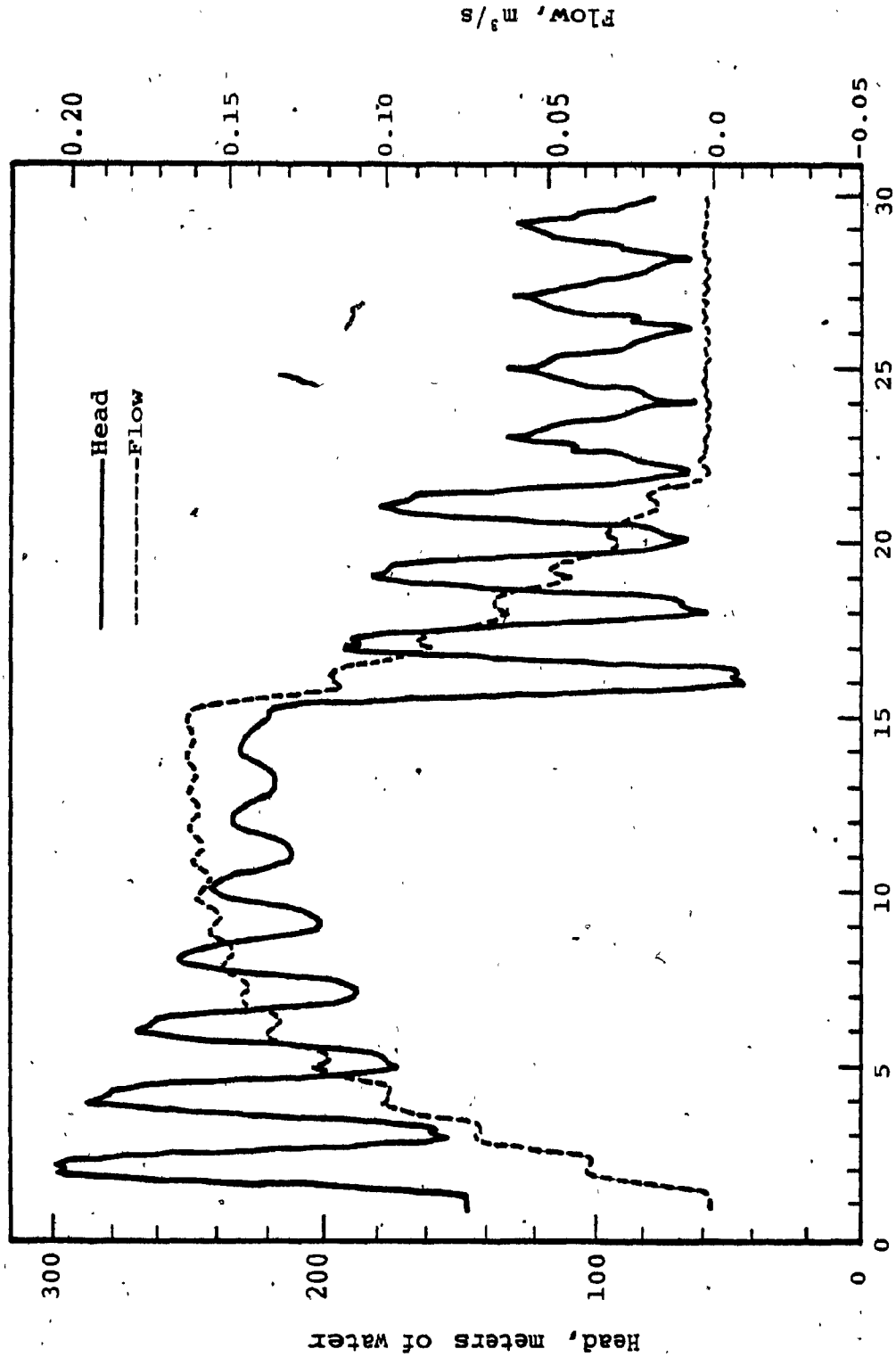

Figure 6-7. Head and Flow Directly Upstream from Valve vs Time

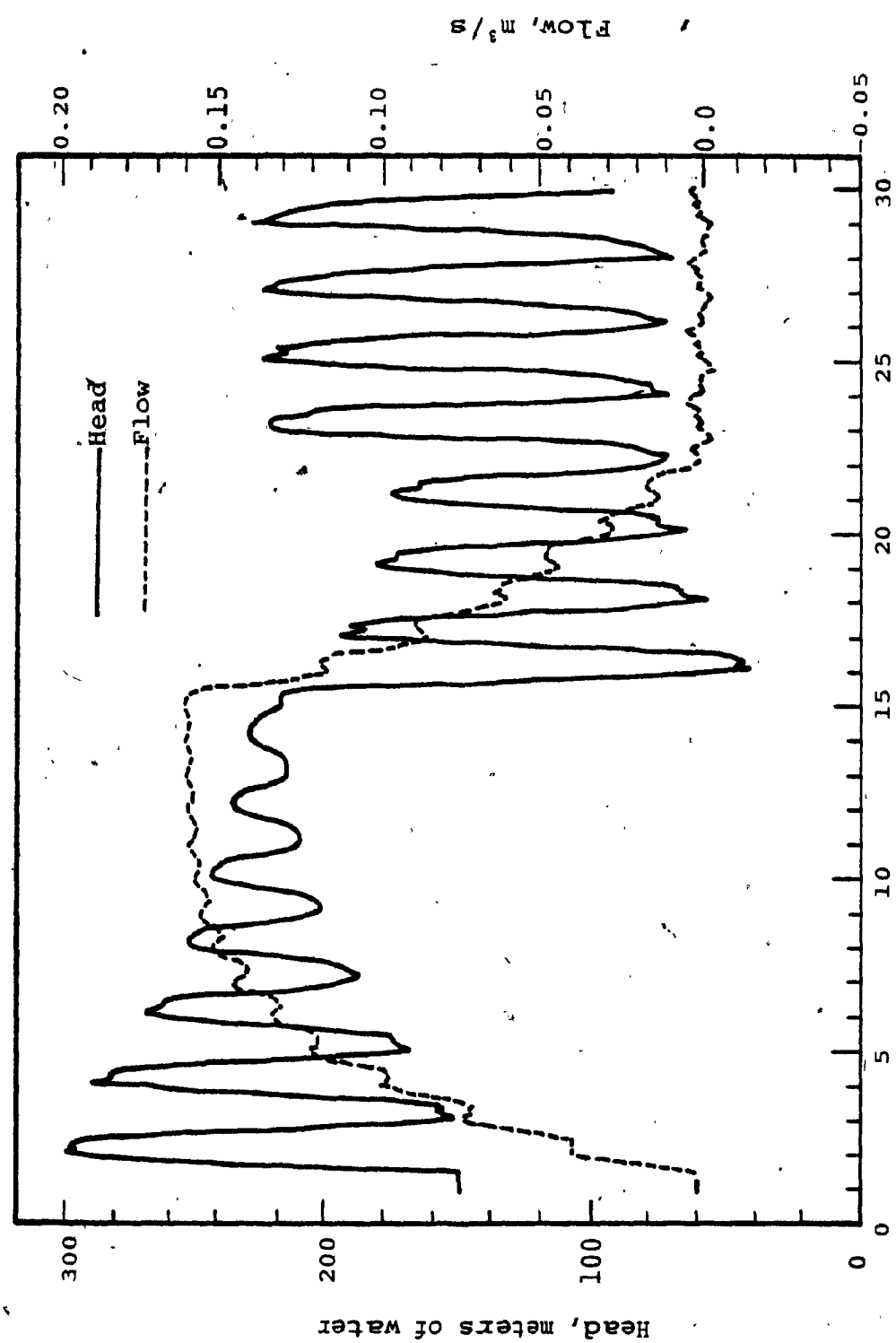

Figure 6-8. Head and Flow Directly Downstream from Valve vs Time

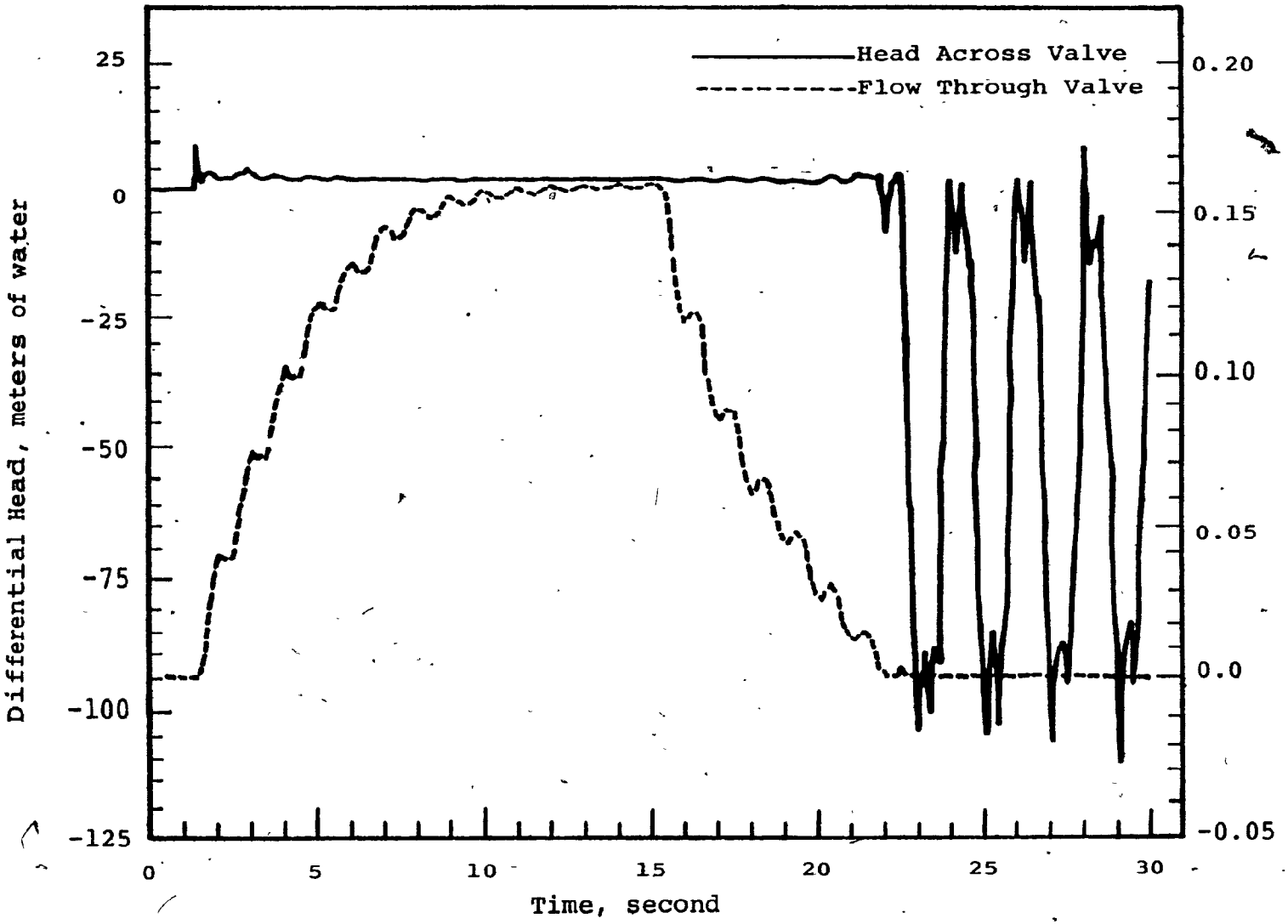

Figure 6-9. Head Across Valve and Flow Through Valve vs Time

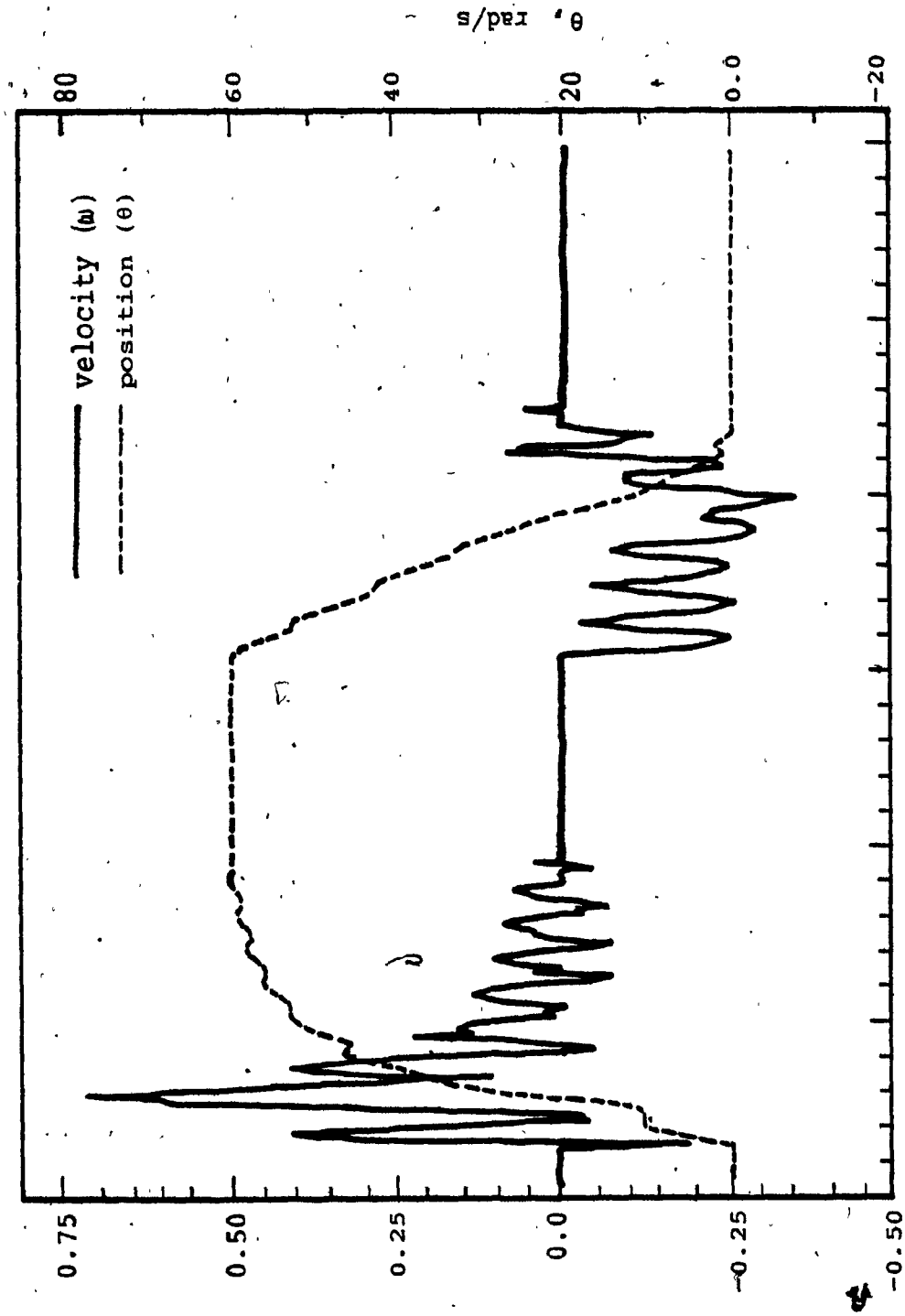

Figure 6-10. Disc Angle and Velocity vs Time

CHAPTER 7

CONCLUSION

7.1 Summary

The objective of this thesis is to optimize the design of wafer swing-disc check valves. Optimal valve design considers two major aspects of the valve performance. The first performance criterion is minimum pressure loss when the valve is fully opened. The second valve performance criterion requires minimum waterhammer pressure and non-slam seating action resulting from the valve closure. Also, the optimized valve design desires the wafer-type advantages of simplicity, compactness and light-weight features to be retained.

In Chapter 2, wafer swing-disc check valve pressure loss minimization is investigated by considering the valve orifice and fully opened disc to be two restrictions in series. Initial consideration of the orifice and disc restrictions indicated that the valve pressure loss may be reduced by providing smooth entrance and exit regions for each restriction. This task was not performed since alteration of the valve exterior dimension would be required which would result in a lost of the desirable compact and light-weight features. Results from this initial study concluded that a well rounded orifice entrance helps reduce

a minor portion of the valve pressure loss.

The valve pressure loss is minimized by considering various combinations of orifice restrictions and fully opened disc restrictions. A certain amount of disc area overlapping the orifice area relates the two corresponding diameters for a given valve size. Each restriction, when considered separately, decreases in pressure drop as the flow passage area ratio with respect to the pipe increases. Corresponding to the pressure drop across each restriction is characterized by respective flow coefficients. The overall flow coefficient characterizing the pressure drop across both restrictions in series assumes that the individual restrictions are independent of each other and are unaffected when combined. A large flow coefficient is equivalent to a small pressure drop across the restriction. For the wafer-type swing-disc check valve, the pressure drop depends on the ratio of orifice diameter to pipe diameter and on the amount of disc to orifice overlap. For each particular overlap there is an optimum diameter ratio that produces the least pressure drop across the valve.

Experiments performed on a 50-mm valve size confirmed the valve analysis and the least pressure drop occurred at the expected diameter ratio. Thus, the valve analysis provides the valve manufacturers with a method to predict and to minimize the energy losses across wafer-type

swing-disc check valves.

In Chapter 3, wafer swing-disc check valves manufactured by Ritepro Inc. in Montreal are studied to reduce the pressure drop across these valves. Ritepro manufactures two types of wafer check valves. The difference between the valve seating arrangement distinguishes the two valve types.

The soft seal valve type consists of the metal disc seating on an O-ring seal. This valve type is used in fire prevention systems and requires a pressure drop not exceeding 20.7 kPa when the water flow velocity is 4.57 m/s in Schedule 40 pipe. The hard seal valve type consists of the metal disc seating on a metal seat ring. This type of valve is used in general industrial applications and there is no pressure drop limit requirement. The hard seal valve pressure drop is reduced to give the valve an improved performance characteristic.

The pressure drop minimization concept developed in Chapter 2 is applied to reduce the pressure loss across Ritepro valves. For a given valve overlap, further pressure loss reduction is achieved by changing the location of the disc pivot. It is concluded from the analysis that shorter hinge arm length and further the pivot location away from the orifice, yields larger disc opening angles. The larger

disc opening results in an increased disc to pipe flow passage area ratio. Elimination of the disc cone and considering the effects of the hinge arm thickness, are included in increasing the disc flow passage area. Providing the valve with more flow area around the disc increases the valve overall flow coefficient and the least pressure drop occurs at larger orifice to pipe diameter ratios.

Final valve design considers clearances to prevent the disc from wedging into the pipe walls when fully opened. Free disc swing clearance from the downstream connecting pipe is also considered. For both valve types, the pressure drop is reduced for valve sizes from 50-mm to 300-mm.

It was noted that as the valve size increases the required overlap decreases. As realized through the investigation, a higher overall flow coefficient can be achieved by reducing the overlap. But, as the valve size increases, the angle of disc final opening also decreases since the valve body length does not grow proportionally with the valve size. Smaller disc openings increases the pressure drop.

Evaluation of production prototypes, soft seal valve sizes from 65-mm to 300-mm, tested by the Hydraulics Laboratory at NRC, are well below the 20.7 kPa pressure drop

limit. Although the 50-mm valve body length was extented to permit more disc opening, this valve size still does not meet the pressure drop limit. Large discrepancies between test values and expected values occur for the last three bigger valve sizes. The discrepancies are attributed to the lack of knowledge of the entrance loss to the disc restriction as a function of disc angle.

The overall research effort for the soft seal valve was a success in helping reduce the pressure drop across the valve, except for the 50-mm valve which is above the pressure drop requirement. A comparison between newly designed valves and existing Ritepro valves indicate a significant pressure drop improvement.

The new hard seal valve design is an offshoot from the soft seal valve design. This is because the latter valve's disc-arm assembly and hinge location are the same as used for the hard seal valves. The orifice diameter for the hard seal valves is determined from the overlap specification. The exception is the 50-mm valve which is designed in the same way as the soft seal valve type. This deviation from the design procedure results from the fact that two sets of disc assembly and hinge location for two identical sizes of valves, being only different in valve overlap, is neither production efficient nor stock management efficient. It should be remembered that no

pressure drop limit is required from the hard seal valve type and pressure drop minimization is recommended only to provide the valve with a better performance characteristic.

Experiments were performed only on small valve model sizes of 50-mm, 80-mm and 100-mm. This is considered sufficient since it is more difficult to achieve a low pressure drop for small valve sizes due to the large overlap.

Test results are especially poor for the 100-mm valve as compared with calculations. Discrepancies are attributed to lack of knowledge of the entrance losses to the orifice. The errors are compounded by not knowing the disc entrance losses as a function of disc angle. The orifice entrance is not smooth as compared to the soft seal valve type. Due to the seat ring, the orifice consists of a smooth entrance followed by an abrupt square edged reduction in diameter. The entrance loss associated with such an orifice is not known. A constant coefficient was assumed similar to the loss coefficient for a sudden contraction although the loss is a function of contraction diameter ratio. This assumption did not prove to be entirely correct. For better agreement between test results and theory, more experiments are required to determine the effect of the orifice with the step.

The 100-mm valve had a large difference in pressure drop as compared with calculations. However, if all other untested valves would have an increase in pressure drop by this same percentage, their losses would still be below the 20.7 kPa limit. A comparison between the tested and expected loss values with those measured for existing Ritepro valves show a significant pressure drop improvement. Further tests, by providing the 100-mm hard seal valve with a well rounded smooth orifice, indicate that the pressure drop may be reduced well beyond that of the soft seal valve type.

In Chapter 4, a hydro-pneumatic mechanism acting as a combination spring and damper for the wafer swing-disc check valve is reviewed from the work of Reference [8][9][10]. The mechanism provides valve closing speed and non-slamming control. Correlation between experimental and model simulation results concluded that the model equations describing the valve mechanism are adequate. A more critical summary by the authors is provided in the reference. The hydro-pneumatic valve mechanism is simulated with unsteady pipe flow in Chapter 6, and will be further summarized later in this section.

In Chapter 5, the pressure drop across the wafer swing-disc check valve and the fluid forces acting against the valve disc are presented. Test results of these two

variables are measured for forward and reverse steady-flow conditions at various positions of disc angles. In steady-flow conditions, these two flow forces are related to the flow through the valve. For any combination of valve flow rate and disc opening, these flow force relations are unique and no other steady-flow condition is possible. In unsteady-flow conditions, the valve flow, the valve pressure drop, the fluid forces against the disc, as well as the disc position, are assumed related to their equivalent steady-flow conditions at each instant of time. These unique steady-flow conditions are the flow characteristics of the valve.

The equations describing the flow through the valve to the pressure drop across the valve are developed in Chapters 2 and 3. Applying these equations to the pressure drop test measurements, the entrance contraction loss coefficient to the disc restriction is determined as a function of disc angle. The disc loss coefficient together with its describing equations characterizes the flow and pressure drop relation for the wafer swing-disc check valve of any size.

An expression relating the force (or torque) created by the moving fluid against the valve disc is formulated. This equation applies to both a stationary and to a moving disc within the flow stream. The equation is characterized

by a normal drag coefficient evaluated from the force measurements. A comparison of the drag coefficient varies with disc opening in a similar manner as the disc flow coefficient. This indicates that a relation exists between the disc pressure drop and the fluid flow forces acting against the disc. Thus, the definition of a normal drag coefficient does not require determining the pressure distribution around the disc and the location of the pressure centre. The normal drag coefficient together with the governing equation fully chatacterizes the torque and flow relation for the wafer swing-disc check valve of any size.

Chapter 6 presents the computer simulation study of the hydro-pneumatic spring-damper check valve dynamics when the fluid flow through the valve is unsteady. The valve is placed between two pipes of equal length with a reservoir head source at one pipe end and a constant head tank at the other pipe end. Unsteady pipe flow is established by changing the reservoir head. The valve characteristics relate the pipeline flow to the valve pressure drop and to the flow forces against the valve disc. The pipe flow results from the waterhammer modelling of the pipeline.

The pipeline modelling consists of sectioning the pipe into finite equal lengths where the fluid inertia, capacitance and pipe resistance are lumped. A valve in the

piping system is simply considered as a lumped resistance. This model enables the representation of the piping system by a circuit diagram from which the head and flow equations corresponding to each pipe section are directly written from. The system equations and system lumped representation by a circuit has a one to one correspondance and the significance of the physical system is clear and concise.

Before analyzing the check valve dynamics, simulation of a simple pipeline compares the transient response between the lumped-parameter method to the method of characteristics. The results yield a qualitative adequacy of the lumped-parameter model using the latter established method as a standard.

The period of waterhammer oscillation and pressure wave propagation speed for the lumped parameter method does not deviate greatly from the method of characteristics and is considered an adequate approximation. The major deviation occurs at oscillation peaks. As the number of pipe sections decreases, the model behaves as a low-pass filter. With increasing number of sections, higher frequencies are superimposed on the tops of the oscillating heads and decays quickly. It is expected that with more number of sections the lumped-parameter results will approach the response given by the characteristics method. The waterhammer solution by the lumped-parameter method with

a finite number of pipe sections only approximates the true solution.

Simulation study of the hydro-pneumatic spring-damper check valve indicates that the speed of valve closure depends on the accumulator precharged pressure and on the setting of the viscous restrictor. Under normal steady-flow, the flow forces against the fully opened disc should just balance the accumulator closing force. This allows the accumulator to force the disc to close as soon as the pipe flow drops below normal operating flow. Also, the viscous restrictor should provide low damping for quick valve closure. For minimum waterhammer pressures the check valve is required to close at the instant when the pipe flow decelerates to zero before reverse flow develops.

The non-slamming effect provided by the lower cushion significantly reduces the disc opening velocity. Thus, the hydro-pneumatic spring and lower cushion limits the disc impact force and avoids damage to the opening check valve. The upper cushion is provided to slow down the valve closing speed in order to reduce the disc impact force upon closure. The upper cushion is not neccessary if the valve closes at the instant when the valve forward flow decelerates to zero.

Some conclusions derived from the study of the check valve effects on waterhammer pressures are as follows:

Tensions provided for spring forces should just balance the normal forward steady flow forces. This allows the spring to force the disc to close as soon as the forward flow slows down. When the forward flow in the pipe decelerates slowly, all dampers provided to control the speed of valve closure should have low damping values. This allows the disc to respond quickly and move with the flow. The disc readjustes its position to the flow and causes minor throttling of the valve flow. In this way, the disc will seat at about the same time as the flow decelerates to zero. For minimum waterhammer pressures to occur at valve closure, the disc is required to seat at the instant the flow decelerates to zero.

When reverse flow has been developed before the valve did close, a damper provided for the final stages of valve closure helps reduce waterhammer effects. The developed reverse flow will urge the disc to close rapidly. Because the disc is moving in fast response with the flow, the check valve causes minor throttling of the flow. When the closing disc velocity is suddenly reduced by the damper, the reverse flow experiences a situation similar to that of a partial instantaneous valve closure. The sudden change in valve resistance requires the flow to readjust to the new resistance. Hence, the flow is suddenly throttled and waterhammer pressures result. For the final angles of valve

closure, since the damper is in effect, the check valve moves slowly in response to the reverse flow and gradually throttles the flow to zero to reduce the waterhammer pressures upon valve closure.

If the check valve is provided with a damper control from its fully opened to its fully closed position, a high damping value may be counterproductive. A high damping value allows the forward flow to decelerate and reverse before the valve could close. Although the damper will throttle the flow to zero and waterhammer pressures will be reduced upon valve closure, excessive reverse flow may have been permitted to occur.

For all cases where reverse flow has been established, a compromise is required between the maximum amount of permissible reverse flow and the maximum disc impact force (or waterhammer pressure) upon valve closure. This compromise is decided upon by the adjustment of the valve dampers provided to control the speed of valve closure. The most desired performance from the check valve is valve closure at the instant the forward flow decelerates to zero.

7.2 Suggestions for Future Work

The pressure loss across the 50-mm soft seal valve is above the 20.7 kPa pressure drop requirement. Possibilities to further reduce the pressure drop include reducing the hinge arm thickness and offsetting the orifice above the pipe axis to shorten the hinge arm length. These considerations provide more disc opening and hence the disc flow passage area is increased. As a consequence to more disc opening the valve length is required to be increased. Suggestions for this work require more experiments and modifications of the existing theory. Also, the suggestion increases the complexity and weight of the valve design.

In predicting the pressure drop across the soft seal valves, the discrepancy between expected and test results were attributed to the lack of knowledge of the disc entrance loss as a function of disc opening angle. The discrepancy was larger for bigger valve sizes. Also, as noted through the investigation, the valve body length does not grow proportionally with increasing valve size and this results in smaller final disc openings. Estimation of the disc entrance loss is required to predict the pressure drop across the remainder of valve sizes from 350-mm to 1050-mm and to provide an improved loss prediction for the bigger valve sizes tested. This requirement is provided by the entrance loss versus disc opening test results given in

Figure 5-6.

The pressure drop prediction across hard seal valves were inaccurate due to the entrance loss assumed for the orifice. To improve the loss prediction, it is suggested that more experiments are necessary to determine the effect of the step reduction in orifice diameter provided by the seat ring. Experiments similar to that performed on the soft seal orifice as described in Chapter 2 would be neccessary. Experimental results indicate that the pressure loss is improved beyond those of the soft seal valve type by providing the hard seal valve with a completely smooth orifice. A method allowing the removal of the seat ring without the step reduction in orifice diameter should be investigated.

Simulation of the hydro-pneumatic check valve showed that the disc closed at the instant when the valve flow decelerated to zero. With this speed of valve closure minimum waterhammer pressures resulted. The check valve was placed between two pipes of equal lengths and pressure fluctuations originated from the reservoir upstream from the valve. This is not the worst possible location for a valve since it takes time for flow reversal starting at the reservoir to travel to the valve. If the pipe completely breaks directly upstream adjacent to the check valve, the most severe situation occurs, since reverse flow would

originate at the valve. Also, water column separation must be considered downstream from the valve. If the valve does not close before reverse flow develops, severe waterhammer pressures may result. In this situation, if the valve closes quick enough before reverse flow occurs, then the valve closure speed is safe for all cases for this particular piping arrangement. This is an important situation to be considered for future investigation.

In the situation just described, if reverse flow does develop before valve closure, the situation including the effect produced by the viscous resistor and by the upper cushion is an important case to study. The purpose of the restrictor and cushion is to act as a damper to protect the valve from excessive shocks upon closure by reducing the disc closing velocity. The slow valve closure throttles the reverse flow to reduce waterhammer pressures upon closure. These effects may be counterproductive since slow valve closure permits more reverse flow to occur. The compromise between the damping velocities and the maximum amount of permissible reverse flow should be studied. It must be remembered that this compromise is dependent on the particular piping system under study.

Using the lumped-parameter method to estimate pipeline waterhammer transients was considered sufficient. Although the model representation conveys a clear and

concise understanding to the physical problem, the method requires excessive computer time. To complete the simulation studied in Chapter 6 required a computing time of 100:1 real time. One of the advantages by the characteristic method is the small computer time required for solution. For example, the characteristic method is a finite difference scheme that evaluates the next time step solution based on the immediate past solution. The lumped-parameter method describes the system pressures and flows by coupled non-linear differential equations using a fourth-order Runge-Kutta integration solution method. This integration method requires two intermediate solution approximations between time steps. This shows that the characteristic solution method is faster than the integration method (assuming that both methods have the same number of pipe sections and time steps). The disadvantage of the characteristic method is that it does not convey a clear and simple representation of the piping system as given by the lumped-parameter method.

The hydro-pneumatic valve mechanism was modelled by ordinary differential equations using a fourth-order Runge-Kutta integration solution method. As mentioned previously, the fourth-order integration method requires two intermediate solution approximations between time steps. The characteristic method only requires a knowledge of its immediate past solution. If these two methods are combined,

the characteristic method requires an interpolation scheme since the fourth-order integration method needs two intermediate solution approximations. An interpolation scheme would increase the complexity and solution time for the characteristic method. But, the characteristic method is an established procedure to calculate pipeline transients and is an accurate representation of the distributed-parameter nature of the fluid pipeline. A marriage between the pipeline characteristic method and the valve mechanism lumped-parameter method is an interesting avenue for future investigation.

The lumped-parameter method, as applied to fluid transient calculations, needs still be researched in many areas. Some of the important questions concerned are:

1. the minimum number of sections required to accurately represent the wave propagation speed and waterhammer pressures

2. methods to minimize the excessive computing time

REFERENCES AND BIBLIOGRAPHY

1. Esleeck, S.M. and Rosser, R.M., "Check Valve Water Hammer Characteristics", Transactions, American Nuclear Society, vol. 2, November 1959, pp. 180-181.

2. Pool, E.B., Porwit, A.J. and Carlton, J.L., "Prediction of Surge Pressure from Check Valves for Nuclear Loops", Paper 62-WA-219, American Society of Mechanical Engineers, October 1962.

3. Pool, E.B., "Minimization of Surge Pressure from Check Valves for Nuclear Loops", Paper 62-WA-220, American Society of Mechanical Engineers, October 1962.

4. Csemniczky, J., "Hydraulic Investigations of the Check Valves and Butterfly Valves", Proceedings of the Fourth Conference on Fluid Machinery, AKADEMIA, 1972, pp. 293-305.

5. Krane, R.S. and Cho, S.M., "Hydraulic Performance of Tilting-Disk Check Valves", ASME Journal of Hydraulic Division, vol. 102, no. 1, January 1976, pp. 57-73.

6. Gwinn, J.M., "Swing-Check Valves Under Trip Loads", ASME paper no. 3, July 1977.

7. Uram, E.M., "A Method for Estimating Steam Hammer Effects on Swing-Check Valves During Closure", Transactions, ASME Journal of Engineering for Power, vol. 99, series A, no. 3, July 1977.

8. Svoboda, J. and Lee, R., "Dynamic Model of Hydraulically Damped Swing-Disc Check Valves", 10th Modelling Simulation Conference, sponsored by ISA, Pittsburgh, April 1979.

9. Lee, R.S., "Dynamic Performance of Hydraulically Damped Swing-Disk Check Valve", Master of Engineering Thesis, Concordia University, March 1981.

10. Lee, R.S., Svoboda, J.V. and Kwok, C.K., "Computer Aided Dynamic Analysis of the Hydraulically Damped Check Valves", 8th Canadian Congress of Applied Mechanics, Moncton, June 1981.

11. Svoboda, J.V., Hong, H. and Katz, S., "Optimum Design of Swing-Disc Check Valves", PRAI Grant No. P-7902, volumes 1 and 2, Department of Mechanical Engineering, Concordia University, 1981.

12. Svoboda, J., Katz, S. and Fitch, W., "Minimizing the Pressure Loss of Wafer Type Swing Check Valves", Paper 79-WA/NE-5, ASME Winter Annual Meeting, New York, December 1979.

13. Streeter, V.L. and Wylie, E.B., "Fluid Mechanics", Seventh Edition, McGraw-Hill Book Co., Inc., New York, N.Y., 1979.

14. Miller, D.S., "Internal Flow Systems", Published by BHRA Fluid Engineering, 1978, pp. 268-269.

15. "Flow of Fluids Through Valves, Fittings and Pipes", Technical Paper 410C, Crane Company, Chicago, Ill., 1957.

16. "Standard for Check Valves for Fire Protection Service", UL 312, Fifth Edition, Underwriters' Laboratory, Inc., May 1975.

17. "Wafer-Type Check Valves", API Standard 594, Second Edition, American Petroleum Institute, December 1977.

18. "ULC List of Equipment and Materials", vol. 1, Guide No. 2100 I22.90, File CEx429, Underwriters' Laboratories of Canada, February 1980.

19. Pratte, B.D. and Aitkin, R.B., "Evaluation of Ritepro Swing-Disc Model 212 Wafer Check Valves", Hydraulics Laboratory Report HY-239, Natural Research Council, Division of Mechanical Engineering, Ottawa, Canada, October 1982.

20. Bergeron, L., "Water Hammer in Hydraulics and Wave Surges in Electricity", (translated under the sponsorship of the ASME), John Wiley and Sons, Inc., New York, 1961.

21. Hong, H. and Svoboda, J., "Model of Swing-Disc Check Valve Suitable for Lumped Parameter Piping Network Simulation", 12th Modelling and Simulation Conference sponsored by ISA, Pittsburgh, April 1981.

22. Shearer, J.L., Murphy, A.T. and Richardson, H.H., "Introduction to System Dynamics", Addison-Wesley Publishing Co., 1967.

23. Wylie, E.B. and Streeter, V.L., "Fluid Transients", McGraw-Hill Book Co., Inc., New York, 1978.

24. "Maintenance and Operation Manual, Controlled Cushion Check Valve", 8"-300 lbs Series, Model 215-800-I, Rite Manufacturing Ltd., Montreal, Canada, December 1977.

25. "Rite Manufacturing Ltd. - Catalogue of Check Valves, Couplings, Nozzles, Swivel Joints, Fluid Handling Equipment, Service Station Equipment", Montreal, Canada, 1978.

26. "Fluid Meters: Their Theory and Application", edited by H.S. Bean, Report of ASME Research Committee on Fluid Meters, The American Society of Mechanical Engineers, New york, 1971.

27. Carnahan, B., Luther, H.A. and Wilkes, J.O., "Applied Numerical Methods", John Wiley and Sons, Inc., New york, 1969.

28. Burden, R.L., Faires, J.D. and Reynolds, A.C., "Numerical Analysis", Prindle, Weber and Schmidt, Boston, Massachusetts, 1978.

29. "Symposium on Water Hammer", (Under the Joint Auspices of ASME Power Division and ASME Hydraulic Division), The American Society of Mechanical Engineers, New York, 1961.

30. Benedict, R.P., "Fundamentals of Temperature, Pressure, and Flow Measurements", John Wiley and Sons, Inc., 1977.

31. Chaudhry, M.H., "Applied Hydraulic Transients", Van Nostrand Reinhold Company, New York, 1979.

32. Chirlian, P.M., "Signals, Systems, and the Computer", Intext Educational Publishers, New York, 1973.

33. Doebelin, E.O., "Measurement Systems: Application and Design", McgGraw-Hill Book Co., Inc., New York, 1966.

34. Dorf, R.C., "Modern Control Systems", Addison-Wesley Publishing Co., 1980.

35. Fox, J.A., "Hydraulic Analysis of Unsteady Flow in Pipe Networks", The MacMillan Press Ltd., London, England, 1977.

36. Jaeger, C., "Fluid Transients in Hydro-Electric Engineering Practice", Blackie and Son Limited, London, England, 1977.

37. Kirshner, J.M. and Katz, S., "Design Theory of Fluidic Components", Academic Press, Inc., New York, 1975.

38. Merritt, H.E., "Hydraulic Control Systems", John Wiley and Sons, Inc., New York, 1967.

39. McCloy, D. and Martin, H.R., "The Control of Fluid Power", Longman Group Limited, London, England, 1973.

40. Parkmakian, J., "Waterhammer Analysis", Dover Publications, Inc., New York, 1963.

41. Takahashi, Y., Rabins, M.J. and Auslander, D.M., "Control and Dynamic Systems", Addison-Wesley Publishing Co., Inc., Reading, Massachusetts, 1972.

42. Watters, G.Z., "Modern Analysis and Control of Unsteady Flow in Pipelines", Ann Arbor Science Publishers Inc., Ann Arbor, Michigan, 1979.

43. Yeaple, F.D., "Hydraulic and Pneumatic Power and Control", McGraw-Hill Book Co., Inc., New York, 1966.

APPENDIX A

FLOW PASSAGE AREA RATIO PROVIDED BY WIDE OPENED DISC

The flow passage area provided by the wide opened disc within the pipe is not known with certainty. As a first approximation to derive the disc flow passage area, the opening of the disc is simplified as shown in Figure A-1. The transverse view, Figure A-1b, shows the disc of diameter d_3 partially opened at angle θ within pipe diameter d_1. It is assumed that the disc is thin with negligible thickness. Also, the transverse thickness of the hinge arm is neglected. This results in the hinge arm and disc assembly to form a straight line pivoting about point (O). The axial view of the disc partial opening is shown in Figure A-1a. The disc is seen as an ellipse within the pipe shown as a circle. The XY coordinate system is with respects to the disc centre. With reference to the figure, the disc has a major diameter:

$$2 \cdot a = d_3 \tag{A.1}$$

and the pipe centre below the X-axis is expressed as:

$$c = \frac{d_1}{2} (1 - \cos\theta) \tag{A.2}$$

The equation for the pipe circle is:

$$x^2 + (y+c)^2 = (d_1/2)^2 \qquad (A.3)$$

When the disc is fully opened, it is assumed that the disc is tilted open until its diameter d_3 becomes a chord of the pipe circle d_1. Therefore, at $x = a = d_3/2$ gives $y = 0$. Substituting this condition in Equation A.3 and solving for the disc full opening angle results in:

$$\cos\theta = 1 - \sqrt{1 - \left(\frac{d_3}{d_1}\right)^2} \qquad (A.4)$$

The flow area A_4 provided by the wide opened disc, neglecting the area created by the hinge arm interferring the flow path, is:

$$A_4 = A_1 - A_3 \cos\theta \qquad (A.5)$$

where A_1 is the pipe area and A_3 is the disc area. The second term on the right hand side of Equation A.5 is the projection of the disc area normal to the flow. Substituting Equation A.4 in Equation A.5 and dividing both sides of the equation by the pipe area, results in the flow passage area ratio provided by the wide opened disc as:

$$\frac{A_4}{A_1} = 1 - \left(\frac{d_3}{d_1}\right)^2 \cdot \left[1 - \sqrt{1 - \left(\frac{d_3}{d_1}\right)^2}\right] \qquad (A.6)$$

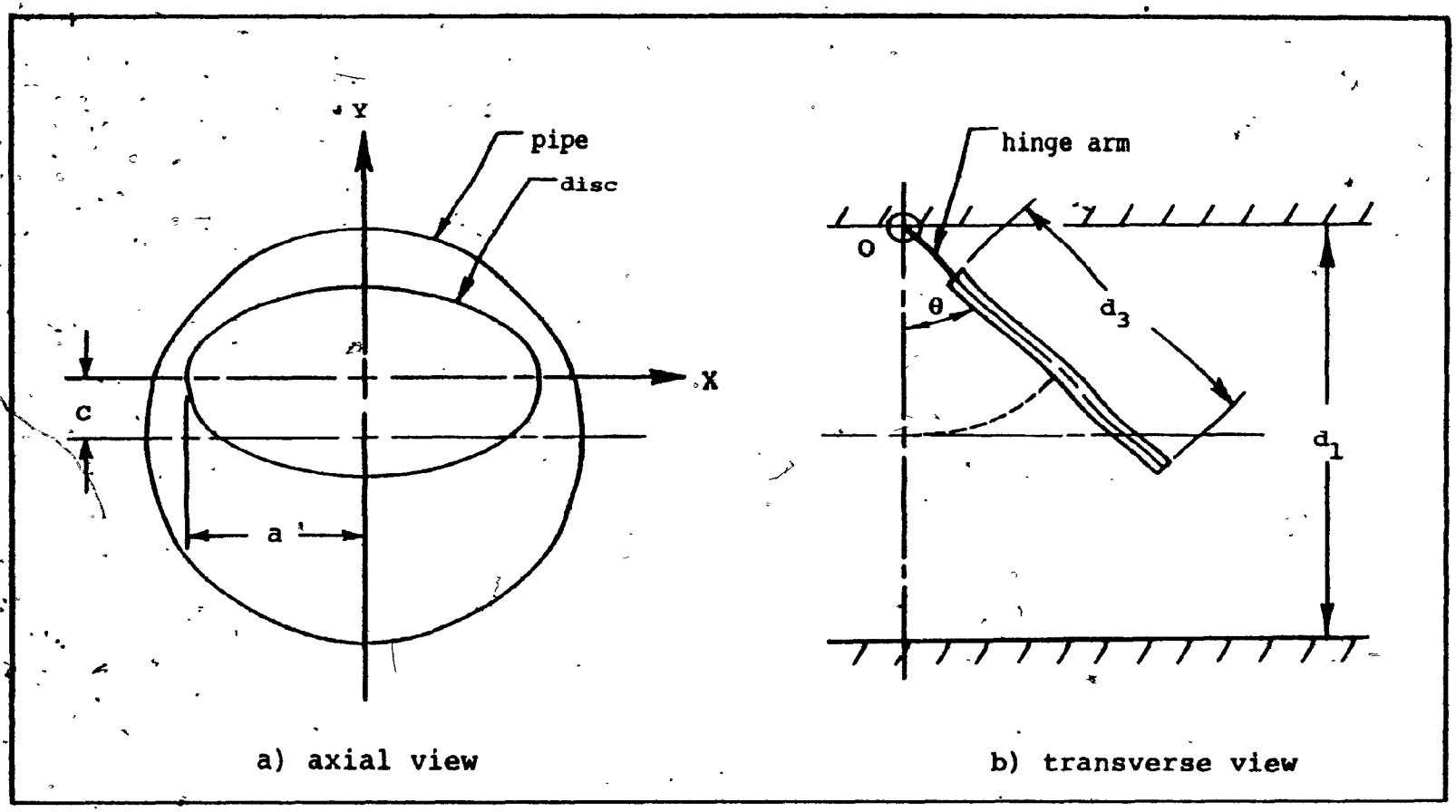

Figure A-1. Simplified Schematics of Disc Opening Within Pipe

APPENDIX B

TEST ARRANGEMENT AND PROCEDURE TO VERIFY VALVE ANALYSIS

B.1 Test Arrangement

A schematic drawing of the experimental set-up to verify the valve analysis of Chapter 2 is shown in Figure B-1. A centrifugal pump supplies water to the test and bypass line. The pump is capable of producing a maximum head of 30 m of water and a maximum flow rate of 0.1133 m^3/s. Flow through the 50-mm Schedule 40 steel test line is metered by a globe valve and measured by a calibrated 80-mm venturi meter using a U-tube manometer. More than 10 pipe diameters preceed the venturi meter to ensure a fully developed flow. Appendix E shows the venturi meter calibration curve.

The test valve is mounted between flanges downstream from the on-off gate valve that supplies flow to the test line. The flanges are counterbored to the outside diameter of the test valve to ensure pipe and valve longitudinal axis alignment. The test valve allows for testing the orifice alone, disc alone, and the orifice and disc together. Figure B-2 shows the construction of the test valve.

Static pressure taps are located upstream and downstream from the valve. Tap locations are indicated in

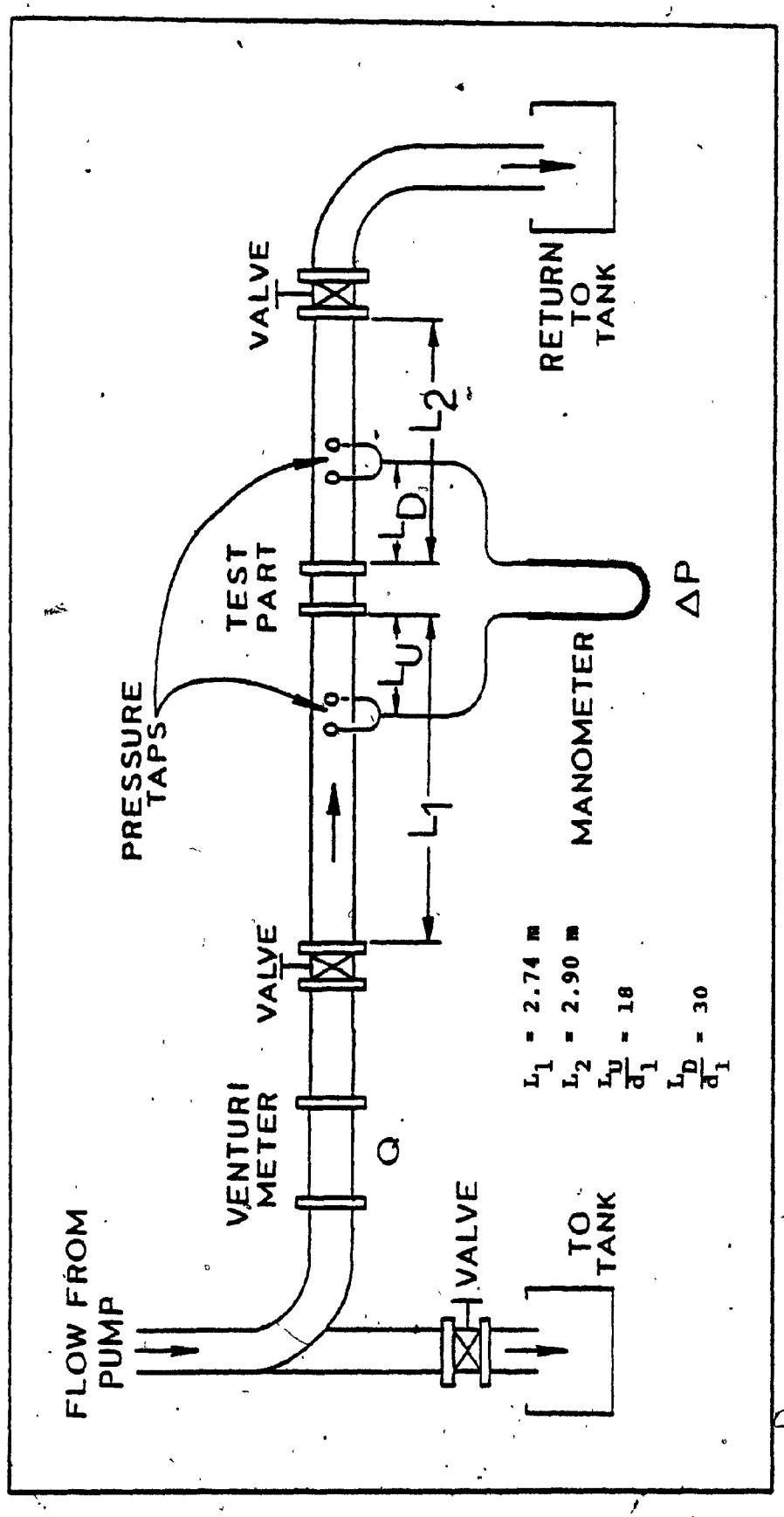

Figure B-1. Schematic Drawing of Test Arrangement

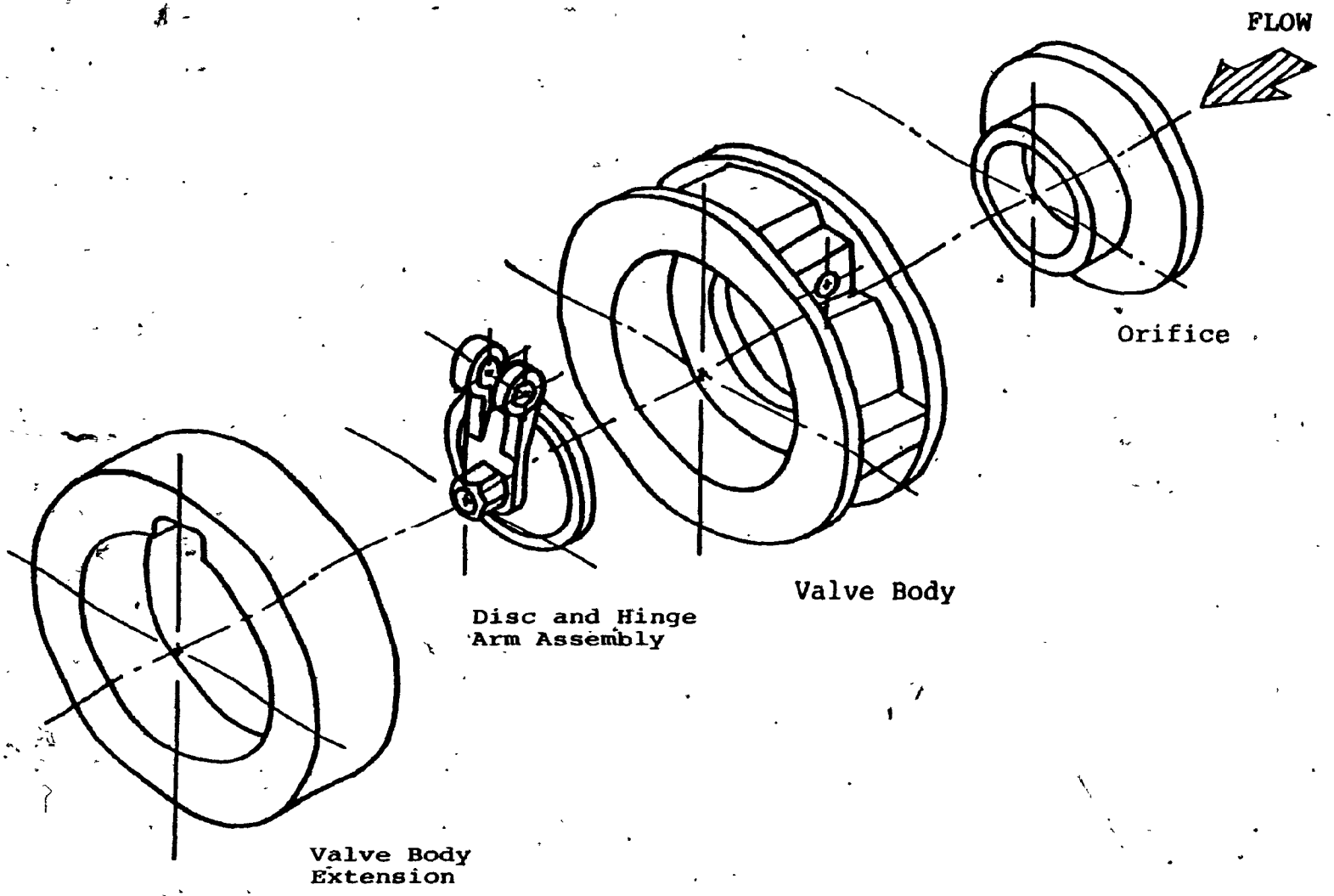

Figure B-2. Exploded View of Test Valve Construction

Figure B-1, and are based on flow entrance development and exit redevelopment to and from the test valve. At each pressure measuring cross section two 1.6 mm pressure taps on opposite ends of a diameter are connected together. The differential pressure between the measuring stations is obtained with a U-tube manometer. Between the pressure measuring stations and manometer are variable restrictions and volume wells to eliminate manometer fluctuations. A similar arrangement is provided for the venturi meter manometer.

All manometer spans are 2.54 m, and manometer fluids used are specific gravity 1.75, 2.95 and mercury 13.58. The water temperature is approximately 20 ^{o}C. Figure B-3 shows the pictorial view of the test set-up.

Table B-1 gives the dimensions of the six orifice and disc sizes tested. An overlap γ = 10.6% is chosen to match the overlap used in the valve analysis. Orifice to pipe diameter ratios, d_2/d_1, are selected above and below the one at which minimum pressure drop is expected.

B.2 Test Procedure

Before experimental verification of the valve analysis is performed, tests are performed on the 50-mm valve to ensure full disc opening. A clear plexiglass tube

Figure B-3. Pictorial View of the ΔP Experimental Set-Up

No.	Orifice Diameter d_2 (mm)	Disc Diameter d_3 (mm)	Ratio d_2/d_1
1	31.5	37.1	0.60
2	34.1	39.7	.65
3	35.8	42.3	.70
4	39.4	44.9	.75
5	41.5	47.1	.79
6	44.6	50.2	.85

Value size: 50 mm

Pipe diameter d_1: 52.5 mm

Overlap γ: 10.6%

TABLE B-1. Dimensions of Test Value

of the same pipe diameter placed directly downstream from the valve is installed in the test position. The test valve included its tension spring. By introducing flow through the test line the disc is visually seen fully opened touching the plexiglass pipe walls at a Reynolds number of 5.608×10^4 ($0.0023\ m^3/s$). Since experiments on the valve does not include the tension spring and the interested flow range is beyond the above mentioned value, full disc opening is ensured.

The pressure difference along the test line for various typical flows are first measured with no restriction in the test position. The test valve is replaced by a short test ring of the same pipe diameter. This provides the pipe friction loss to be interpolated and subtracted from the measurement with test restrictions present. Test line pressure loss are always performed on each test day since the steel pipe tended to rust. Also, the test line is cleared by water flow for a half to one hour before tests are performed.

Various pipe flows with and without test restrictions are adjusted by the metering valve. With increasing pipe flow the pump head is readjusted between 250 kPa and 300 kPa by the bypass line. By loading the pump head and by adjusting the variable resistors reduces manometer fluctuations to 3 mm per leg.

When the desired steady flow is obtained the flow rate is measured by the venturi meter and U-tube manometer. Manometer fluid of specific gravity 1.75 is used. This fluid gives a wide manometer span corresponding to the flow range of interest. For each restriction under test the flow velocity is adjusted between 2.29 m/s (1.220×10^5 Re) and 4.57 m/s (2.440×10^5 Re).

Tests are performed on eighteen different restrictions for the valve as follows:

a. six tests with orifice restriction alone

b. six tests with disc restriction alone

c. six tests with corresponding orifice and disc together

Each test measures the pressure drop across the restriction with a U-tube manometer for descrete flows in the desired flow range. Manometer fluids used are specific gravity 2.95 for lower pressure differences and mercury 13.58 for higher differences.

APPENDIX C

TEST ARRANGEMENT AND PROCEDURE TO VERIFY RITEPRO VALVE DESIGNS

This appendix describes the test arrangement and procedure to verify the Ritepro valve designs of Chapter 3. Tests are performed for valve sizes of 50-mm, 80-mm and 100-mm. The experimental set-up for the 50-mm valve test is exactly the same as that described in Appendix B. For the 100-mm valve size, the test arrangement is similar to the 50-mm test set-up, and is shown in Figure B-1. Only differences in experimental set-up are described in the following.

Flow through the 100-mm Schedule 40 steel test line is measured by a 150-mm venturi meter. A description of the venturi meter with its calibration curve is given in Appendix F. The test valve is mounted between counterbored flanges between the test line. Static pressure taps on the test line are located upstream and downstream from the test valve. Referring to Figure B-1, tap location dimensions are:

$$\frac{L_D}{d_1} = 27$$

These dimensions are based on flow development and exit redevelopment to and from the test valve.

The test arrangement for the 80-mm valve is the same as that used for the 100-mm valve. Referring to Figure B-1, on the test line flange upstream from the test part is added a 100-to-80 mm reducer section followed by 1.22 m of 80-mm Schedule 40 PVC pipe. Following the PVC pipe is a counterbored flange to ensure valve axis alignment. A similar 1.22 m PVC pipe arrangement is connected to the downstream flange. This arrangement provides mounting of the 80-mm valve to be tested.

The three sizes of valve tested, both hard and soft seal valve type, are according to valve dimensions given from Tables 3-1 and 3-2, respectively. The 50-mm and 80-mm valves tested are modified existing Ritepro valves according to the design dimensions. For the 100-mm test a specially built test valve capable of orifice and disc dimension changes is tested. This specially built valve is similar to the 50-mm valve shown in Figure B-2.

For both 50-mm and 80-mm valve test, venturi manometer fluid used is specific gravity 1.75. Manometer

fluid of specific gravity 2.95 is used for the 100-mm test. These fluids give a wide manometer span corresponding to the flow range of interest. Manometer fluids used to measure the pipe friction along the test line and pressure drop across the valve are specific gravity 2.95 for lower differences and mercury 13.58 for higher differences. All manometer spans are 2.54 m.

The experimental procedure for all valves tested are exactly the same as that described in Appendix B. Only differences in test procedures are described in the following. First, all valves are tested at their full open position. Also, for the 100-mm hard seal valve a smooth orifice is replaced for the orifice with a step and tested. Then, for only the 50-mm valve, a specially built anti-wedging nut providing the limited opening is tested. For the 100-mm valve the hinge arm is locked by set-screws at the limited anti-wedging opening and then tested. Also, for the 100-mm hard seal valve a smooth orifice is replaced for the orifice with a step and tested. The 80-mm valve is not tested at is limited opening. All valves are tested twice for repeatability.

$$L_1 = 3.353 \text{ m}$$

$$L_2 = 4.877 \text{ m}$$

$$\frac{L_U}{d_1} = 13$$

APPENDIX D

FLOW FORCE TEST ARRANGEMENT AND PROCEDURE

D.1 Test Valve and Test Arrangement

Flow force measurements are performed on an aluminum-plexiglass test valve shown schematically in Figure D-1. A pictorial view of the valve is shown in Figure D-2. The test valve parts has dimensions equivalent to a 100-mm soft seal valve, as given in Table 3-2. The plexiglass valve body design provides a cavity chamber to house a load cell so as to shield it from the flow stream. Load cell calibration for tension and compression are provided in Appendix G.

The flow force F is measured by a 3-bar linkage where the load cell is incorporated in variable link $\overline{BC}$. The load is measured directly on a voltmeter across the output terminals of the cell. Disc opening angle θ is determined by adjusting the length of link $\overline{BC}$.

With reference to Figure D-1, the fluid torque T_o acting on the disc shaft is given by:

$$T_o = F \cdot \overline{AC} \cdot \sin\phi \qquad (D.1)$$

where angle ϕ is a function of link length $\overline{BC}$ and is given

by:

$$\phi = \cos^{-1}\left[\frac{\overline{BC}^2 + \overline{AC}^2 - \overline{AB}^2}{2 \cdot \overline{AC} \cdot \overline{BC}}\right] \qquad (D.2)$$

Dimensions $\overline{AB}$ and $\overline{AC}$ are constant and their values are indicated in Figure D-1.

The test arrangement for the aluminum-plexiglass valve is the same as that described in Appendix C for the 100-mm valve size experiments.

D.2 Test Procedure

To ensure constant load cell enviroment for different flow conditions, the cell housing is bled constantly so as to fully submerge the load cell in water. Also, the pressure within the cell housing is kept at a constant value in the range between 20 kPa and 110 kPa. This pressure is first measured with no flow by closing the metering valve. The load due to this pressure acts as a constant bias and is subtracted from the flowing force measurements. Load cell readings are recorded in millivolts when the voltmeter fluctuations are within 5 mV. Simultaneous readings of the pressure drop, the flow rate, and the load on the disc are recorded. The procedure to regulate and measure the pipe flow and to measure the valve pressure drop is similar to

that described in Appendix C.

The flow force F and the valve pressure drop ΔP for various positions of disc angle θ versus forward flow rates are measured. Similarly, by turning the valve around, the force and the pressure drop for reverse flow are measured. Only a few test runs were repeated to ensure repeatability for both flow conditions.

The pressure drop due to the orifice alone is also tested for both forward and reverse flow. This provides the orifice pressure loss to be subtracted from the overall valve pressure loss in order to determine the loss contributed by the disc alone.

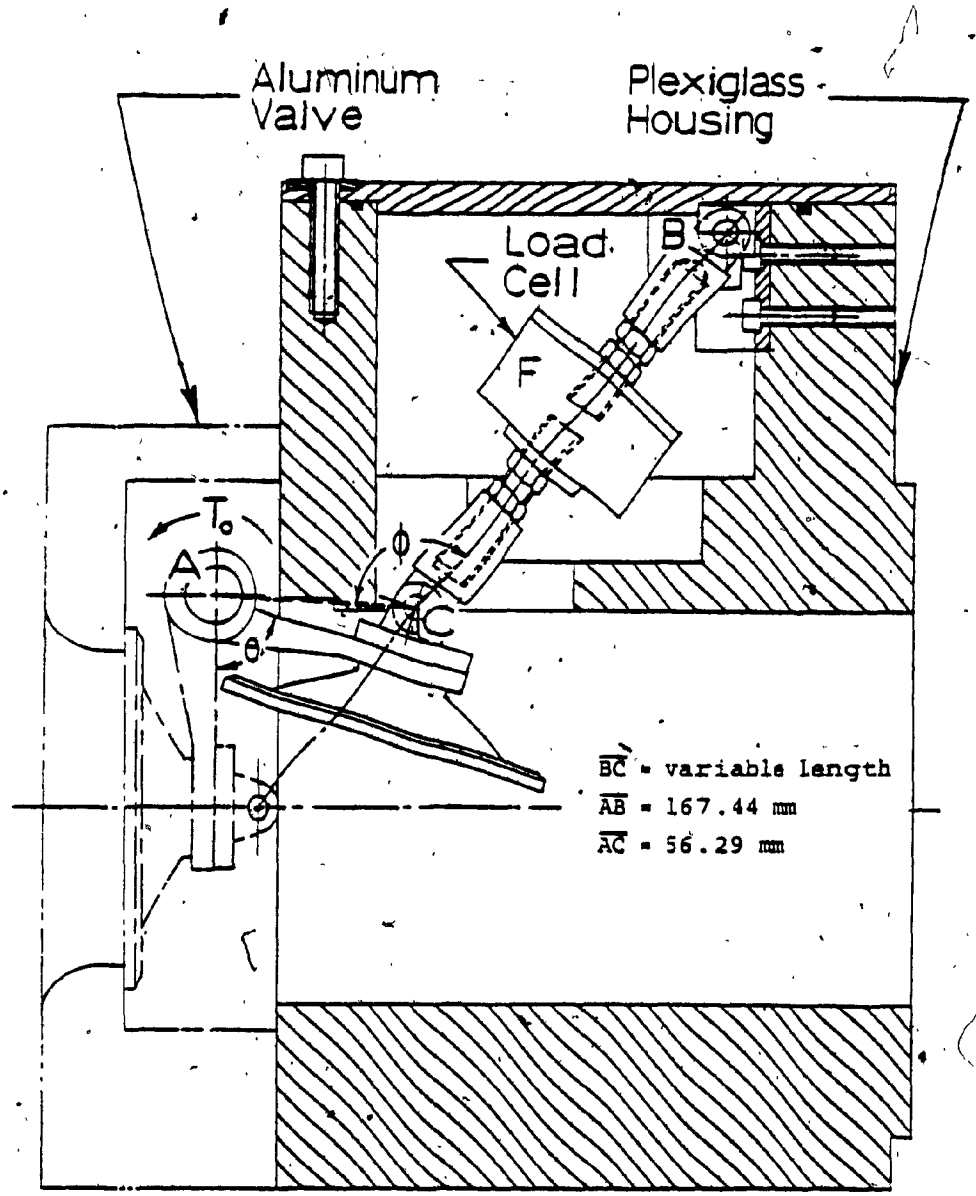

Figure D-1. Schematics of Flow Force Test Rig

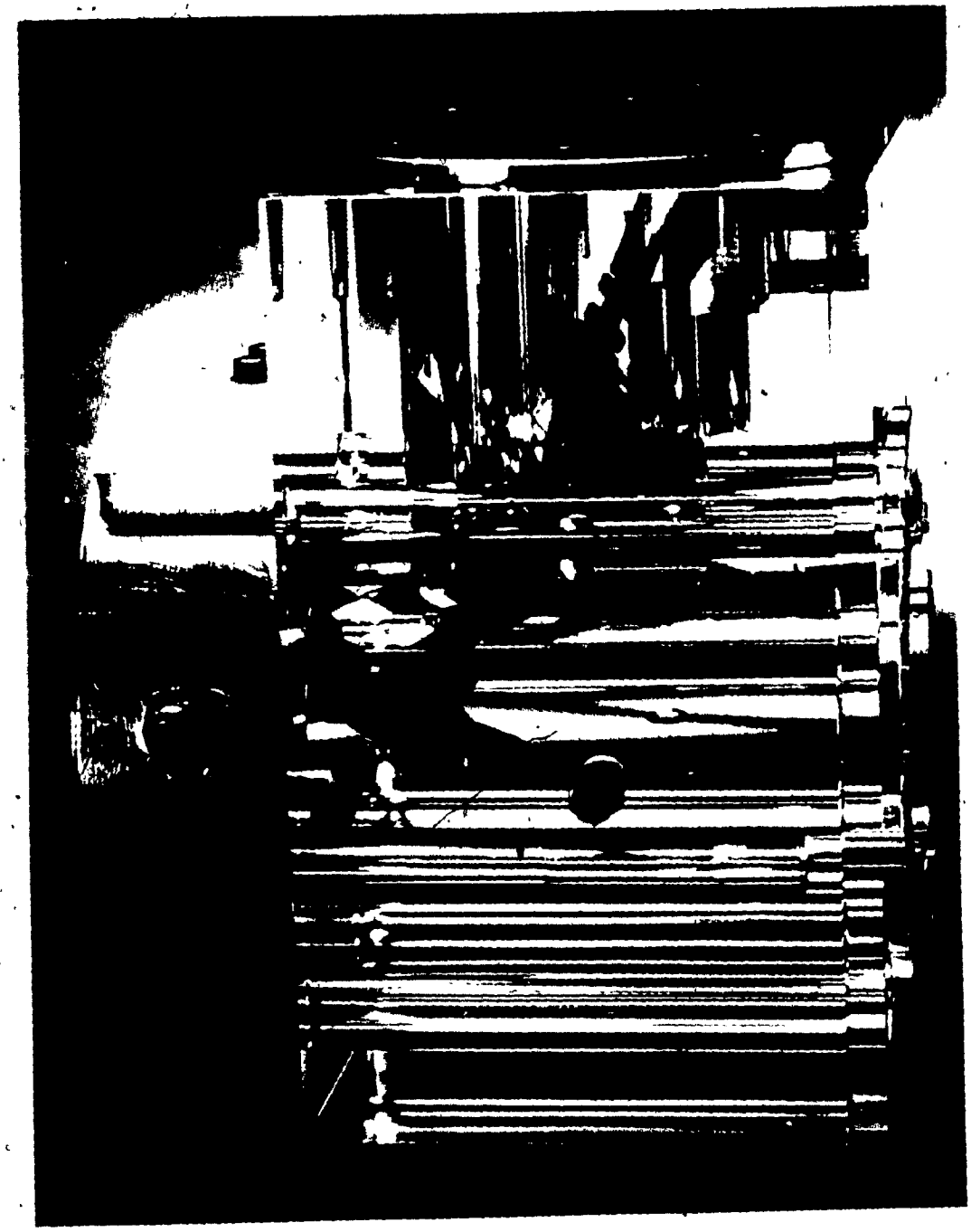

Figure D-2a. Pictorial View of Aluminum-Plexiglass Flow Force Test Rig (transverse view)

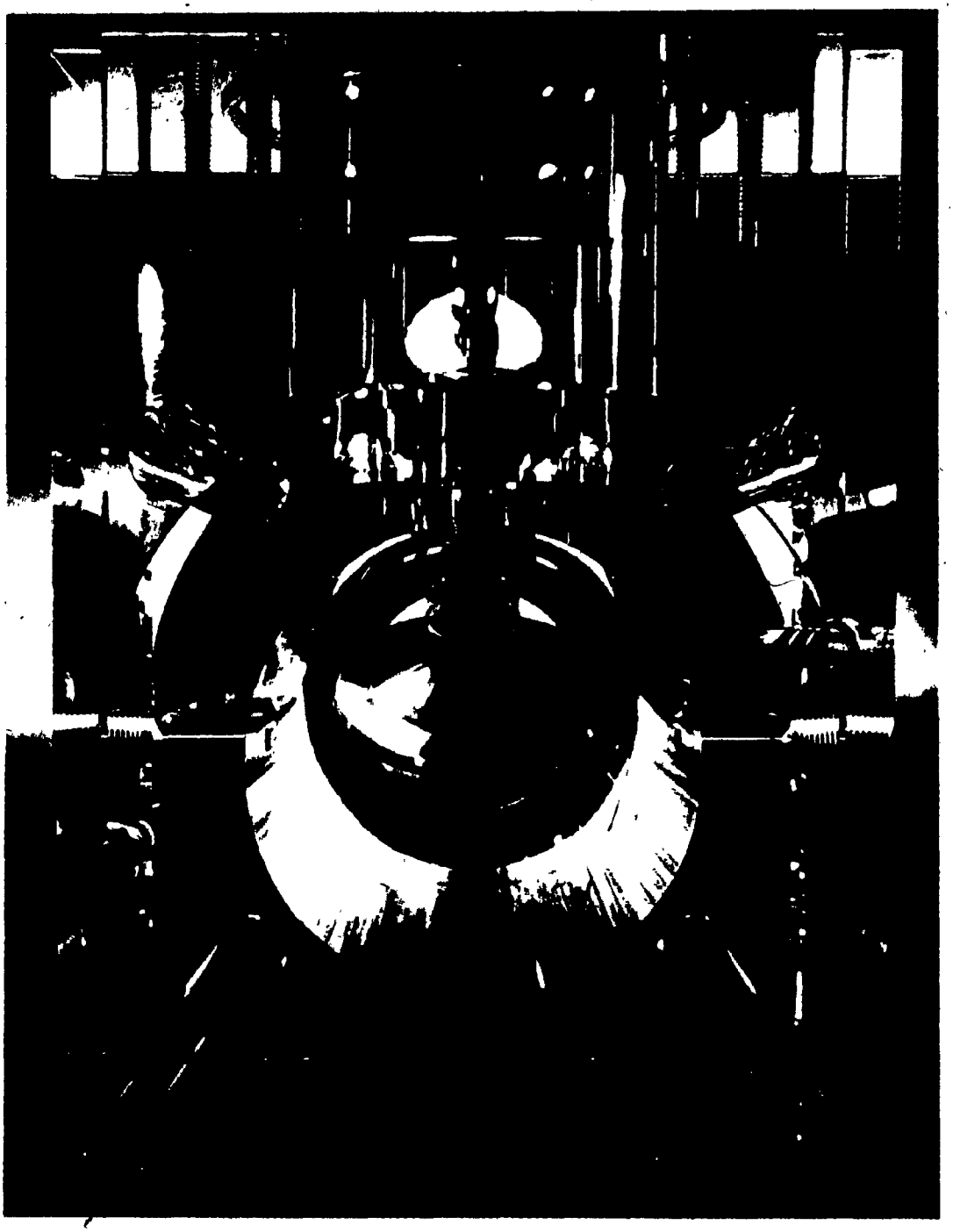

Figure D-2b. Pictorial View of Aluminum-Plexiglass Flow Force Test Rig (downstream rear view)

APPENDIX E

80-mm VENTURI METER CALIBRATION

The 80-mm venturi meter was obtained from the Civil Engineering Department at Concordia University. The venturi meter has a throat diameter of 59.7 mm and an upstream diameter of 72.4 mm. The venturi meter is calibrated against a 90° V-notch weir, designed by the Civil Engineering Department according to ASME [26] specifications. For further comparison, the weir flow rate is compared to the flow rate measured by a 50-mm type S 100-series Trident flow meter manufactured by the Neptune Measurement Company. The flow range for the Trident meter is from $0.0001 m^3/s$ to $0.0101 m^3/s$, while the flow range for the weir is from $0.0013 m^3/s$ to $0.0099 m^3/s$. The venturi meter flow rate is measured in terms of its pressure drop by a U-tube manometer in millimeters of specific gravity 1.75 manometer fluid. The data for the venturi meter calibrated against the flow measured by the weir and by the Trident flow meter is given in Table E-1. The difference in flow rate measurements between the Trident meter with respect to the weir is small. Also given in the table is the flow rate calibration equation for the venturi meter in terms of manometer fluid height. Figure E-1 shows the venturi meter calibration curve in height of manometer fluid with respects to the weir flow measurements.

No.	Venturi h-mm of Sp.Gr. 1.75	90° V-Notch Weir $Q \times 10^3 (m^3/s)$	Trident Flow Meter $Q \times 10^3 (m^3/s)$	% Difference with respect to Weir
1	33	2.55	2.61	2.4
2	65	3.54	3.57	0.8
3	130	5.07	4.98	-1.7
4	175	5.52	5.89	6.7
5	214	6.37	6.40	0.4
6	263	7.14	7.08	-0.8
7	288	7.39	7.39	0
8	329	7.96	7.90	-0.7
9	359	8.38	8.24	-1.7
10	388	8.61	8.55	-0.7
11	425	8.89	8.92	0.3
12	458	9.37	9.29	-0.9
13	487	9.51	9.54	0.3
14	512	9.85	9.77	-0.8
	Weir:	$\log Q = 0.4956 \log h - 3.3473$		
	Trident:	$\log Q = 0.4842 \log h - 3.3217$		

TABLE E-1. 80-mm Venturi Meter Calibration Data

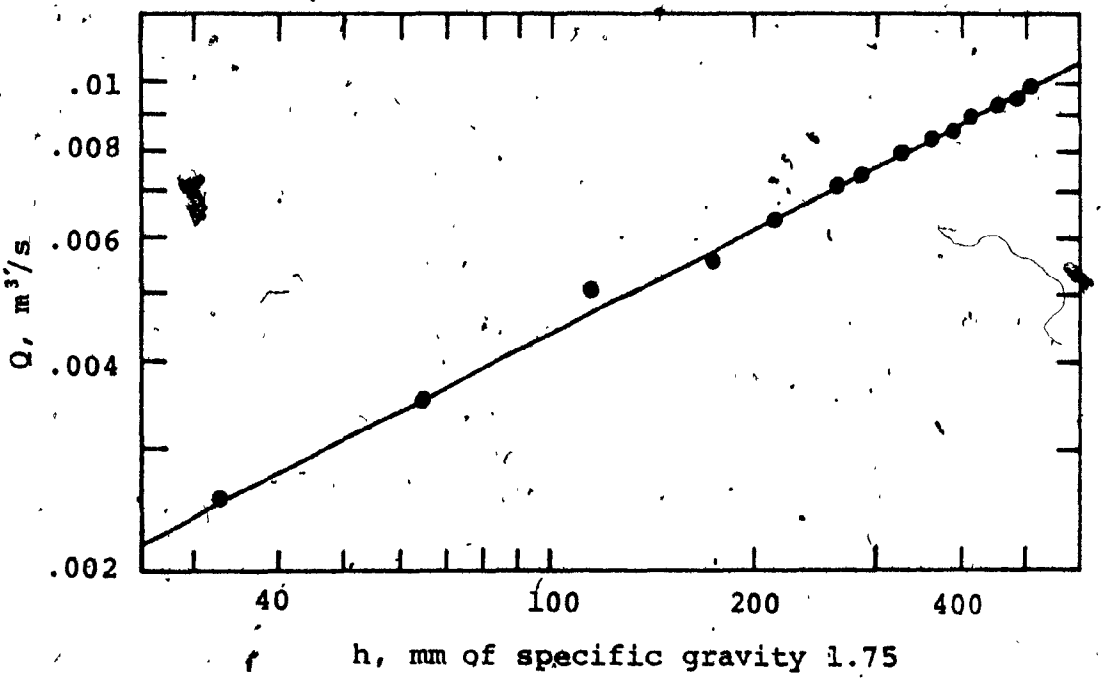

Figure E-1. 80-mm Venturi Meter Calibration Curve

APPENDIX F

150-mm VENTURI METER CALIBRATION

The 150-mm venturi meter has a throat diameter of 89.1-mm and an upstream diameter of 146.1-mm. The venturi meter is designed according to ASME [26] specifications. A detail drawing of the venturi meter is shown in Figure F-1. The venturi meter is calibrated against a 60^{o} V-notch weir designed according ASME [26] specifications by the Civil Engineering Department at Concordia University. The flow range for the weir is from $0.0008 m^3/s$ to $0.0425 m^3 s$. Table F-1 gives the calibration data for the venturi meter. The venturi meter pressure drop corresponding to the pipe flow rate measured by the weir is in millimeters of manometer fluid. Manometer fluid of specific gravity 1.75 is used for low flow rates, while the fluid of specific gravity 2.95 is used for higher flow rates. The venturi meter flow calibration equation expressed in height of manometer fluid specific gravity 2.95 is given in the table. The calibration curve for the venturi meter is shown in Figure F-2 plotted against manometer fluid of specific gravity 2.95.

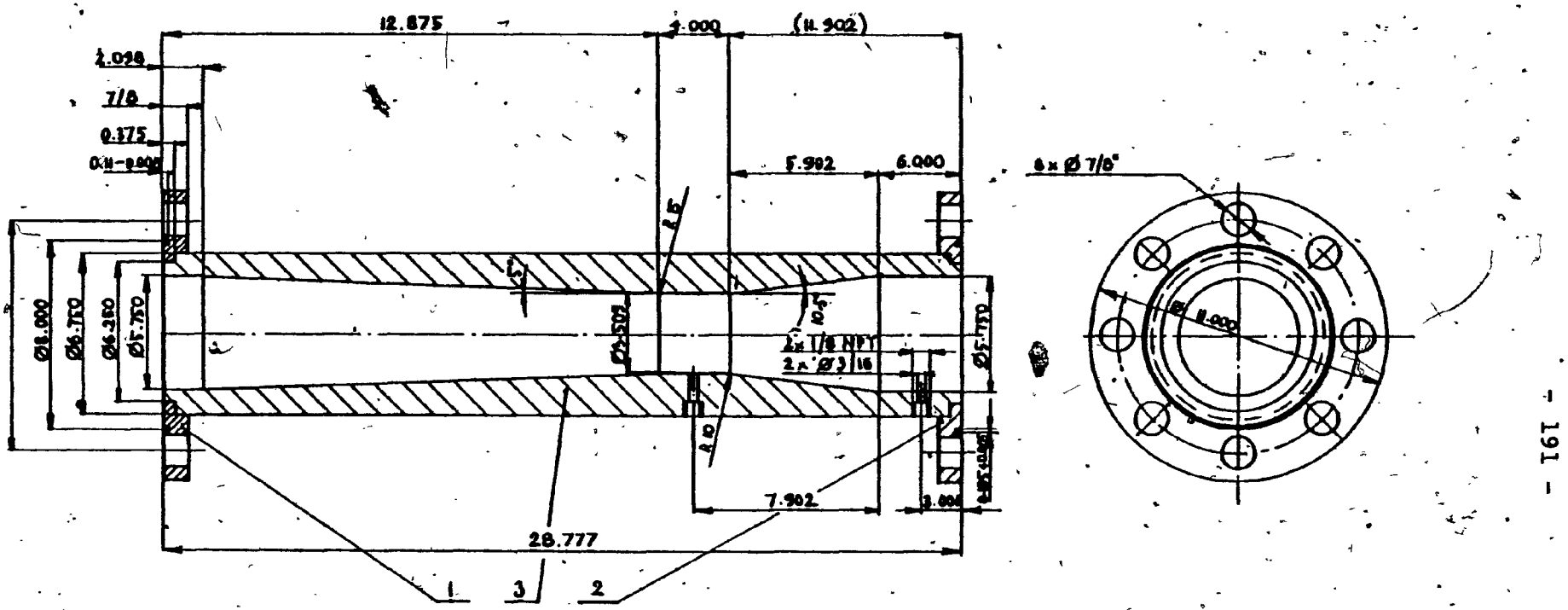

1 inch = 25.4 mm

3	VENTURIMETER	1	BRONZE
2	FLANGE	1	M.S.
1	FLANGE	1	M.S.
No.	PART NAME	REQD	MAT.

Figure F-1. 150-mm Venturi Meter Detail Drawing

No.	Venturi h-mm of Sp.Gr. 2.95 (Sp.Gr. 1.75)	60° V-Notch Weir $Q \times 10^3$ (m^3/s)	No.	Venturi h-mm of Sp.Gr. 2.95 (Sp.Gr. 1.75)	60° V-Notch Weir $Q \times 10^3$ (m^3/s)
1	(24)	3.88	16	(657)	20.39
2	(38)	4.98	17	(704)	21.18
3	(50)	5.64	18	(757)	22.00
4	(69)	6.68	19	307	22.63
5	(102)	8.13	20	370	24.83
6	(151)	9.88	21	414	26.25
7	(203)	11.50	22	466	27.89
8	(255)	12.88	23	518	29.39
9	(304)	14.02	24	569	30.75
10	(354)	15.18	25	612	31.97
11	(404)	16.17	26	663	33.39
12	(457)	17.10	27	716	34.57
13	(505)	17.98	28	817	36.84
14	(556)	18.86	29	975	40.13
15	(606)	19.74	30	1082	42.16

$$\log Q = 0.4990 \log h - 2.8864$$

Q (m^3/s) h (mm of Sp.Gr. 2.95)

TABLE F-1. 150-mm Venturi Meter Calibration Data

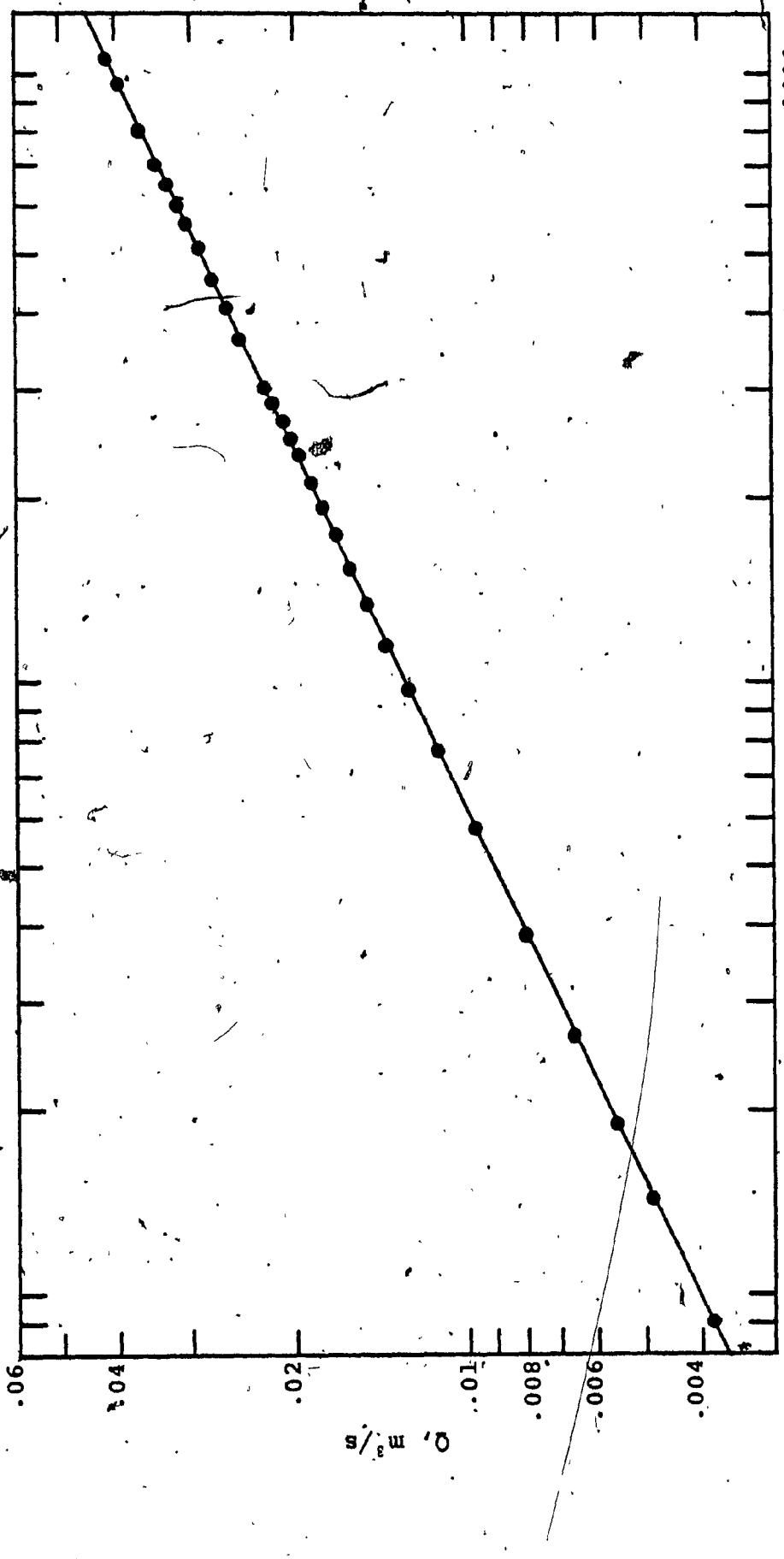

Figure F-2. 150-mm Venturi Meter Calibration Curve

APPENDIX G

LOAD CELL CALIBRATION

The force transducer used to measure the flow forces acting on the valve disc is a type TC-2000-100 bi-directional load cell manufactured by Kulite Semiconductor Inc. The load cell is comprised of a Wheatstone semiconductor bridge, compensated for thermal changes. Force measurements are read directly from a milli-voltmeter connected across the output terminals. The load cell specifications are:

Rated load	:	444.8 N (100 lb_f)
Diapharm thickness	:	0.74 mm (0.029 in)
Nominal deflection	:	0.018 mm (0.0007 in)
Natural frequency	:	5.4 kHz
Overload	:	150%
Operation mode	:	tension and compression
Rated electrical excitation	:	10 VDC/AC (RMS)
Maximun electrical excitation	:	15 VDC/AC (RMS)
Input impedence	:	2047 ohms
Output impedence	:	788 ohms
Full scale output	:	155 mV FSO (nominal)
Residual output	:	+2%
Non-linearity	:	0.5% FSO
Hysteresis	:	0.1% FSO
Repeatability	:	0.1%

Resolution : infinite

Operating temperature range : -40 °C to +120 °C.

The calibration data for the load cell, for tension and for compression, is given in Table G-1. Both modes of operation has the same slope. The tension data are plotted in Figure G-1. Also plotted on the same figure is the compression data. Thus, given any initial static load reading from the voltmeter, the force difference from the initial load is calculated by knowing the transducer calibration slope.

No.	TENSION		COMPRESSION	
	N(+)	mV(-)	N(-)	mV(+)
1	5.8	16.8	19.1	-11.0
2	28.0	26.9	36.9	- 3.1
3	50.3	37.8	54.7	4.8
4	72.5	47.4	72.5	12.3
5	117.0	67.7	90.3	20.6
6	161.5	88.1	108.1	28.3
7	237.1	121.8	125.9	37.3
8	259.3	131.9	143.7	44.5
9	281.6	142.0	161.5	52.9
10	326.0	161.6	179.3	61.0
11	397.2	193.3	197.0	68.9
12			214.8	77.2
SLOPE (N/mV)	-2.20		-2.20	

TABLE G-1. Force Transducer Calibration Data

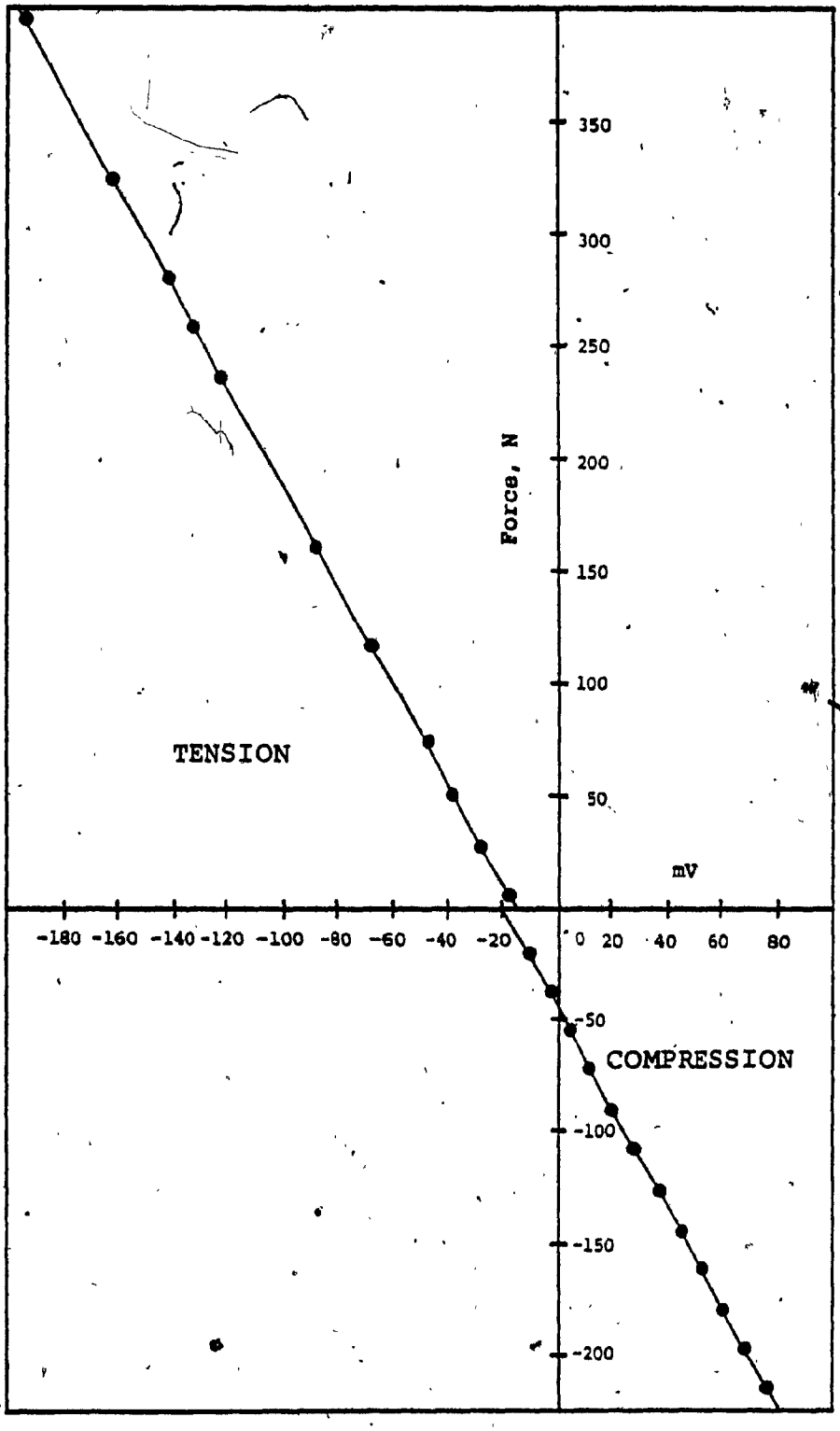

Figure G-1. Force Transducer Calibration Curve

APPENDIX H

FORTRAN PROGRAM LISTING OF VALVE-PIPELINE SIMULATION

```
      PROGRAM MAIN(INPUT,OUTPUT,TAPE1)
*****************************************************************
C  THIS PROGRAM SIMULATES THE TRANSIENT FLOW AND
C  CHECK VALVE RESPONSE FOR THE PIPING SYSTEM
C  DESCRIBED IN CHAPTER 6.
*****************************************************************

      DIMENSION Y(44),F(44)

C  N = NUMBER OF DIFFERENTIAL EQUATIONS

      N=44
      M=0
      ICOUNT=0
      DUMMY=0.0
      CALL SPLINE(DUMMY)

      X=25.0
      H=.00005
      STEP=H
      H3=H/1000.
      DT=.1
      DTOUT=X+DT
      TMAX=30.

*  INITIAL CONDITIONS FOR PIPES
      HR=150.
      QV=0.0
      DO 5 II=1,10
      Y(II)=150.
      Y(II+20)=150.
      Y(II+10)=0.0
    5 Y(II+31)=0.0
      Y(31)=150.
*  INITIAL CONDITIONS FOR THE SWING-DISC CHECK VALVE
      Y(N-2)=0.0
      Y(N-1)=1.0472
      Y(N)=4.9161E-04

   10 FORMAT(1H1,3X,*TIME*,6X,*CVN*,6X,*ANGLE*,19X,
     +*PIPE 1  /  PIPE 2*,62X,*DTETA*)
   15 FORMAT(1H0,2(2X,F7.4),5X,F8.4,3X,*H=*,6(2X,F7.3),2X,
```

```
     +*TCY=*,E13.6,/,35X,*Q=*,6(2X,F7.4),3X,*PA=*,E13.6,
     +8X,E13.6)
  20 FORMAT(35X,*H=*,6(2X,F7.3),2X,*CND=*,E13.6,/,35X,
     +*Q=*,6(2X,F7.4),2X,*TO=*,E13.6)


      CALL PIPE(N,HR,QV,Y,F)
      CALL VALVE(N,Y,F,PA,CVN,ANGLE,DTETA,QV,CND,TO,TCY)

      PRINT 10
      PRINT 15,X,CVN,ANGLE*57.29578,HR,(Y(J),J=2,10,2),
     +TCY,(Y(J),J=11,19,2),QV,PA,DTETA
      PRINT 20,(Y(J),J=21,31,2),CND,(Y(J),J=32,40,2)
     +,Y(41),TO

C   INTEGRATION.......

   30 CONTINUE
      CALL RUNGE(N,Y,F,X,STEP,ICOUNT)
      IF(ICOUNT.EQ.0) GO TO 40
   35 CONTINUE

* * *  RESERVOIR HEAD VARIATIONS * * * *

      IF(X.LE.1.0) HR=150.
      IF((X.GT.1.0).AND.(X.LE.1.5)) HR=300.*X-150.
      IF((X.GT.1.5).AND.(X.LE.15.)) HR=300.
      IF((X.GT.15.).AND.(X.LE.15.5)) HR=-400.*X+6300.
      IF(X.GT.15.5) HL=100.

      CALL VALVE(N,Y,F,PA,CVN,ANGLE,DTETA,QV,CND,TO,TCY)
      CALL PIPE(N,HR,QV,Y,F)
      GO TO 30

C   PRINTING CONTROL
   40 CONTINUE
      IF((X.LT.DTOUT+H3).AND.(X.GT.DTOUT-H3)) GO TO 50
      GO TO 35
   50 CONTINUE
      DTOUT=DTOUT+DT
      PRINT 15,X,CVN,ANGLE*57.29578,HR,(Y(J),J=2,10,2),
     +TCY,(Y(J),J=11,19,2),QV,PA,DTETA
      PRINT 20,(Y(J),J=21,31,2),CND,(Y(J),J=32,40,2),
     +Y(41),TO
      IF(X.GE.TMAX) STOP
      GO TO 35

      END
```

```
      SUBROUTINE RUNGE(N,Y,F,X,H,M)
C*************************************************************
C  1) FOURTH-ORDER RUNGE-KUTTA INTEGRATION METHOD
C  2) KUTTA'S COEFFICIENTS A=1/6 B=1/3 C=1/3 D=1/6
C  3) INTEGRATE SYSTEM OF N SIMULTANEOUS FIRST ORDER
C     DIFFERENTIAL EQUATIONS F(J)=DY(J)/DT
C     WHERE J=1,2,.....,N
C  4) SUBJECT TO INITAIAL CONDITIONS Y(J)
C     WHERE J=1,2,.....,N
C  5) INTEGRATION ACROSS ONE STEP OF LENGTH H IN
C     INDEPENDENT VARIABLE X
C  6) METHOD REQUIRES 4 CALLS, PASS(1).....PASS(4)
C  7)   N-NUMBER OF DIFFERENTIAL EQUATIONS
C       Y-SOLUTION VECTOR
C       F-DERIVATIVE VECTOR
C       H-STEP SIZE
C       M-DUMMY VARIABLE TO TELL CALLING PROGRAM IF
C         M.EQ.0  H STEP COMPLETED
C         M.NE.0  H STEP NOT COMPLETED
C   SAVEY-USED TO SAVE INITIAL VALUES OF Y(J)
C   SAVEF-WEIGHTED AVERAGES OF DERIVATIVES
C  8) VARIABLES WITH DIMENSIONS MUST BE STATED IN
C     MAIN PROGRAM'S DIMENSION STATEMENT

C  SOURCE: REFERENCE [27]  PP.361-380
*************************************************************
      DIMENSION Y(N),F(N),SAVEY(44),SAVEF(44)

      M=M+1
      GO TO (1,2,3,4),M

C..... PASS 1 .....
    1 DO 10 J=1,N
      SAVEY(J)=Y(J)
      SAVEF(J)=F(J)
   10 Y(J)=SAVEY(J)+0.5*H*F(J)
      X=X+0.5*H
      RETURN

C..... PASS 2 .....
    2 DO 20 J=1,N
      SAVEF(J)=SAVEF(J)+2.0*F(J)
   20 Y(J)=SAVEY(J)+0.5*H*F(J)
      RETURN

C..... PASS 3 .....
    3 DO 30 J=1,N
      SAVEF(J)=SAVEF(J)+2.0*F(J)
   30 Y(J)=SAVEY(J)+H*F(J)
```

```
      X=X+0.5*H
      RETURN

C..... PASS 4 .....
    4 DO 40 J=1,N
   40 Y(J)=SAVEY(J)+(SAVEF(J)+F(J))*H/6.0
      M=0
      RETURN

      END
```

```
      SUBROUTINE PIPE(N,HR,QV,Y,F)
*****************************************************************
C  THIS SUBROUTINE CALCULATES PIPE HEAD AND FLOW
C  DERIVATIVES REQUIRED FOR THE RUNGE-KUTTA INTEGRATION
C  ROUTINE.
C  WITH REFERENCE TO FIGURE 6-4, FOR I=1 TO 10
C  F(I)=DH(I)/DT                    Y(I)=H(I)
C  F(I+10)=DQ(I)/DT                 Y(I+10)=Q(I)
C  F(I+20)=DH(I+10)/DT              Y(I+20)=H(I+20)
C  F(I+30)=DQ(I+10)/DT              Y(I+30)=Q(I+10)
C  F(41)=DH(TANK)/DT                Y(41)=H(TANK)
*****************************************************************
      DIMENSION Y(N),F(N)
      DATA XRE,XCA,XIN,XCAH/289.752,1.3187E-05,189.576,
     +6.5937E-06/

      DO 10 I=1,9
      I11=I+10
      I12=I11+1
      YI12=Y(I12)
      F(I)=(Y(I11)-YI12)/XCA
   10 F(I12)=(Y(I)-Y(I+1)-XRE*YI12*ABS(YI12))/XIN
      Y11=Y(11)
      F(11)=(HR-Y(1)-XRE*Y11*ABS(Y11))/XIN
      F(10)=(Y(20)-QV)/XCAH

      DO 20 J=22,30
      J32=J+10
      J33=J32+1
      YJ33=Y(J33)
      F(J)=(Y(J32)-YJ33)/XCA
   20 F(J33)=(Y(J)-Y(J+1)-XRE*YJ33*ABS(YJ33))/XIN
      Y32=Y(32)
      F(32)=(Y(21)-Y(22)-XRE*Y32*ABS(Y32))/XIN
      F(21)=(QV-Y32)/XCAH
      F(31)=0.0

      RETURN
      END
```

```
      SUBROUTINE VALVE(NN,Y,F,PA,CVN,ANGLE,DTETA,QV,CND,
     +TO,TCY)
*****************************************************************
C  DYNAMIC SIMULATION OF THE HYDRAULIC SPRING-DAMPER
C  SWING-DISC CHECK VALVE.

C  REFER TO CHAPTER 4 FOR DETAILS.

*****************************************************************
      DIMENSION Y(NN),F(NN)
      LOGICAL SET1,SET2,SET3,PDY,UPCU,LOCU
      LOGICAL PTDF,NTDF,OPHD,CLHD

      DATA A1,A2,XJ/2.3742E-03,3.1613E-03,1.0122E-01/
      DATA RV,RC,RUC,RLC/5.1348E+13,3.8511E+12,2.5674E+13
     +,2.0539E+13/
      DATA VAO,PAO/4.9161E-04,1034214.0/
COMMENT ** 'DTETA','TETA1', AND 'VA' INITIAL CONDITIONS
C         MUST BE PASSED FROM MAIN PROGRAM

      N=NN-3
      DTETA=Y(N+1)
      TETA1=Y(N+2)
      VA=Y(N+3)

C**  THE ACCEPTABLE ANGULAR DISPLACEMENT VALUE IS FROM 0. TO
1.0472 RAD
      SET1=TETA1.LE.0.0
      SET2=TETA1.GE.1.0472
      SET3=SET1.OR.SET2
      TETA=TETA1
      IF(SET1) TETA=0.0
      IF(SET2) TETA=1.0472

C** HYDRAULIC ACTUATOR DISPLACEMENT
      YY=SQRT(4.9677E-02-4.0311E-02*(COS(0.5877+TETA)))

C** TO FIND ANGLE ALFA
      FN=(YY*YY-2.9032E-02)/(0.2032*YY)
      ALFA=ACOS(FN)

C** HYDRAULIC ACTUATOR VELOCITY
C   WITH PHYSICAL LIMITATIONS IN CONSIDERATION
      IF(SET3) GO TO 70
      DY=4.0311E-02*SIN(0.5877+TETA)*DTETA/(2.*YY)
      GO TO 80
   70 DY=0.0
   80 CONTINUE

C** ROD END FLUID FLOW RATE
```

```
      Q1=A1*DY
C** PISTON END FLUID FLOW RATE
      Q2=A2*DY
C** ACCUMULATOR FLUID FLOW RATE
      QA=Q2-Q1

C** INSTANTANEOUS ACCUMULATOR PRESSURE
      PA=PA0*VA0/VA
      P1=PA


C** POSITIVE ACTUATOR VELOCITY
      PDY=DY.GT.0.0
C** UPPER CUSHION REGION IS 1.9050E-02 M FROM THE END OF
STROKE
      UPCU=YY.GT.0.2096
C** LOWER CUSHION REGION IS 1.9050E-02 M FROM THE END OF
STROKE
      LOCU=YY.LT.0.1461


C** THE P2 VALUE DEPENDS ON THE FLUID RESTRICTION
      IF(PDY) GO TO 100
      IF(DY.EQ.0.0) GO TO 120
      IF(LOCU) GO TO 90
      P2=P1+RC*Q2*Q2
      GO TO 130
   90 P2=P1+RLC*Q2*Q2
      GO TO 130
  100 IF(UPCU) GO TO 110
      P2=P1-RV*Q2*Q2
      GO TO 130
  110 P2=P1-RUC*Q2*Q2
      GO TO 130
  120 P2=P1
  130 CONTINUE


**** TORQUE INPUT FROM PIPE-LINE

      ANGLE=1.0472-TETA
      HEADL=Y(10)
      HEADR=Y(21)
      ANVEL=DTETA
      IF(SET3) ANVEL=0.0
      CALL CVNCND(ANGLE,ANVEL,HEADL,HEADR,CVN,CND,QV,TO)

C**  HYDRAULIC CYLINDER TORQUE AT ANGLE ALFA
      TCY=(P2*A2-P1*A1)*SIN(ALFA)*0.1016
C**  DISK ANGULAR ACCELERATION IS OBTAINED FROM DIVIDING
C    TORQUE DIFFERENCE BY INERTIA
      TDIFF=(TCY-TO)/XJ
```

```
C**  WHEN LIMIT CONDITION IS SATISFIED THE ACCELERATION IS
SET TO ZERO
      PTDF=TDIFF.GE.0.0
      NTDF=TDIFF.LT.0.0
      OPHD=SET1.AND.NTDF
      CLHD=SET2.AND.PTDF
      TDIFF1=TDIFF
      IF(OPHD.OR.CLHD) GO TO 20
      GO TO 30
   20 TDIFF1=0.0
      DTETA=0.0
      Y(N+1)=DTETA
      Y(N+2)=TETA
   30 CONTINUE


C**  TO FIND ANGULAR VELOCITY BY INTEGRATING ACCELERATION
      F(N+1)=TDIFF1


C**  TO FIND ANGULAR DISPLACEMENT BY INTEGRATING ANGULAR
VELOCITY
      F(N+2)=DTETA


C**  THE COMPRESSED GAS VOLUME IS OBTAINED BY INTEGRATING
C    THE ACCUMULATOR FLUID FLOW RATE
      F(N+3)=QA

      RETURN
      END
```

```
      SUBROUTINE CVNCND(ANGLE,DTETA,HEADL,HEADR,CVN,CND
     +,QV,TO)
*****************************************************************
C  THIS SUBROUTINE CALCULATES THE FLOW COEEFICIENTS
C  TO DETERMINE THE SWING-DISC VALVE PRESSURE DROP AND
C  THE NORMAL DRAG COEFFICIENT TO DETERMINE THE FORCE
C  ACTING AGAINST THE VALVE DISC.

C  REFER TO CHAPTER 5 FOR DETAILS.
*****************************************************************
      COMMON/BLK1/P(4,14),Q(4,14),R(4,14),S(4,14)
      COMMON/BLK2/XX(4,15),YY(4,15)

COMMENT: THIS SUBROUTINE IS IN BRITISH UNITS.
C        1-FEET = 0.3048-M
      REAL KL3,KL3I
      DATA A1,A2,A3,AL/3.4741E-01,2.3044E-01,2.7688E-01
     +,0.375/
      DATA A1INCH/50.0270/
      DATA D3D1S,RO2CON,HLRAC/0.797,14.5311,1.3627E-01/
      DATA CV1F,CV1R/1.5163,0.7746/


      IF(ANGLE.GT.0.0) GO TO 10
      CVN=0.0
      CND=0.0
      TO=(HEADL*A2-HEADR*A3)*104.0
      QV=0.0
      RETURN

   10 DEG=ANGLE*57.29578
      COST=COS(ANGLE)
      SINT=SIN(ANGLE)
      ARAT=(-0.948+1.7039*COST+1.2696*SINT)/A1INCH
      Z=1.0-D3D1S*COST-ARAT
      ZS=(Z-1.0)**2
      IF(HEADL.LT.HEADR) GO TO 100

********** F O R W A R D   F L O W **********

      K=0
      DO 20 J=1,14
      K=K+1
   20 IF((DEG.GE.XX(1,J)).AND.(DEG.LE.XX(1,J+1))) GO TO 30
   30 DIFF=DEG-XX(1,K)
      KL3I=P(1,K)+DIFF*(Q(1,K)+DIFF*(R(1,K)+S(1,K)*DIFF))
      CNDI=P(2,K)+DIFF*(Q(2,K)+DIFF*(R(2,K)+S(2,K)*DIFF))
      KL3=1.0/KL3I
      CND=1.0/CNDI
```

```
      CV2=Z/SQRT(KL3+ZS)
      CVN=CV1F*CV2/SQRT(CV1F*CV1F+CV2*CV2)
      QE=CVN*A1*SQRT(HEADL-HEADR)*RO2CON
      QV=QE*2.8317E-02
      VFLOW=QE/A2
      VARM=AL*DTETA*COST
      VREL=VFLOW+VARM
      VEL=VREL*ABS(VREL)
      TO=HLRAC*VEL*CND
      IF(-VARM.LE.VFLOW) RETURN
      TO=(HEADL*A2-HEADR*A3)*104.0
      CND=0.0
      RETURN

********** R E V E R S E     F L O W **********

  100 CONTINUE
      K=0
      DO 120 J=1,14
      K=K+1
  120 IF((DEG.GE.XX(3,J)).AND.(DEG.LE.XX(3,J+1))) GO TO 130
  130 DIFF=DEG-XX(3,K)
      KL3I=P(3,K)+DIFF*(Q(3,K)+DIFF*(R(3,K)+S(3,K)*DIFF))
      CNDI=P(4,K)+DIFF*(Q(4,K)+DIFF*(R(4,K)+S(4,K)*DIFF))
      KL3=1.0/KL3I
      CND=1.0/CNDI
      CV2=Z/SQRT(KL3+ZS)
      CVN=CV1R*CV2/SQRT(CV1R*CV1R+CV2*CV2)
      QE=CVN*A1*SQRT(HEADR-HEADL)*RO2CON
      QV=-QE*2.8317E-02
      VFLOW=-QE/A1
      VARM=AL*DTETA*COST
      VREL=VFLOW+VARM
      VEL=VREL*ABS(VREL)
      TO=HLRAC*VEL*CND
      IF(VARM.LE.-VFLOW) RETURN
      TO=(HEADR*A3-HEADL*2)*104.0
      CND=0.0
      RETURN

      END
```

```
      SUBROUTINE SPLINE(DUMMY)
*****************************************************************

C  THIS SUBROUTINE CALCULATES THE NATURAL CUBIC SPLINE
C  INTERPOLATION CURVES GIVEN IN FIGURES 5-6 AND 5-7,
C  RESPECTIVELY FOR FORWARD AND REVERSE FLOW. DATA
C  CORRESPONDING TO FIGURES 5-2 AND 5-3 FOR FORWARD FLOW
C  AND FIGURES 5-4 AND 5-5 FOR REVERSE FLOW ARE READ
C  AND STORED AS FOLLOWS:

C    XX(L,N)  = DISC OPENING ANGLES
C    YY(L,N)  = DISC ENTRANCE LOSS COEFFICIENT (1/KL3)
C               OR THE NORMAL DRAG COEFFICIENT (1/CND)

C       L = 1   1/KL3   FORWARD FLOW
C       L = 2   1/CND   FORWARD FLOW
C       L = 3   1/KL3   REVERSE FLOW
C       L = 4   1/CND   REVERSE FLOW

C       N = 15    EACH FIGURE FROM FIGURES 5-2 TO 5-5 HAS
C                 14 EXPERIMENTAL AVERAGE POINTS PLUS 1
C                 ADDITIONAL DATA FOR THE CLOSED DISC

C  THE NATURAL CUBIC SPLINE COEFFICIENTS ARE CALCULATED
C  AND STORED IN ARRAYS P, Q, R AND S WITH INDICES (L,K).
C  INDEX L IS DESCRIBED ABOVED. INDEX K IS 14 SINCE
C  THERE ARE 15 DATA POINTS.

C  THE NATURAL CUBIC SPLINE ALGORITHM WAS OBTAINED
C  FROM REFERENCE [28], PP.116-121.

*****************************************************************

      COMMON/BLK1/P(4,14),Q(4,14),R(4,14),S(4,14)
      COMMON/BLK2/XX(4,15),YY(4,15)
      DIMENSION X(15),Y(15),AL(14),U(15),V(15),W(15)
      DIMENSION B(14),C(14),D(14)


      L=0
    5 L=L+1
      READ(1,*) N
      DO 6 M=1,N
    6 READ(1,*) X(M),Y(M)

      N1=N-1
      N2=N-2
      DO 10 I=1,N2
   10 AL(I+1)=3.0*(Y(I+2)*(X(I+1)-X(I))-Y(I+1)*
     +(X(I+2)-X(I))
     ++Y(I)*(X(I+2)-X(I+1)))/(X(I+2)-X(I+1))/(X(I+1)-X(I))

      U(1)=1.0
```

```
      V(1)=0.0
      W(1)=0.0

      DO 20 I=1,N2
      U(I+1)=2.0*(X(I+2)-X(I))-(X(I+1)-X(I))*V(I)
      V(I+1)=(X(I+2)-X(I+1))/U(I+1)
   20 W(I+1)=(AL(I+1)-W(I)*(X(I+1)-X(I)))/U(I+1)

      U(N)=0.0
      C(N)=0.0
      J=N-1

   30 C(J)=W(J)-V(J)*C(J+1)
      B(J)=(Y(J+1)-Y(J))/(X(J+1)-X(J))
     +-(X(J+1)-X(J))*(C(J+1)+2.0*C(J))/3.0
      D(J)=(C(J+1)-C(J))/3.0/(X(J+1)-X(J))
      J=J-1
      IF(J.GE.1) GO TO 30


      DO 40 K=1,N1
      P(L,K)=Y(K)
      Q(L,K)=B(K)
      R(L,K)=C(K)
      S(L,K)=D(K)
      XX(L,K)=X(K)
   40 YY(L,K)=Y(K)
      YY(L,N)=Y(N)
      XX(L,N)=X(N)


      KPRNT=0
      IF(KPRNT.NE.1) GO TO 110
      DO 80 K=1,N1
      PRINT 70,L,K,P(L,K),Q(L,K),R(L,K),S(L,K)
   70 FORMAT(2X,2I5,3X,4(E13.6),/)
   80 CONTINUE
      DO 100 K=1,N
      PRINT 90,XX(L,K),YY(L,K)
   90 FORMAT(2X,*DEG=*,F9.6,10X,*COEFF=*,E13.6,/)
  100 CONTINUE
  110 CONTINUE

      IF(L.EQ.4) RETURN
      GO TO 5

      END
```

PROGRAM DATA

```
15
0.          0.
5.25        0.3889
10.24       1.2253
14.99       2.3305
20.16       2.3213
24.71       1.7819
29.73       1.5785
34.54       1.4806
39.98       1.5564
44.87       1.6567
49.71       1.8083
54.63       2.1164
60.28       2.8514
64.97       3.7397
69.97       5.9137
```

```
15
0.          0.
5.25        0.02953
10.24       0.05959
14.99       0.08621
20.16       0.1018
24.71       0.1079
29.73       0.1305
34.54       0.1628
39.98       0.2254
44.87       0.3110
49.71       0.4151
54.63       0.5851
60.28       0.8865
64.97       1.2806
69.97       2.1935
```

15

0.	0.
4.70	0.6501
9.60	3.560
14.99	5.8480
20.27	2.9061
24.74	1.6955
29.70	1.7224
34.35	2.0161
40.00	1.7618
44.89	1.5848
49.92	1.5307
55.22	1.5853
60.34	1.8215
65.00	2.3283
69.97	3.2552

15

0.	0.
4.70	0.01124
9.60	0.02983
14.99	0.03808
20.27	0.03932
24.74	0.03771
29.70	0.04853
34.35	0.06459
40.00	0.08294
44.89	0.1008
49.92	0.1277
55.22	0.1527
60.34	0.1903
65.00	0.2379
69.97	0.3067